Magnetic Properties of Amorphous Oxides and Related Materials

Hirofumi Akamatsu

2009

Contents

General Introduction

An amorphous oxide magnet is of great interest because it is a typical example of a random magnet. In magnetic oxide glasses, magnetic cations are randomly distributed in three-dimensional disordered networks. Most oxide glasses are insulating so that their magnetic properties are dominated by short-range superexchange interaction via an oxide ion, in contrast to a canonical spin glass, an archetype of random magnetic systems, where the long-range Ruderman-Kittel-Kasuya-Yoshida interaction via a conduction electron plays an important role for the spin glass ordering [1]. According to the Kanamori-Goodenough rule, the sign and strength of superexchange interactions depend on the sorts of magnetic ions, the distance between them, and the angles of *M*-O-*M* where *M* and O are a magnetic ion and an oxide ion, respectively, in insulating oxides [2,3]. The latter two ingredients have a wide distribution in an amorphous oxide. This introduces a random distribution in the sign and strength of the superexchange interaction. Antiferromagnetic interactions prevail against ferromagnetic ones in most of magnetic oxide glasses, as indicated by neutron magnetic scattering [4] and the fact that they have negative Weiss temperatures (θ_W's) [5-8]. The random distribution of magnetic moments and the antiferromagnetic interactions between them inevitably cause so-called magnetic frustration of geometrical origin in the alignment of the magnetic moments. Also, the magnetic frustration possibly arises from the competition of ferromagnetic and antiferromagnetic superexchange interactions. Due to the combination of the randomness and frustration, which is the key concept for description of spin glasses [1], spin freezing as observed in spin glasses is expected to occur in amorphous oxide magnets as well.

For these three decades some researchers have experimentally investigated the random spin freezing in magnetic oxide glasses of a variety of systems at low temperatures from several hundreds millikelvins to several kelvins [5-22]. As long as the author knows, Verhelst *et al*. [5] first observed the random spin freezing of oxide

glasses for the CoO-Al_2O_3-SiO_2 and MnO-Al_2O_3-SiO_2 systems in 1975, just three years after the discovery of the canonical spin glass, i.e., the *Au*-Fe alloys. Assuming the presence of magnetic clusters, they explained the sharp peak in temperature variation of ac magnetic susceptibility on the basis of a simple superparamagnetic model, i.e. a thermally activated freezing process of the magnetic clusters. They indicated that a spin glass model is also capable of accounting for the spin freezing although they did not attempt a critical comparison of various models to explain the magnetic anomaly. Around the same time, Moran *et al*. [9] investigated the sound velocity, which is concerned with the specific heat, for these glass systems. They also utilized the superparamagnetic model in order to interpret the temperature dependence of the sound velocity. Rechenberg *et al*. [10] reported the relaxation process of remanent magnetization below the spin freezing temperature for the CoO-Al_2O_3-SiO_2 glass system. They measured the time dependence of remanent magnetization after an external field was turned off for the field cooled sample, and analyzed the experimental results by the superparamagneic model assuming a distribution of anisotropy energy for the superparamagnetic clusters. Later, further extensive investigations of these magnetic alminosilicate glasses were made by dc and ac susceptibility [11], magnetic specific heat [12], and Mössbauer spectra measurements [13], and the experimental results were discussed in terms of a superparamagnetic model. On the other hand, Ferré *et al*. [6] performed the detailed dc and ac magnetization measurements and suggested that the MnO-Al_2O_3-SiO_2 glasses have similar magnetic properties to canonical spin glasses. In particular, the frequency dependence of spin freezing temperature derived from the ac susceptibility measurement was found to be unsuitable for the Arhenius law, indicating that the thermally activated process can not explain the spin freezing. Ito *et al*. [7] measured the temperature dependence of ac susceptibility and Mössbauer spectra for the FeO-Al_2O_3-SiO_2 glasses. They also suggested that no physically acceptable values are yielded by fitting the Arrhenius law to the variation of spin freezing temperature with frequency of ac field along with the precession time of

^{57}Fe nuclear spin. They indicated that a spin glass phase transition model is more appropriate than a superparamagnetic model for the description of magnetic behavior of this glass system since the hyperfine Mössbauer spectrum rapidly vanishes around spin freezing temperature with an increase in temperature. Sanchez *et al.* studied the temperature dependence of ac susceptibility and the ^{57}Fe Mössbauer spectrum for FeO-Al_2O_3-SiO_2 [14] and Li_2O-B_2O_3-Fe_2O_3 [15] glasses. They found that the empirical Vogel-Fulcher relation explain well the variation of spin freezing temperature with the observation time scale for the glasses for the glasses. Beauvillain *et al*. [16-18] performed the scaling analysis of the non-linear susceptibility for the MnO-Al_2O_3-SiO_2 system and obtained the critical exponents comparable to other spin glasses. They also analyzed the frequency dependence of peak temperature in ac magnetic susceptibility by using the Vogel-Fulcher relation for the glass system. These results suggest that the spin freezing is not explainable in terms of a simple superparamagnetism, but attributed to a spin glass transition. Wallance and coworkers [19,20] investigated the field and temperature dependence of specific heat for the CoO-Al_2O_3-SiO_2 and MnO-Al_2O_3-SiO_2 systems. Combined with the temperature dependence of dc susceptibility, the specific heat was analyzed on the basis of the scaling hypothesis. The critical exponents obtained by this analysis have approximately the same values as those yielded by the scaling analysis of nonlinear susceptibility. These results provide further credence to the phase transition picture.

The superexchange interactions between the rare-earth ions are much weaker than those between the 3*d* transition metal ions. While most oxide glasses bearing rare-earth ions remain paramagnetic even at low temperatures, random spin freezing was also reported for a few oxide glasses containing Ho^{3+} and Tb^{3+} [21,22]. In contrast to the glasses having 3*d* transition metal ions mentioned above, the frequency-dependent peak temperature in the magnetic susceptibility was explained well by the Arrhenius relation for the Ho_2O_3-Al_2O_3-B_2O_3 glass. This result indicates that the magnetic anomaly is not a spin glass transition but a simple superparamagnetic

blocking.

As mentioned above, magnetic oxide glasses often manifest spin freezing like those of spin glasses and superparamagnets at very low temperatures. On the other hand, 'ferromagnetic' behavior was found in amorphous oxides containing Fe_2O_3 such as Fe_2O_3-Bi_2O_3-ZnO [23], Fe_2O_3-Bi_2O_3-CaO [24,25], Fe_2O_3-Bi_2O_3-Li_2O [26,27], Fe_2O_3-Bi_2O_3-CuO [28], Fe_2O_3-SrO, and Fe_2O_3-Bi_2O_3 [29] systems in the late 1980's and early 1990's. The magnetization of these amorphous oxides was reported to be saturated under a magnetic field of several Teslas at room temperature. It should be noted that these iron-containing amorphous oxides do not exhibit any hyperfine sextet splitting in the ^{57}Fe Mössbauer spectra at room temperature, evidently suggesting that the ferromagnetic order does not extend over a long range, but is restricted within a localized region. Nakamura *et al*. [25] concluded that the ferromagnetic behavior in the Fe_2O_3-Bi_2O_3-CaO and Fe_2O_3-Bi_2O_3-Li_2O systems was attributed to some ferrimagnetic nanocrystalline phases embedded in the amorphous matrix, although the lattice images of the regions which they regarded as the nanocrystals in their transmission electron micrographs are not so clear. Coey *et al*. found ferromagnetic behavior of semiconducting amorphous iron gallium oxide films in which Fe^{2+} and Fe^{3+} ions coexist [30]. They suggested that the ferromagnetic interactions were caused by double-exchange interactions via hopping electrons between the Fe^{2+} and Fe^{3+} ions. The amorphous film had remanent magnetizations below 155 K. However, the hyperfine sextet splitting was not clearly observed in the ^{57}Fe Mössbauer spectra at 80 K, indicating that the film also demonstrated no long-range magnetic order. Also, they did not present the conclusive evidences for the existence of ferromagnetic interactions.

There is a rare case where ferromagnetic interactions are obviously predominant in oxide glasses. In 1979, Shoenes *et al*. reported a positive value of θ_W for the binary europium silicate glass in which Eu^{2+} ions account for 27 mol% of the whole cations [31]. This glass is a paramagnet with θ_W = +1 K, indicating that ferromagnetic

interactions prevail, and remains paramagnetic down to 1.5 K. The magnetic properties of Eu^{2+}-containing oxide glasses have not been investigated extensively since this fascinating discovery. The origin of the observed ferromagnetic interaction and the magnetic ground state remains to be clarified.

As described above, the amorphous oxide magnets exhibit diverse magnetic properties. The magnetic behavior is considered to depend on not only the sorts, concentrations, and distribution states of magnetic ions but the glass hosts. However, the magnetic properties of amorphous oxides have not been studied systematically at all. Especially, there is little investigation on the nature of low-temperature phases such as spin dynamics peculiar to the random magnets. Detailed investigations on magnetic properties of various oxide systems are required for the full understanding of the mechanism of magnetic transitions.

From the viewpoint of application of magnetic oxide glasses, magneto-optical properties such as the Faraday effect are of considerable importance. The Faraday rotation devices can be utilized as an optical isolator, an optical switch and an optical modulator. A great deal of attention has been paid to the Faraday effect of the glasses having a high concentration of 4*f* rare-earth ions such as Eu^{2+} and Tb^{3+} [32-36]. The glasses exhibit rather high transmittance and large Faraday effect in the visible to ultraviolet wavelength region. On the other hand, there are few reports on the Faraday effect of glasses containing 3*d* transition metal ions, because the glasses bearing only a few molar percents of these ions often have intense absorption in the visible range. The 3*d* transition metal ions such as iron ions are abundant in the earth. Hence, the investigation of magneto-optical properties of glasses containing 3*d* transition metal ions must be important, although the fabrication of relatively transparent glasses containing these ions is necessary.

Another example of random magnets is a spinel-type oxide with a random cation distribution. Zinc ferrite ($ZnFe_2O_4$) possesses a normal spinel structure as its stable phase, where Zn^{2+} and Fe^{3+} ions occupy the tetrahedral sites (A sites) and the

octahedral sites (B sites), respectively, in a face-centered-cubic close packing of oxide ions. While a normal spinel $ZnFe_2O_4$ behaves like an antiferromagnet with Néel temperature T_N = 13 K [37], a site-disordered $ZnFe_2O_4$ exhibits ferromagnetic behavior even at room temperature [38,39]. This is due to the formation of ferrimagnetic clusters by the strong antiferromagnetic superexchange interaction between the Fe ions in the A and B sites [40]. This type of random magnets is fascinating in that a disorder in the site occupation of cations leads to magnetic order even at higher temperatures.

This thesis deals with the magnetic properties of a series of random magnetic oxides including bulk oxide glasses, amorphous oxide thin films, and nanocrystalline oxide thin films from the viewpoint of fundamental interest as well as possibility of application.

Chapter 1 describes the magnetic properties of iron-based bulk oxide glasses. Section 1.1 reports the magnetic properties of binary Fe_2O_3-TeO_2 glasses. The present glasses exhibit a paramagnetic-spin glass transition at low temperatures. In particular, $20Fe_2O_3 \cdot 80TeO_2$ (mol%) glass shows a critical slowing down near the transition temperature and a slow spin dynamics such as magnetic aging and memory effects unique to spin glasses. Section 1.2 deals with the magnetic properties of glasses in FeO-Fe_2O_3-P_2O_5 system where Fe^{2+} and Fe^{3+} ions coexist. The molar ratio of Fe^{3+} to the total iron ions, $[Fe^{3+}]/[Fe_{total}]$, is controlled by melting the glass in a carbon crucible at various temperatures. These glasses also undergo paramagnetic-spin glass transitions at low temperatures as well as the Fe_2O_3-TeO_2 glasses. The magnetic frustration becomes relaxed with a decrease in $[Fe^{3+}]/[Fe_{total}]$. Section 1.3 shows the magnetic properties of Fe_2O_3-Bi_2O_3-B_2O_3 glasses, the composition of which is denoted by $x Fe_2O_3 \cdot (80.0\text{-}x)Bi_2O_3 \cdot 20.0B_2O_3$ in mol% ($18.2 \leq x \leq 40.0$). The glasses manifest complicated magnetic behavior explainable in terms of the coexistence of spin glass phase and magnetic clusters which exhibit superspin glass-like transition. The contribution of magnetic clusters to the magnetic properties becomes more significant

as the content of Fe_2O_3, x, is increased. Exchange bias effects have been examined in order to clarify the interaction between the spin glass phase and the magnetic clusters.

In Chapter 2, amorphous oxide thin films of Fe_2O_3-R_2O_3 (R = La, Gd and Tb) systems have been prepared by using a radio frequency sputtering method, and the magnetic properties of the thin films have been examined. It is revealed that the magnetic moments of iron ions take part in the formation of a spin glass state, as indicated by the magnetic aging effects, while those of rare-earth ions remain to be in a paramagnetic state even at very low temperatures.

Chapter 3 reports the fabrication of borate, aluminoborate, and aluminoborosilicate glasses containing a high concentration of Eu^{2+} ions and their magnetic properties. The Eu^{2+} ions interact with each other ferromagnetically, as indicated by the positive value of θ_W. A reentrant spin glass-like transition is demonstrated by the temperature dependence of ac and dc magnetic susceptibilities as well as specific heat.

Chapter 4 reports the magneto-optical properties of highly transparent iron phosphate glasses in which almost all the iron ions are present as Fe^{2+}. Large Faraday effect has been observed in the ultraviolet wavelength range due to the charge transfer transition from O^{2-} to Fe^{2+}.

Chapter 5 gives the structural and magnetic properties of sputtered $CdFe_2O_4$ thin films. The as-deposited film consists of $CdFe_2O_4$ nanocrystals with a random cation distribution, demonstrates magnetic transition like that of cluster-spin glass or superspin glass, and possesses large magnetization even at room temperature. The effect of annealing on the magnetic properties has been discussed in terms of the change of microstructure as well as chemical structure of the thin films.

Finally, the whole results and discussions are summarized in the last chapter.

References

[1] J. A. Mydosh, *Spin glasses: an Experimental Introduction* (Taylor &Francis Ltd., London, 1993).

[2] J. B. Goodenough, *Phys. Rev.* **100**, 564 (1955).

[3] J. Kanamori, *J. Phys. Chem. Solids* **10**, 87 (1959).

[4] F. A. Wedgwood and A. C. Wright, *J. Non-Cryst. Solids* **21**, 95 (1976).

[5] R. A. Verhelst, R. W. Kline, A. M. de Graaf, and H. O. Hooper, *Phys. Rev. B* **11**, 4427 (1975).

[6] J. Ferre, J. Pommier, J. P. Renard, and K. Knorr, *J. Phys. C: Solid State phys.* **13**, 3697 (1980).

[7] A. Ito, E. Torikai, H. Yamauchi, and Y. Syono, *J. Phys. C: Solid State phys.* **15**, 2759 (1982).

[8] J. L. Shaw, A. C. Wright, R. N. Sinclair, G. K. Marasinghe, D. Holland, M. R. Lees, and C. R. Scales, *J. Non-Cryst. Solids* **345&346**, 245 (2004).

[9] T. J. Moran, N. K. Batra, R. A. Verhelst, and A. M. de Graaf, *Phys. Rev. B* **11**, 4436 (1975).

[10] H. R. Rechenberg, L. H. Bieman, F. S. Huang, and A. M. de Graaf, *J. Appl. Phys.* **49**, 1638 (1978).

[11] F. S. Huang, L. H. Bieman, A. M. de Graaf, and H. R. Rechenberg, *J. Phys. C: Solid State phys.* **11**, L271 (1978).

[12] L. E. Wenger and P. H. Keesom, in: Amorphous Magnetism II, eds. Levy and Hasegawa (Plenum, New York, 1977)

[13] L. H. Bieman, P. F. Kenealy, and A. M. de Graaf, in: Amorphous Magnetism II, eds. Levy and Hasegawa (Plenum, New York, 1977)

[14] J. P. Sanchez, J. M. Friedt, R. Horne, and A. J. Van Duyneveldt, *J. Phys. C* **17**, 127 (1984).

[15] J. P. Sanchez and J. M. Friedt, *J. Physique* **43**, 1707 (1982).

[16] P. Beauvillain, C. Dupas, J. P. Renard, and P. Veillet, *J. Magn. Magn. Mater.* **31-34**, 1377 (1983).

[17] P. Beauvillain, C. Dupas, J. P. Renard, and P. Veillet, *Phys. Rev. B* **29**, 4086 (1984).

[18] P. Beauvillain, C. Chappert, J. P. Renard, and J. Seiden, *J. Magn. Magn. Mater.* **54-57**, 127 (1986).

[19] W. D. Wallance, G. W. Hunter, and L. E. Wenger, *J. Appl. Phys.* **61**, 3630 (1987).

[20] G. W. Hunter, L. E. Wenger, and W. D. Wallance, *Phys. Rev. B* **36**, 5750 (1987).

[21] C. Chappert, P. Beauvillain, J. P. Renerd, and K. Knorr, *Solid State Commun.* **31**, 213 (1979).

[22] K. Sato, K. Yamaguchi, F. Maruyama, and N. Nishi, *Phys. Rev. B* **63**, 104416 (2001).

[23] N. Ota, M. Okubo, S. Matsuda, and K. Suzuki, *J. Magn. Magn. Mater.* **54-57**, 293 (1986).

[24] S. Nakamura and N. Ichinose, *J. Non-Cryst. Solids* **95&96**, 849 (1987).

[25] S. Nakamura, Y. Hirotsu and N. Ichinose, *Jpn. J. Appl. Phys*. **30**, L844 (1991).

[26] S. Nakamura and N. Ichinose, *Jpn. J. Appl. Phys*. **28**, 984 (1989).

[27] J. Chen, S. Cheney and G. Srinivasan, *J. Appl. Phys*. **75**, 6828 (1994).

[28] S. Soeya, S. Nakamura and N. Ichinose, *J. Appl. Phys*. **68**, 2875 (1990).

[29] K. Tanaka, K. Hirao, and N. Soga, *J. Appl. Phys*. **69**, 7752 (1991).

[30] J. M. D. Coey, E. Devlin, and R. J. Gambino, *J. Appl. Phys*. **53**, 7810 (1982).

[31] J. Shoenes, E. Kaldis, W. Thöni, and P. Wachter, *Phys. Stat. Sol.* **51**, 173 (1979).

[32] N. F. Borrelli, *J. Chem. Phys.* **41** 3289 (1964).

[33] K. Tanaka, K. Hirao and N. Soga, *Jpn. J. Appl. Phys.* **34**, 4825 (1995).

[34] K. Tanaka, K. Fujita, N. Soga, J. Qiu and K. Hirao, *J. Appl. Phys.* **83**, 840 (1997).

[35] K. Tanaka, K. Fujita, N. Matsuoka, K. Hirao and N. Soga, *J. Mater. Res.* **13**, 1989 (1998).

[36] T. Hayakawa, M. Nogami, N. Nishi and N. Sawanobori, *Chem. Mater.* **14**, 3223

(2002).

[37] K. Kamazawa, Y. Tsunoda, H. Kadowaki, and K. Kohn, *Phy. Rev. B* **68**, 024412 (2003).

[38] K. Tanaka, S. Nakashima, K. Fujita, and K. Hirao, *J. Phys*.: *Condens*. *Matter* **15**, L469 (2003).

[39] S. Nakashima, K. Fujita, K. Tanaka and K. Hirao, *J. Phys*.: *Condens*. *Matter* **17**, 137 (2005).

[40] S. Nakashima, K. Fujita, K. Tanaka, K. Hirao, T. Yamamoto and I. Tanaka, *Phy. Rev. B* **75**, 174443 (2007).

CHAPTER 1: Magnetic properties of iron-containing oxide glasses

Section 1.1 Spin dynamics in Fe_2O_3-TeO_2 system

1.1.1 Introduction

Spin glasses have attracted considerable attention as a prototype of many-body cooperative phenomena since Cannella and Mydosh [1] observed a magnetic anomaly in the temperature dependence of susceptibility for binary *Au*Fe alloys with very low concentrations of Fe. In such a canonical spin glass, the magnetic moments are frozen in the random direction via Ruderman-Kittel-Kasuya-Yoshida interaction via a conduction electron, by which the spin pairs couple ferromagnetically or antiferromagnetically depending on the distance between the spins [2]. Edwards and Anderson [3] suggested a simplified theoretical model of spin glass where the nearest neighboring spins have interactions with the signs distributed randomly from pair to pair, and defined an order parameter of spin glass as follows:

$$q(t_1, t_2) = \overline{\langle S_i(t_1) S_i(t_2) \rangle}, \qquad (1.1)$$

where the angle brackets denote the thermal average and the bar denotes the spatial average over the spins. Their theory implies that the components characteristic to spin glass are summarized as randomness and frustration. Later, Sherrington and Kirkpatrick [4] developed a mean field theory for an infinite-range model of spin glass, where the signs of interactions for all spin pairs have a gaussian distribution, so as to indicate the existence of multi-valley landscape for the free energy of the system. Recently, the systematic and precise mathematical analysis for spin glass has been extended beyond the framework of the original aim, i.e., the clarification of the magnetism of spin glass. The recent theoretical studies of spin glass have established a new physical picture and concept for random systems with competing interactions

such as neural network and optimization problems [5]. On the other hand, the search for spin glass materials has been also performed for various random magnets. Consequently, spin glass behavior has been found not only in alloys but also in insulators: $Eu_xSr_{1-x}S$ (3D Heisenberg) [6], $Fe_xMn_{1-x}TiO_3$ (3D Ising) [7] and so forth.

Magnetic oxide glasses, where the magnetic cations are randomly distributed in the glass matrix, are one of typical random magnets. In most of magnetic oxide glasses, antiferromagnetic superexchange interactions between magnetic ions via oxide ions are prevailing. Due to the structural randomness, the magnetic oxide glasses can not achieve the arrangement of magnetic moments where all pairs are antiferromagnetically coupled: the systems are magnetically frustrated. So, magnetic oxide glasses satisfy the condition necessary for the occurrence of spin glass transition. Actually, random freezing phenomena of magnetic moments have been reported for some oxide glasses with a high concentration of magnetic ions [8-15]. Since the first observation of spin freezing in oxide glasses by Verhelst *et al*. [8], extensive experimental investigations have been made in order to clarify the mechanism of the spin freezing. The observed anomalies have been explained in terms of either a spin glass transition or a blocking of superparamagnet [8-15].

On the other hand, recently, a great deal of attention has been paid to the spin dynamics in spin glasses, superparamagnets, and other related random magnets [16-39]. In particular, spin glasses exhibit unique slow spin dynamics including magnetic aging effects [16-29]. Intriguing phenomena such as temperature chaos and rejuvenation effects have been discovered experimentally [16-29], and interpreted in terms of both the droplet model [30-32] and the hierarchical energy model [33]. Superparamagnets also exhibit a slow dynamics below the blocking temperature. However, the spin dynamics in spin glasses and superparamagnets is quite different from each other [16]. Owing to the development of procedures for detecting magnetic aging effects, the investigation of spin dynamics is becoming one of the experimental ways of distinguishing spin glasses from superparamagnets [16-18]. Also, spin glasses show

the divergence of relaxation time near the transition temperature, i.e., critical slowing down [34-36] in contrast to superparamagnets [37]. Hence, the analysis of critical slowing down is also very useful for differentiating spin glasses from superparamagnets.

This section deals with the fundamental structural and magnetic properties of the Fe_2O_3-TeO_2 glass system, and examine a spin dynamics including magnetic aging and memory effects as well as critical slowing down for the $20Fe_2O_3 \cdot 80TeO_2$ (mol%) glass. The temperature-dependent magnetic susceptibilities of the present glasses exhibit similar behavior to those found in spin glasses at low temperatures. The temperature and field dependence of nonlinear susceptibility near the spin freezing temperature are analyzed on the basis of the scaling hypothesis. The critical exponents obtained by this analysis are similar to those of other spin glasses. A dynamical scaling analysis of relaxation time reveals that the $20Fe_2O_3 \cdot 80TeO_2$ (mol%) glass exhibits a critical slowing down around the spin freezing temperature as observed in prototype of spin glasses. The magnetic aging and memory effects peculiar to spin glasses have been observed below the spin freezing temperature. These experimental results strongly confirm that the present glasses form a spin glass phase at low temperatures.

1.1.2 Experimental procedure

Glasses with a nominal composition of $x Fe_2O_3 \cdot (100-x)TeO_2$ (mol%) (x=10, 15, and 20) were prepared by using a conventional melt-quenching method. Fe_2O_3 and TeO_2 were used as starting materials. The raw materials were mixed thoroughly and melted in a platinum crucible at 1000°C for 1-2 h, and then the melt was poured onto a stainless steel plate and cooled in air. X-ray diffraction analysis with CuK_α radiation was carried out to confirm that the sample was amorphous. ^{57}Fe Mössbauer spectroscopy was performed at room temperature to elucidate the chemical state of iron

ions. As a γ-ray source, 10 mCi ^{57}Co in metallic Rh was used. Calibration of Doppler velocity and estimation of isomer shift were made by using a spectrum of α-Fe foil at room temperature. The glass samples were subjected to measurements of magnetic properties such as dc and ac susceptibilities by using a SQUID magnetometer (Quantum Design MPMS).

1.1.3 Results and discussions

1.1.3.1 ^{57}Fe Mössbauer spectroscopy

The Mössbauer spectra for Fe_2O_3-TeO_2 glasses with 10, 15, and 20 mol% of Fe_2O_3 are illustrated in Fig. 1.1. All the spectra manifest a paramagnetic doublet attributable to Fe^{3+} ion: absorption peaks ascribable to Fe^{2+} ion are not observed in all the spectra. Table 1.1 summarizes the values of isomer shift (IS) and quadrupole splitting (QS) for these glasses. The values of isomer shift, larger than 0.35 mm/s, indicate that most of the Fe^{3+} ions occupy octahedral sites surrounded by six oxide ions [40] in these tellurite glasses. These results are consistent with those of Fe_2O_3-TeO_2 glasses prepared by a rapidly quenching method with a twin-roller [41].

1.1.3.2 The temperature dependence of dc magnetic susceptibility

Figure 1.2(a) and (b) shows the temperature variation of dc susceptibility $\chi(T)$ for the present glasses. The susceptibility measurements for both field cooling (FC) and zero field cooling (ZFC) were performed for all the specimens with a magnetic field of 50 Oe. The $\chi(T)$ curves obtained under conditions of FC and ZFC are different from each other below the spin-freezing temperature, T_f, at which $\chi(T)$ for ZFC manifests a maximum. The $\chi(T)$ curve obtained under the ZFC condition demonstrates a sharp cusp at T_f, and that under FC is apt to become constant below T_f. These phenomena are very similar to those of conventional spin glasses of alloys and oxide crystals

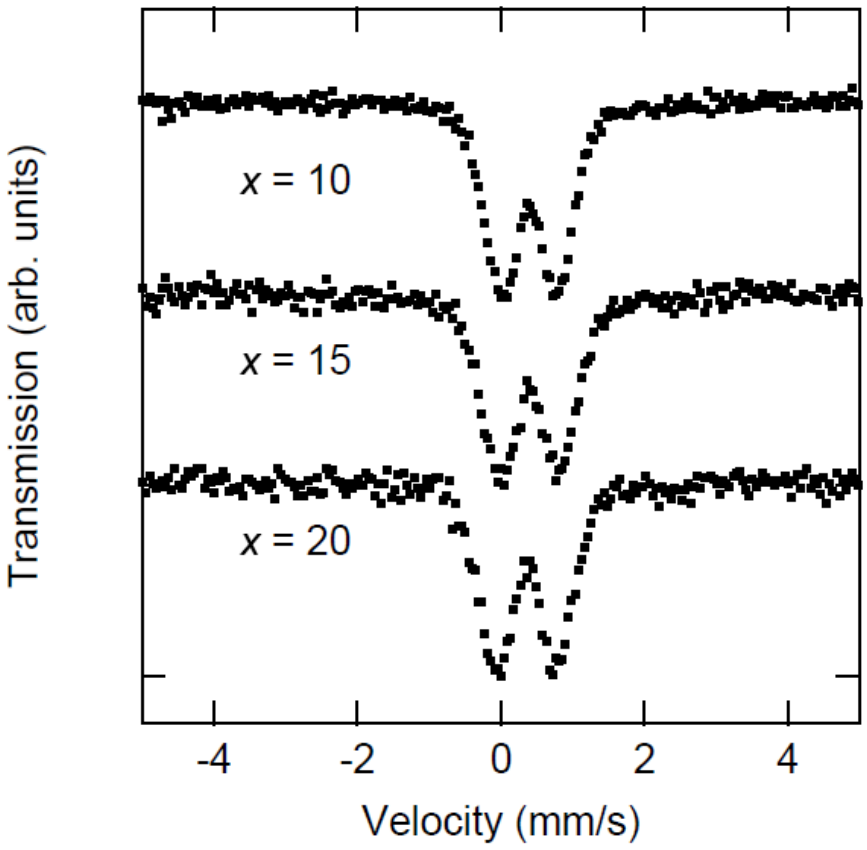

Figure 1.1: ^{57}Fe Mössbauer spectra for the xFe$_2$O$_3$·(100-x)TeO$_2$ glasses with x=10, 15, and 20 at room temperature.

Table 1.1: Mössbauer parameters: Isomer shift (IS) and Quadrupole splitting (QS), and magnetic parameters: spin-freezing temperature (T_f), Weiss temperature (θ_W), and effective number of Bohr magnetons (M_B) for the Fe_2O_3-TeO_2 glasses.

x	IS (mm/s)	QS (mm/s)	T_f (K)	θ_W (K)	M_B
10	0.40	0.77	3.5	-57	6.0
15	0.40	0.83	7.3	-111	6.0
20	0.36	0.84	8.9	-142	5.5

[17,19,42]. Table 1.1 gives the values of T_f for the present glasses. The value of T_f is higher with an increase in the Fe_2O_3 content.

Figure 1.3 depicts the inverse dc susceptibility as a function of temperature, $\chi^{-1}(T)$, for the present glasses. All the glasses manifest a linear relation at high temperatures, suggesting that these glasses are paramagnetic at high temperatures like room temperature. These results are in agreement with the room temperature Mössbauer spectra illustrated in Fig. 1.1. In other words, $\chi^{-1}(T)$ at high temperatures for these glasses is describable in terms of the following Curie-Weiss law:

$$\chi^{-1} = \frac{3k_B(T-\theta_W)}{NM_B{}^2\mu_B{}^2}, \qquad (1.2)$$

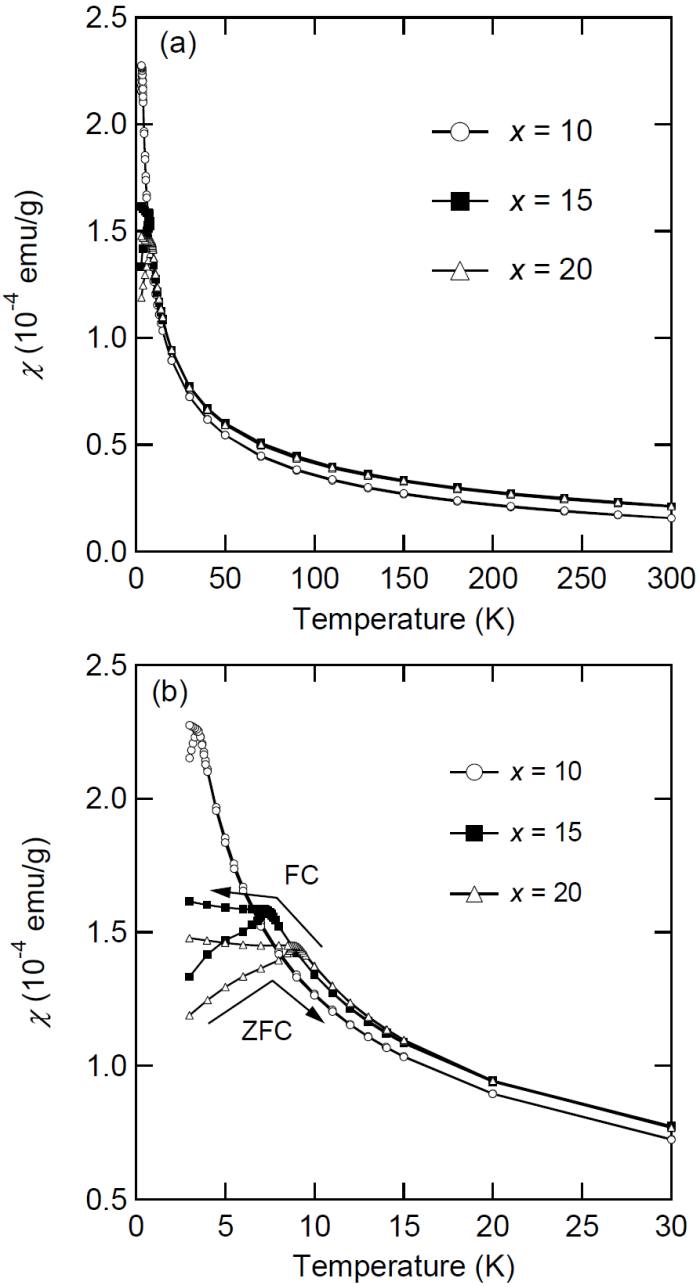

Figure 1.2: Temperature dependence of dc susceptibility for the xFe$_2$O$_3$·(100-x)TeO$_2$ glasses with x=10 (open circles), 15 (closed squares), and 20 mol% (open triangles) in the temperature range of (a) 0 to 300 K and (b) 0 to 30 K. FC and ZFC denote field cooling and zero field cooling, respectively.

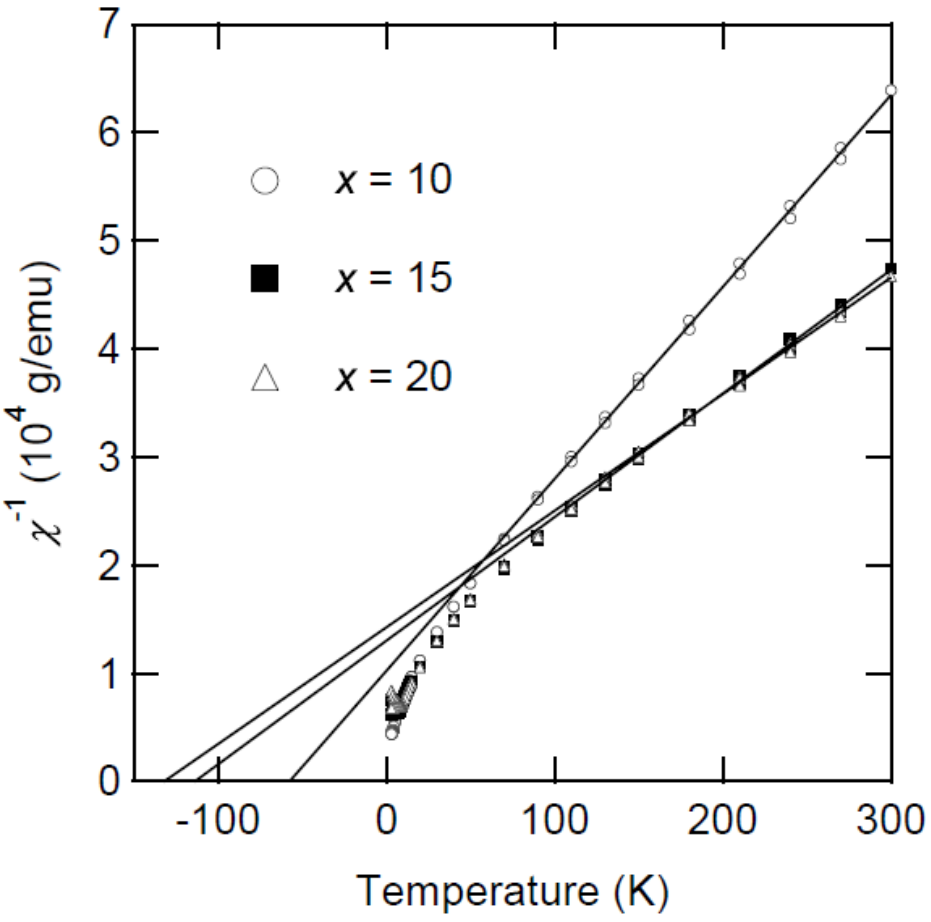

Figure 1.3: Temperature dependence of inverse dc susceptibility for the xFe$_2$O$_3$·(100-x)TeO$_2$ glasses with x=10 (open circles), 15 (closed squares), and 20 mol% (open triangles). The solid lines are obtained by fitting Eq. (1.2) to the experimental data at high temperatures.

where θ_W is the Weiss temperature, N the number of magnetic ions per unit mass, M_B the effective number of Bohr magnetons, μ_B the Bohr magneton, and k_B the Boltzmann constant. By fitting Eq. (1.2) to the experimental data at high temperatures, the θ_W and M_B were evaluated and summarized in Table 1.1. From Table 1.1, some characteristics relevant to magnetism for the present glasses can be derived. The values of effective number of Bohr magnetons for the present glasses, i.e., 5.5-6.0, are very similar to that for theoretical spin-only value of Fe^{3+}, i.e., 5.92. This is coincident with the result of Mössbauer measurements [see Fig. 1.1]. The value of θ_W is negative for all the present glasses. This fact indicates that the superexchange interaction among magnetic ions is antiferromagnetic in these glasses. Here, it is worth noticing the ratio of the absolute value of θ_W to T_f, f, which is an empirical measure of magnetic frustration as discussed for a number of geometrically frustrated magnets [43]. For the present glasses, the value of f is found to be 15 to 16. The fact the value of f is large enough compared to unity indicates that magnetic frustration is inherent in the present glasses. Almost all the geometrical frustrated magnets with the value of $f > 10$ contain highly isotropic ions such as S-state ions like Fe^{3+} and Mn^{2+} as well as transition metal ions with fully quenched orbital moments like Cr^{3+} [43,44]. A close look at Fig. 1.3 reveals that the $\chi^{-1}(T)$ curve deviates from the Curie-Weiss law far above T_f. For instance, for the $20Fe_2O_3 \cdot 80TeO_2$ glass, the deviation takes place below about 70 K. A similar phenomenon was reported for other oxide glasses containing transition metal ions [8,9]. This fact implies that the short-range magnetic correlation emerges even at the temperature one order of magnitude higher than T_f, and the correlation range spreads with a decrease in temperature.

1.1.3.3 The magnetic field dependence of dc magnetization

Figure 1.4 shows the dependence of magnetization on magnetic field, $M(H)$, for the $20Fe_2O_3 \cdot 80TeO_2$ glass at varied temperatures. The measurement temperatures are 3 K (open circles), 15 (closed triangles), and 300 (closed squares). The main panel

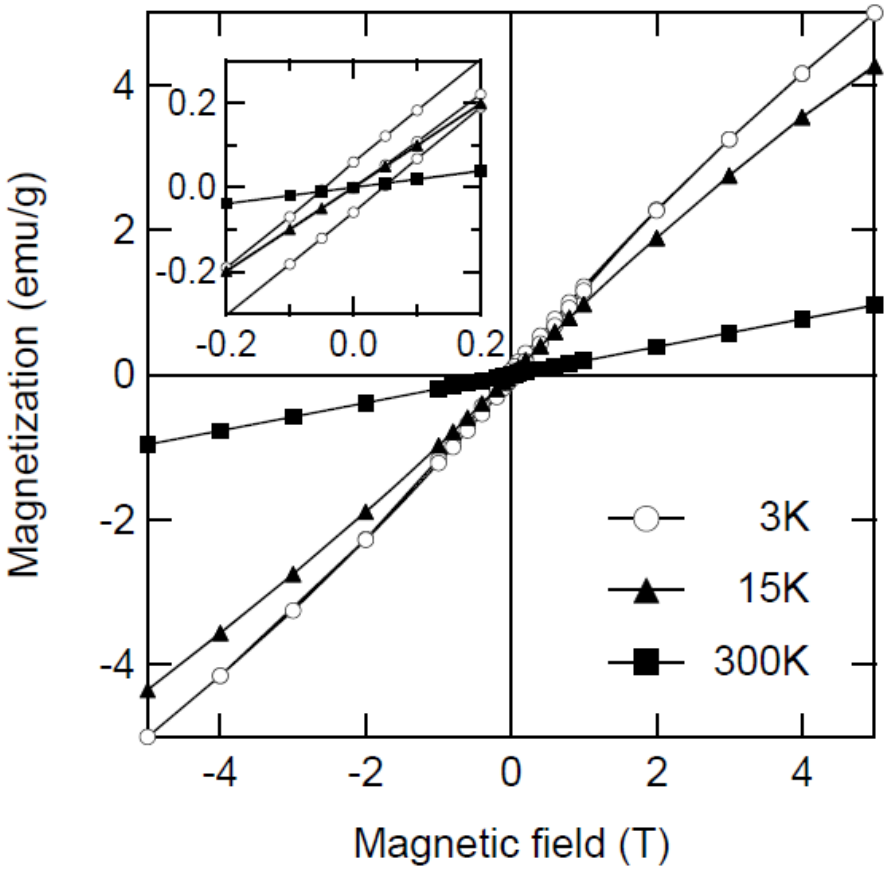

Figure 1.4: Variation of magnetization with magnetic field for the $20Fe_2O_3{\cdot}80TeO_2$ glass at 3 (open circles), 15 (closed triangles), and 300 K (closed squares). The inset displays a restricted range of magnetic field.

and inset of Fig. 1.4 correspond to a range of magnetic field of -5 to 5 T and -0.2 to 0.2 T, respectively. In Fig. 1.4, $M(H)$ is proportional to the magnetic field within the given range of magnetic field at 300 K, indicating that the glass is paramagnetic at this temperature. On the other hand, the behavior of $M(H)$ deviates from the linearity at 3 K. Besides, it is found from the inset that the $M(H)$ curve at 3 K manifests a magnetic hysteresis loop. This clearly indicates that some magnetic order is present at 3 K in this glass. The inset also shows that the $M(H)$ curve is not linear at 15 K. The temperature of 15 K is higher than the spin-freezing temperature, but the deviation from Curie-Weiss law is observed at this temperature as mentioned above. Hence, the nonlinear $M(H)$ curve at 15 K can be explained by the emergence of the short-range antiferromagnetic correlation.

1.1.3.4 Scaling analysis of nonlinear magnetic susceptibility

The static nonlinear susceptibility measurements have been carried out for the $20Fe_2O_3{\cdot}80TeO_2$ glass in order to reinforce the presumption of spin glass transition. M. Suzuki *et al*. extended the Landau-type phenomenological of second phase transition so as to predict the scaling relation of nonlinear term of magnetic susceptibility for spin glasses[45]. The static nonlinear susceptibility $\chi_{NL}(T, H)$ is defined as follows:

$$\chi_{NL}(T, H) = M(T, H)/H - \chi_0(T) = -\chi_2(T)H^2 + \chi_4(T)H^4 - \ldots . \quad (1.3)$$

The scaling methods, which have been developed earlier for empirical description of paramagnetic-ferromagnetic transition, provide the scaling relation as follows:

$$\chi_{NL} = -t^{\beta}\Phi\left(\frac{H^2}{t^{\beta+\gamma}}\right), \qquad (1.4)$$

where $t = (T-T_c)/T_c$ is the reduced temperature, β and γ the critical exponents of the spin glass order parameter and the coefficient χ_2 [45], and $\Phi(x)$ the appropriate scaling function. The analysis is based on the data concerning the temperature dependence of

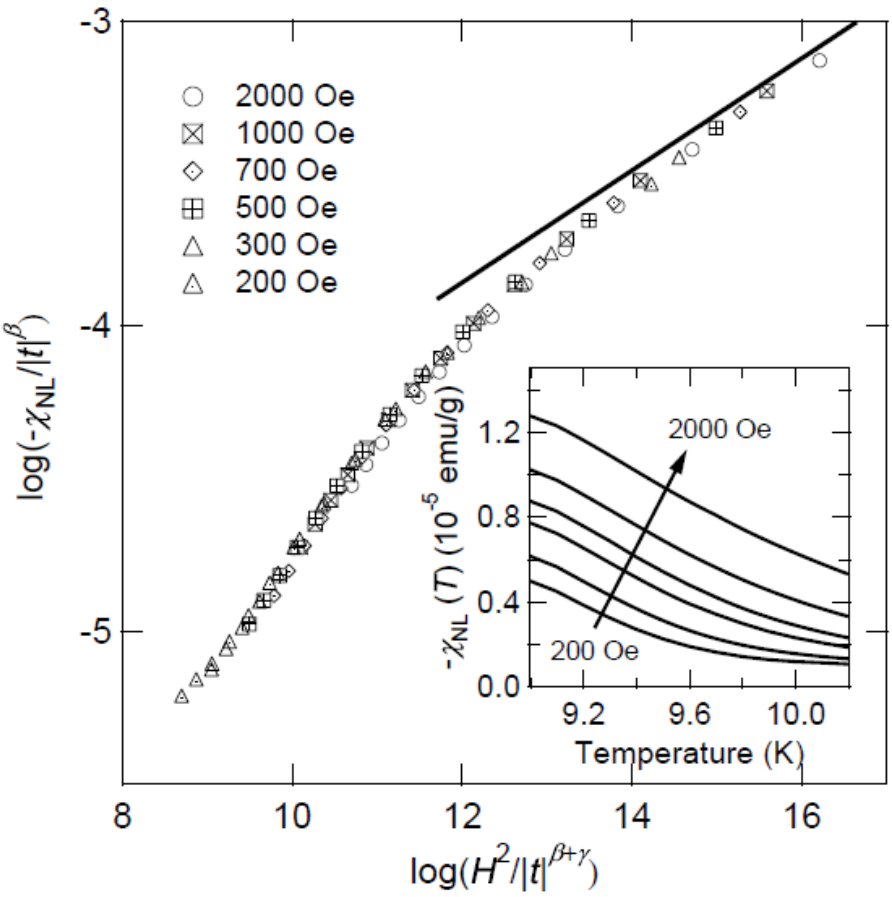

Figure 1.5: Nonlinear susceptibility $\chi_{NL}(T, H)$ for the $20Fe_2O_3 \cdot 80TeO_2$ glass analyzed according to the universal scaling relation of Eq. (1.4). A single curve is yielded by plotting with T_c = 8.9 K, β=0.9 and γ=4.0. The solid line represents the asymptotic limit of the experimental data to the $\beta/(\beta+\gamma)$ value for $T \rightarrow T_f$. The inset shows $\chi_{NL}(T, H)$ as a function of T.

Table 1.2: Critical temperature, T_c, and exponents, β and γ, yielded by scaling analysis of nonlinear susceptibility for some spin glasses.

	T_c/K	β	γ	Reference
*Cu*Mn (4.6 at%)	26.25	1.2	3.4	46
*Cu*Mn (1 at%)	10.05	0.7	3.3	10
*Cu*Mn (0.25 at%)	3.53	1	3.5	10
amorphous *Al*Gd (37 at%)	15.75	0.93	2.7	47
amorphous $Al_2Mn_3Si_3O_{12}$	2.95	1.4	3.4	10,11
$Zn_{0.1}Mn_{0.9}In_2Te_4$	3.4	0.9	3.6	48
$Zn_{0.49}Mn_{0.51}Te$	20.8	0.8	4	49
$Cd_{0.6}Mn_{0.4}Te$	12.37	0.9	3.3	50

FC magnetization measured at various magnetic fields. The temperature dependence of $\chi_{NL}(T, H)$ for the $20Fe_2O_3 \cdot 80TeO_2$ glass measured at varied magnetic fields is shown in the inset of Fig. 1.5, where $\chi_0(T)$ is taken as the dc susceptibility measured at the smallest dc magnetic field in this experiment, i.e., 20 Oe. Figure 1.5 shows the best log-log plot in the temperature region of $T > T_f$ with T_c = 8.9(1) K, β=0.9(1) and γ=4.0(2). The universal scaling curve covers several orders of magnitude along both vertical and horizontal axes. Table 1.2 summarizes the critical temperature and exponents reported for some spin glass materials. The critical exponents obtained for the present glass are in good agreement with those reported for other spin glasses. As T approaches T_c from the higher temperature region (top right part of the curve), the slope tends to be the proper asymptotic value $\beta/(\beta+\gamma)$ [11,48-50]. The static scaling analysis of nonlinear susceptibility gives credence for the spin glass transition picture in the present glasses.

1.1.3.5 Dynamical scaling analysis

Figure 1.6 illustrates the temperature dependence of real part of ac susceptibility obtained by zero-field cooling for the $20Fe_2O_3 \cdot 80TeO_2$ glass. The amplitude of ac magnetic field was kept to be 3 Oe. The ac frequency was varied from 0.1 to 1000 Hz. The spin-freezing temperature $T_f(f)$ dependent on frequency f can be defined as a temperature at which the real part of ac susceptibility $\chi'(T, f)$ manifests a maximum. In other words, the maximum relaxation time of the system τ is equal to $1/f$ at $T_f(f)$. Although $T_f(f)$ is often taken as a temperature at which $\chi'(T, f)$ is 0.98 times the equilibrium susceptibility [34], it is reasonable to define $T_f(f)$ as a temperature of maximum susceptibility in $\chi'(T, f)$ curve for dynamical scaling analysis as demonstrated previously [34-36]. In Fig. 1.6, $T_f(f)$ increases with an increase in f ; τ becomes longer as the temperature is lowered. According to the dynamic scaling hypothesis, provided that this system exhibits a conventional critical slowing down toward the transition temperature T_c, the variation of maximum relaxation time with transition temperature is described by

$$\tau = \tau_0 \left(\frac{T_f(f) - T_c}{T_c} \right)^{-z\nu}, \qquad (1.5)$$

where τ_0 is a microscopic relaxation time, and z and ν are the dynamic critical exponents concerned with the following relationship:

$$\tau \propto \xi^z \quad (1.6) \qquad \textit{and} \qquad \xi \propto \left(\frac{T - T_c}{T_c} \right)^{-\nu}, \quad (1.7)$$

where ζ is the correlation length scale. In the present case, the best fitting of Eq. (1.5) to the experimental data yields $z\nu$=10, T_c=8.8 K, and τ_0=10^{-13} s, as shown in the inset of Fig. 1.6. The dynamical critical exponents reported for some spin glass materials are summarized in Table 1.3. The values of $z\nu$=10 is in good agreement with those reported for various type of spin glasses. In particular, the value of τ_0=10^{-13} s is

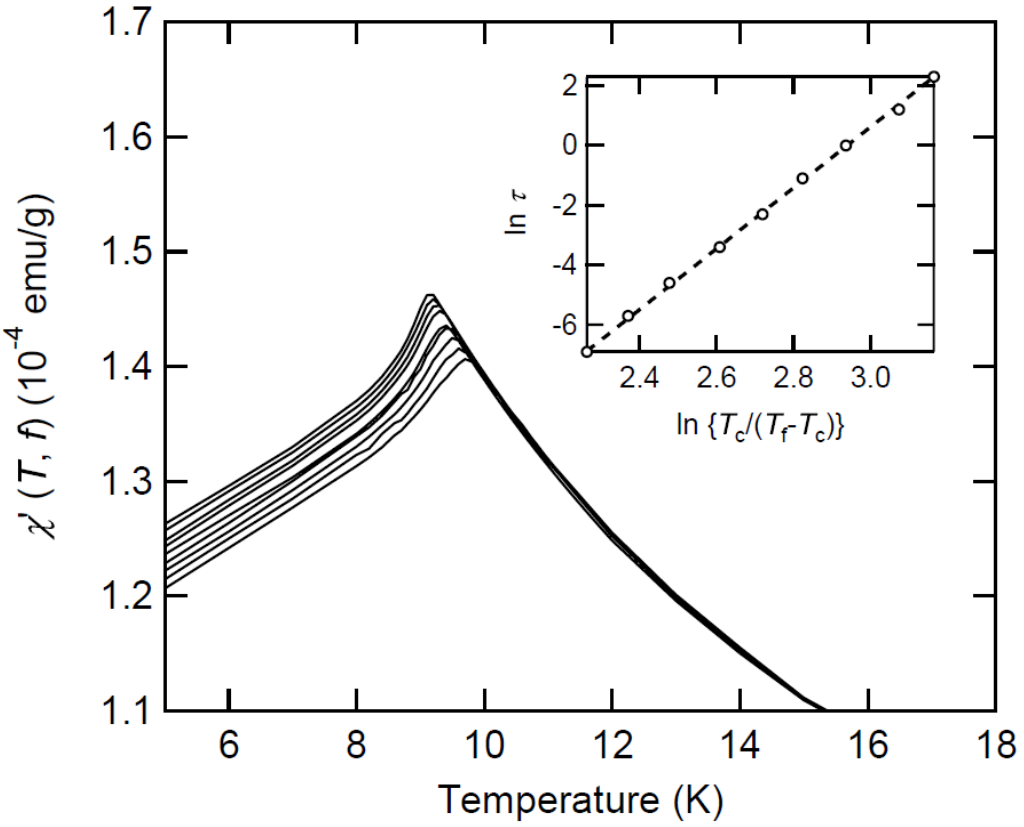

Figure 1.6: Temperature dependence of the real part of ac susceptibility for the $20Fe_2O_3 \cdot 80TeO_2$ glass. The frequency f is 0.1, 0.3, 1, 3, 10, 30, 100, 300, and 1000 Hz (from top to bottom). The inset illustrates the relationship between maximum relaxation time τ and spin-freezing temperature $T_f(T,f)$ in critical slowing down analysis. The broken line demonstrates the fit of the experimental data to Eq. (1.5).

Table 1.3: Critical temperature T_c, microscopic relaxation time τ_0, and dynamical critical exponent zv obtained by the dynamical scaling analysis for some spin glasses.

	T_c/K	τ_0/s	zv	Reference
$Eu_{0.4}Sr_{0.6}S$	1.48	5.2×10^{-11}	9.4	51
*Pt*Mn (5 at%)	7.7	3.9×10^{-9}	4.2	51
AuMn (8 at%)	17.9	0.6×10^{-15}	10.2	51
CuMn (4.6 at%)	27.45	7.7×10^{-13}	5.5	51
amorphous $Al_2Mn_3Si_3O_{12}$	3	1×10^{-14}	8.9	10, 51
$Zn_{0.1}Mn_{0.9}In_2Te_4$	3.1	5.6×10^{-10}	10.3	48

identical in magnitude with those for atomic spin glasses, for which τ_0 denotes a spin flip time of individual magnetic moments belonging to atoms or ions [20,34]. In contrast, it has been observed that τ_0~10^{-6} s for interacting magnetic nanoparticles systems or super spin glasses, for which τ_0 corresponds to the time scale of reversal of superparamagnetic magnetizations [34,35]. The critical temperature is in good agreement with that obtained by the static scaling analysis. The results of this analysis imply that a magnetic transition takes place from paramagnetic phase to atomic spin glass phase in the present oxide glass of Fe_2O_3-TeO_2 system.

The temperature dependence of relaxation time is also fitted well by the Voger-Fulcher law:

$$\tau = \tau_0 \exp\left(\frac{E_a}{k_B(T - T_0)}\right), \qquad (1.8)$$

where E_a and T_0 are the fitting parameters concerned with energy and temperature, respectively. The Voger-Fulcher law has been utilized to analyze the frequency dependence of spin freezing temperature for some magnetic oxide glasses [10,12,13]. A strong motivation in using this empirical law is that the failure of the Arrhenius law in providing an acceptable magnitude of τ_0 can be compensated by using the additional parameter T_0 [51]. Some attempts have been made to relate the parameter to a physically meaning one such as a true transition temperature and a measure of inter-cluster interactions from a viewpoint of cooperative phenomena [52,53]. However, the author does not discuss the validness of the fitting by the Voger-Fulcher law and examine the value of the parameters, because a deep understanding of the parameters is lacking.

1.1.3.6 Magnetic aging and memory effects

In order to discuss magnetic aging effects in the magnetically ordered phase of the $20Fe_2O_3{\cdot}80TeO_2$ glass, the temperature dependence of dc susceptibility $\chi(T)$ was inspected by utilizing a protocol of zero-field cooling memory experiment proposed by Mathieu *et al* [17]. In this protocol, $\chi(T)$ is measured on heating after zero-field cooling with an intermittent stop at a temperature below the transition temperature. Figure 1.7 illustrates the schematic procedure of this experiment. In the present case, the glass was cooled from a temperature well above T_c=8.8 K to a stopping temperature T_s, which was lower than T_c, at a rate of 0.2 K/min, and was kept at T_s for 3 h. Here, T_s was selected to be 7, 6, and 5 K. After a stop for 3 h, the glass was recooled to 3 K

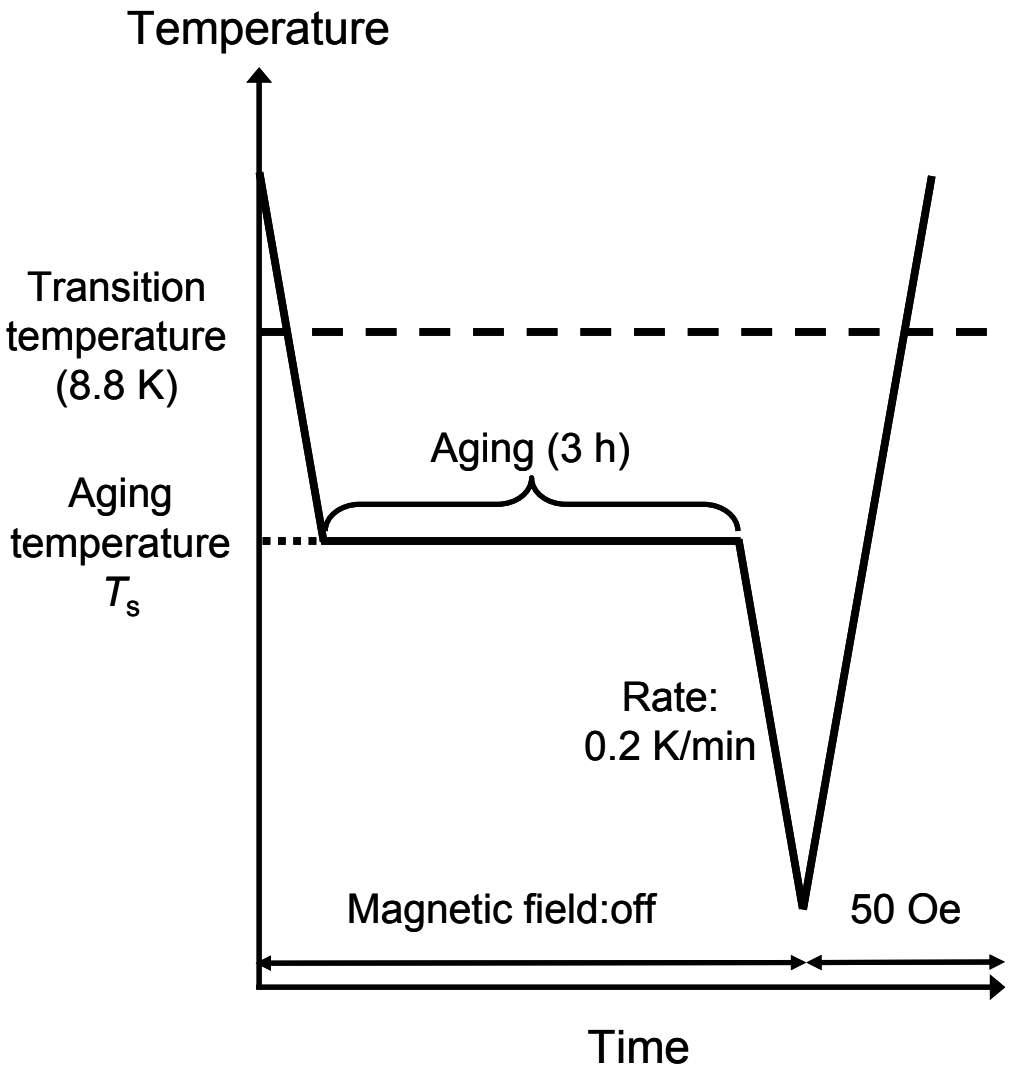

Figure 1.7: Schematic procedure of the zero-field cooling memory experiment proposed by Mathieu *et al*.

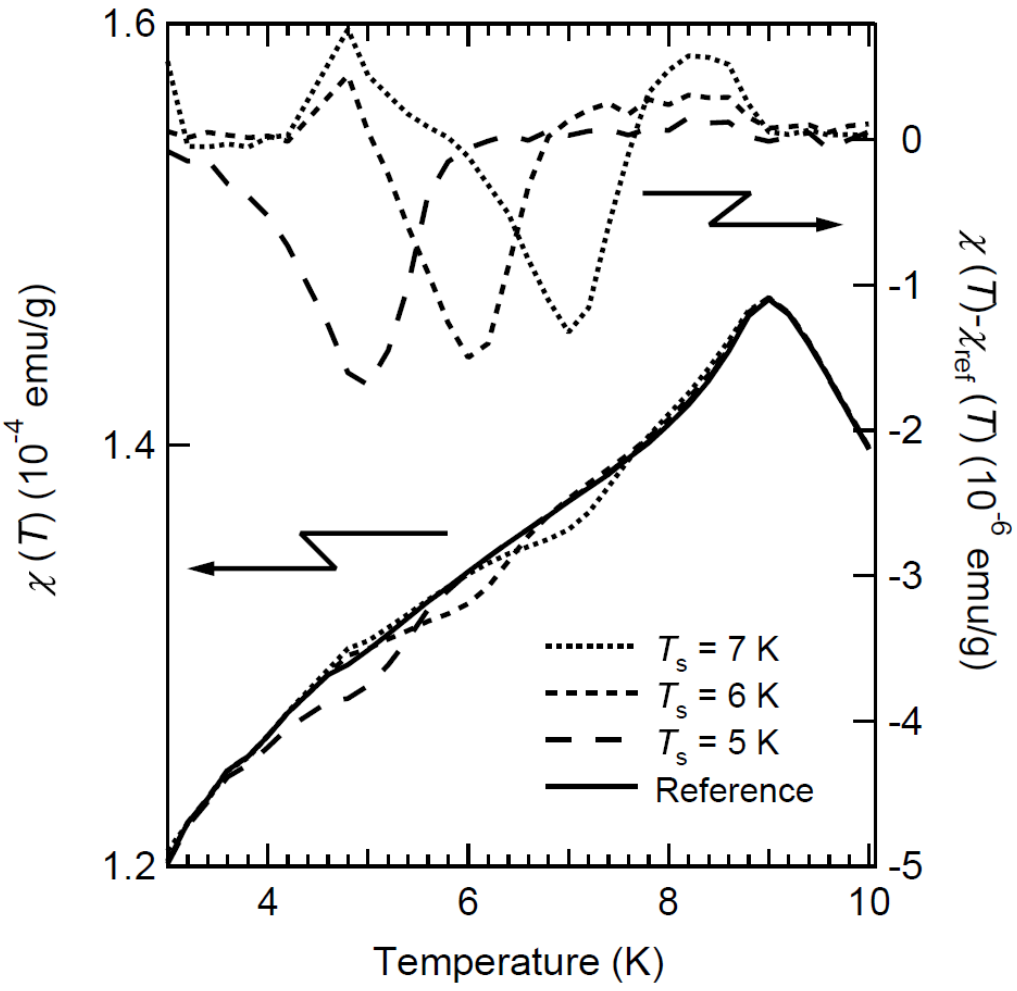

Figure 1.8: Temperature dependence of dc susceptibility measured on heating after zero-field cooling with and without an intermittent stop at T_s. The difference between $\chi(T)$ and $\chi_{ref}(T)$ is illustrated as well.

at a rate of 0.2 K/min. Subsequently, a magnetic field of 50 Oe was applied and $\chi(T)$ was measured on heating at a rate of 0.2 K/min. As a reference, $\chi_{ref}(T)$ was determined by measuring the temperature dependence of zero-field cooled susceptibility without any intermittent stops. The results thus obtained are shown in Fig. 1.8. The $\chi(T)$ curves involving a stop coincide with the $\chi_{ref}(T)$ curve in a temperature range well below T_s. In contrast, the $\chi(T)$ curves deviate downward from the $\chi_{ref}(T)$ curve as the temperature approaches T_s. As the temperature increases in a range above T_s, the $\chi(T)$ curves gradually merge with the $\chi_{ref}(T)$ curve, and eventually coincide with the $\chi_{ref}(T)$. The difference between $\chi(T)$ and $\chi_{ref}(T)$ as a function temperature is also illustrated in Fig. 1.8. The effect of aging at T_s is reflected by a dip at around T_s. For comparison, the same experiment was performed as T_s = 10 K, i.e., a temperature above T_c, and it was found that aging at 10 K had no influence on $\chi(T)$ curve (not shown). The appearance of memory dips indicates that spin configurations attained during a stop at T_s are preserved after cooling and subsequent heating. The finite temperature range of the memory dips reflects a temperature chaos in equilibrium spin configurations. Since an equilibrium spin configuration at a particular temperature T is completely different from another spin configuration at a different temperature $T+\Delta T$ if ΔT is sufficiently large, an aging effect at T does not affect a spin structure at $T+\Delta T$ at all. This memory effect has been confirmed for spin glasses and strongly interacting nanoparticles systems [16-18]. On the other hand, it has been experimentally and theoretically demonstrated that the memory effect according to this protocol is not observed in simple superparamagnets due to the absence of magnetic interactions among magnetic particles [16]. The observation of this memory effect is generally an indication of collective nature in spin dynamics [16,18], so that the present result strongly suggests that low temperature magnetic phase of the $20Fe_2O_3 \cdot 80TeO_2$ glass is a spin glass.

1.1.3.7 Magnetic aging effects in magnetic field

An aging effect in a magnetic field [19] was also explored for the present $20Fe_2O_3 \cdot 80TeO_2$ glass. The experiments were performed in the following way. The glass was cooled from a temperature well above T_c=8.8 K to 3 K at a rate of 0.2 K/min. Subsequently, a magnetic field of 50 Oe was applied and $\chi(T)$ was measured on heating to a stopping temperature T_s, which was 4 or 5 K, at a rate of 0.2 K/min. Then, the temperature was fixed to be T_s for 5.5 h, and $\chi(T_s)$ as a function of time was measured. After the stop at T_s, $\chi(T)$ was determined on heating further at a rate of 0.2 K/min. As a reference, $\chi_{ref}(T)$ was measured in zero-field and field cooling processes without any long term stops (5.5 h in the present case) at fixed temperatures. The $\chi(T)$ and $\chi_{ref}(T)$ curves thus obtained are depicted in Fig. 1.9. As found in the inset of Fig. 1.9, $\chi(T)$ increases logarithmically with time at T_s. After a stop for 5.5 h at T_s, $\chi(T)$ at first decreases with an increase in temperature and merges with the $\chi_{ref}(T)$ curve at a temperature well above T_s. A similar behavior was reported for the ferromagnetic phase of a reentrant spin glass $Cu_{0.2}Co_{0.8}Cl_2$-$FeCl_3$ graphite bi-intercalation compound [21]. The decrease of $\chi(T)$ just above T_s observed in Fig. 1.9 is thought to be a rejuvenation effect attributed to a chaotic nature of spin configurations which depend on temperature. The present behavior is somewhat different than that observed for 3D Ising spin glass $Fe_{0.5}Mn_{0.5}TiO_3$ [19] and $Cu_{0.5}Co_{0.5}Cl_2$-$FeCl_3$ graphite bi-intercalation compound [22]; for these two systems, $\chi(T)$ monotonically increases as the temperature is raised from T_s after a stop and then merges with a reference curve at a temperature well above T_s. It was concluded for the $Fe_{0.5}Mn_{0.5}TiO_3$ that $\chi(T)$ is explained well in terms of a scaling description derived from the droplet theory for spin glasses, where the susceptibility depends on two length scales $R_T(t_w)$ and $L_T(t)$ as follows [19]:

$$\chi(T,t) = F\left(R_T(t_w), L_T(t)\right). \qquad (1.9)$$

Here $R_T(t_w)$ is the mean size of spin glass domains grown during a waiting time t_w (or a stopping time in zero field) and $L_T(t)$ the maximum size of domains excited within a

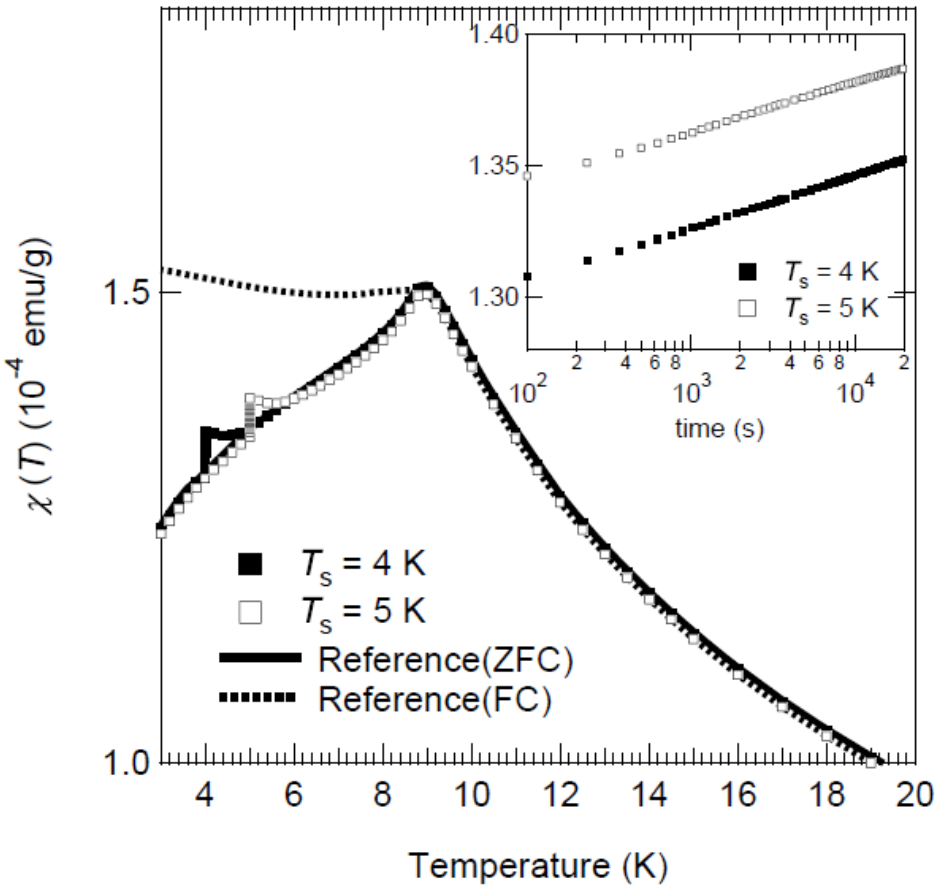

Figure 1.9: Temperature dependence of dc susceptibility measured on heating with and without an intermittent stop at T_s under an external magnetic field of 50 Oe after zero-field cooling. Temperature dependence of field cooled dc susceptibility is also shown. The inset depicts time dependence of susceptibility at T_s.

probing time t. Several kinds of theoretical equations have been suggested to express the growth laws of $R_T(t_w)$ and $L_T(t)$ [30-32]. One of the theories proposes a power law as follows:

$$R_T(t_w) \approx \left(\frac{t_w}{\tau_0}\right)^{\frac{bT}{T_c}} \qquad (1.10)$$

and

$$L_T(t) \approx \left(\frac{t}{\tau_0}\right)^{\frac{bT}{T_c}}, \qquad (1.11)$$

where the exponent $b \approx 0.17$ [30]. For $Fe_{0.5}Mn_{0.5}TiO_3$, by assuming that $L_T(t)$ grows continuously even if the temperature is changed discontinuously, $\chi(T)$ can be scaled by a scaling function F which increases continuously with $L_T(t)$. The validity of this scaling law warrants an accumulative nature of aging dynamics involving the continuous growth of $L_T(t)$ within a laboratory time scale. In the present experiments, $\chi(T)$ does not increase monotonically with time as reflected in the decrease of $\chi(T)$ just above T_s. Hence, it is clear that this scaling law can not be applied to the $20Fe_2O_3 \cdot 80TeO_2$ glass. This indicates that the $20Fe_2O_3 \cdot 80TeO_2$ glass manifests a non-accumulative aging effect presumably due to a chaotic nature within the laboratory time scale.

1.1.4 Conclusion

In conclusion, this section presents the magnetic properties of the binary Fe_2O_3-TeO_2 glasses. The Fe_2O_3-TeO_2 glasses exhibit typical spin glass behavior: the temperature dependence of ZFC and FC susceptibilities, the static and dynamic scaling of nonlinear susceptibility and relaxation time, respectively, and the magnetic aging and

memory effects. In particular, it is of much interest that the critical exponents obtained by scaling analysis are in good agreement with those of other spin glasses although the present glasses have a microscopic picture different from canonical spin glasses. In canonical spin glasses, ferromagnetic and antiferromagnetic interactions are randomly distributed, while the antiferromagnetic superexchange interaction via oxide ions is dominant among Fe^{3+} ions in the Fe_2O_3-TeO_2 glasses as indicated from the negative value of θ_W. It is naturally anticipated that magnetic structure of the present oxide glass depends on the arrangement of Fe^{3+} ions in the glass structure. Magnetic frustration in the oxide glass, revealed by the magnitude of the value f, can be caused by a spatially random distribution of Fe^{3+} ions, which are connected by the antiferromagnetic interaction. The strength of superexchange interactions among Fe^{3+} ions has a distribution due to the site-dependent variations in Fe-O-Fe bond angles and Fe-O bond lengths. Thus, not only randomness but also frustration is present in the magnetic structure of the Fe_2O_3-TeO_2 glasses, leading to transition into spin glass phase at very low temperatures even in the absence of random distributions of magnetic interactions with opposite signs.

References in Section 1.1

[1] V. Cannella and J. A. Mydosh, *Phys. Rev. B* **6**, 4220 (1972).

[2] J. A. Mydosh, *Spin glasses: an Experimental Introduction* (Taylor &Francis Ltd., London, 1993).

[3] S. F. Edwards and P. W. Anderson, *J. Phys. F: Metal Phys.* **5**, 965 (1975).

[4] D. Sherrington and S. Kirkpatrick, *Phys. Rev. Lett.* **35**, 1792 (1975).

[5] J. J. Hopfield, *Proc. Natl. Acad. Sci. USA* **79**, 2554 (1982).

[6] H. Maletta and W. Felsch, *Phys. Rev. B* **20**, 1245 (1979).

[7] A. Ito, H. Aruga, E. Torikai, M. Kikuchi, Y. Shono, and H, Takei, *Phys. Rev. Lett.* **57**, 483 (1986).

[8] R. A. Verhelst, R. W. Kline, A. M. de Graaf, and H. O. Hooper, *Phys. Rev. B* **11**, 4427 (1975).

[9] J. L. Shaw, A. C. Wright, R. N. Sinclair, G. K. Marasinghe, D. Holland, M. R. Lees, and C. R. Scales, *J. Non-Cryst. Solids* **345&346**, 245 (2004).

[10] P. Beauvillain, C. Dupas, J. P. Renard, and P. Veillet, *Phys. Rev. B* **29**, 4086 (1984).

[11] P. Beauvillain, C. Chappert, J. P. Renard, and J. Seiden, *J. Magn. Magn. Mater.* **54-57**, 127 (1986).

[12] J. P. Sanchez, J. M. Friedt, R. Horne, and A. J. Van Duyneveldt, *J. Phys. C* **17**, 127 (1984).

[13] J. P. Sanchez and J. M. Friedt, *J. Physique* **43**, 1707 (1982).

[14] G. W. Hunter, L. E. Wenger, and W. D. Wallance, *Phys. Rev. B* **36**, 5750 (1987).

[15] H. R. Rechenberg, L. H. Bieman, F. S. Huang, and A. M. de Graaf, *J. Appl. Phys.* **49**, 1638 (1978).

[16] M. Sasaki, P. E. Jönsson, H. Takayama, and H. Mamiya, *Phys. Rev. B* **71**, 104405 (2005).

[17] R. Mathieu, P. Jönsson, D. N. H. Nam, and P. Nordblad, *Phys. Rev. B* **63**, 92401

(2001).

[18] C. R. Sankar and P.A. Joy, *Phys. Rev. B* **72**, 132407 (2005).

[19] L. W. Bernardi, H. Yoshino, K. Hukushima, H. Takayama, A. Tobo, and A. Ito, *Phys. Rev. Lett.* **86**, 720 (2001).

[20] P, Nordblad, *J. Phys,:Condens. Matter.* **16**, S715 (2004).

[21] M. Suzuki and I. S. Suzuki, *Phys. Rev. B* **71**, 174437 (2005).

[22] M. Suzuki and I. S. Suzuki, *Eur. Phys. J. B* **41**, 457 (2004).

[23] P. E. Jönsson, R. Mathieu, P. Nordblad, H. Yoshino, H. Aruga Katori, and A. Ito, *Phys. Rev. B* **70**, 174402 (2004).

[24] S. Miyashita and E. Vincent, *Eur. Phys. J. B* **22**, 203 (2001).

[25] V. Dupuis, E. Vincent, J.-P. Bouchaud, J. Hammann, A. Ito, and H. Aruga Katori, *Phys. Rev. B* **64**, 174204 (2001).

[26] K. Jonason, E. Vincent, J. Hammann, J. P. Bouchaud, and P, Nordblad, *Phys. Rev. Lett.* **81**, 3243 (1998).

[27] T. Jonsson, K, Jonsson, P. Jönsson, and P, Nordblad, *Phys. Rev. B* **59**, 8770 (1999).

[28] P. Jönsson, M. H. Hansen, and P, Nordblad, *Phys. Rev. B* **61**, 1261 (2000).

[29] L. Lundgren, P. Svedlindh, P. Nordblad, and O. Beckman, *Phys. Rev. Lett.* **51**, 911 (1983).

[30] T. Komori, H. Yoshino, and H. Takayama, *J. Phys. Soc. Jpn.* **68**, 3387 (1999).

[31] T. Komori, H. Yoshino, and H. Takayama, *J. Phys. Soc. Jpn.* **69**, 1192 (2000).

[32] D. S. Fisher and D. A. Huse, *Phys. Rev. B* **38**, 386 (1988).

[33] M. Sasaki and K. Nemoto, *J. Phys. Soc. Jpn.* **69**, 2283 (2000).

[34] C. Djurberg, P. Svedlindh, P. Nordblad, M. F. Hansen, F. Bødker, and S. Morup, *Phys. Rev. Lett.* **79**, 5154 (1997).

[35] M. H. Hansen, P. E. Jönsson, P. Nordblad, and P. Svedlindh, *J. Phys,:Condens. Matter.* **14**, 4901 (2002).

[36] K. Gunnarsson, P. Svedlindh, P. Nordblad, L. Lundgren, H. Aruga, and A. Ito, *Phys. Rev. Lett.* **61**, 754 (1988).

[37] S. A. Makhlof, F. T. Parker, and A. E. Berkowitz, *Phys. Rev. B* **55**, R14717 (1997).

[38] Y. Sun, M. B. Salamon, K. Ganier, and R. S. Averback, *Phys. Rev. Lett.* **91**, 167206 (2003).

[39] G. M. Tsoi, L. E. Wenger, U. Senaratne, R. J. Tackett, E. C. Buc, R. Naik, P. P. Vaishnava, and V. Naik, *Phys. Rev. B* **72**, 014445 (2005).

[40] C. R. Kurkjian and E. A. Sigety, *Phys.Chem.Glasses* **9**, 73 (1968).

[41] K. Tanaka and N. Soga, *J. Non-Cryst. Solids* **95&96**, 255 (1987).

[42] S. Nagata, P. H. Keesom and H. R. Harrison, *Phys. Rev. B* **19**, 1633 (1979).

[43] A. P. Ramirez, *Annu. Rev. Mater. Sci.* **24**, 453 (1994).

[44] I. S. Hagemann, P. G. Khalifah, A. P. Ramirez, and R. J. Cava, *Phys. Rev. B* **62**, 771 (2000).

[45] M. Suzuki, *Prog. Theor. Phys.* **58**, 1151 (1977).

[46] B. Barbara, A. P. Malozemoff, and Y. Imry, *Phys. Rev. Lett.* **47**, 1852 (1981).

[47] A. P. Malozemoff, Y. Imry, and B. Barbara, *J. Appl. Phys.* **53**, 7672 (1982).

[48] G. F. Goya and V. Sagredo, *Phys. Rev. B* **64**, 235208 (2001).

[49] T. M. Pekarek, E. M. Watson, J. Garner, P. M. Shand, I. Miotkowski, and A. K. Ramdas, *J. Appl. Phys.* **101**, 09D511 (2007).

[50] A. Mauger, J. Ferré, and P. Beauvillain, *Phys. Rev. B* **40**, 862 (1989).

[51] J. Souletie and J. L. Tholemce, *Phys. Rev. B* **32**, 516 (1985).

[52] S. Shtrikman and E. P. Wohlfarth, *Phys. Lett.* **85A**, 467 (1981).

[53] S. Shtrikman and E. P. Wohlfarth, *J. Magn. Magn. Mater.* **31-34**, 1421 (1983).

Section 1.2 Spin glass transition and magnetic frustration in mixed valence iron phosphate glasses

1.2.1 Introduction

Considerable interests in spin glass have been generated recently on the basis of the expectation that it can be a physical model of random systems. The extensive search for new spin glass materials and investigation of their magnetic properties have been performed since Cannella and Mydosh [1] observed magnetic transitions in temperature dependence of susceptibility for binary *Au*Fe alloys with very low concentrations of Fe. A great number of magnetic materials exhibiting spin glass behavior have emerged in crystalline alloys, oxides, sulfides, and so forth. The development of experimental, theoretical, and numerical studies on spin glass has given an insight into their intrinsic nature. Even in this decade, fascinating phenomena involving magnetic aging effects have been reported as unique features of spin glasses [2-6]. Spin glass is also a matter of absorbing interest from a point of view of its analogy to many complex systems such as associative memory in the brain [7].

Magnetic oxide glass is a prototype of a solid in which magnetic moments are spatially distributed in a disordered fashion like a spin glass. In most insulating oxides, magnetic properties are dominated by antiferromagnetic superexchange interaction via an oxide ion. It may be naturally anticipated that all the pairs of magnetic moments antiferromagnetically coupled with each other can not take their own most stable states because of the random distribution of magnetic ions. In other words, the magnetic frustration is inevitably present in the random structure of oxide glasses. Hence, magnetic oxide glass presumably satisfies the conditions necessary for the occurrence of spin glass transition: randomness and frustration [8]. Some efforts to describe the mechanism of magnetic transition in oxide glasses have led to the investigation on temperature dependence of dc and ac magnetic susceptibility, Mössbauer spectrum,

electron spin resonance spectrum, and so forth [9-14]. As a result, magnetic oxide glasses, in particular, those containing 3*d* transition metal ions, have been regarded as a prototype of insulating spin glass. In Section 1.1, the author has described that Fe_2O_3-TeO_2 glasses manifest curious phenomena relevant to spin dynamics including magnetic aging and memory effects as well as critical slowing down similar to those observed in canonical spin glasses. This result strongly confirms that Fe_2O_3-TeO_2 glass system is a typical example of spin glass.

However, there have been few reports about the effects of the sorts and chemical states of magnetic ions on the magnetic properties of insulating amorphous spin glasses [15]. Even the same transition metal ion can have different magnetic moments as well as different single-ion anisotropies depending on its valence state. So, the magnetic properties are expected to depend on the valence states of magnetic ions. This section focuses on the iron phosphate glasses in which Fe ions can be present as either divalent or trivalent states. For iron phosphate glass system, Wedgwood *et al*. [16] confirmed the short range antiferromagnetic ordering at low temperatures for the glasses with a nominal composition of $0.79Fe_2O_3 \cdot P_2O_5$ glass by using neutron magnetic scattering. Shaw *et al*. [17] observed the spin glass-like behavior in the temperature dependence of dc magnetic susceptibility for the glasses with nominal compositions of $x Fe_2O_3 \cdot (100-x)P_2O_5$ ($30 \leq x \leq 44$, in mol%). However, detailed magnetic properties of iron phosphate glasses have not been revealed; especially, the dependence of magnetic behavior on the valence states of iron ions has not been discussed at all. In this section, the iron phosphate glasses with varied $[Fe^{3+}]/[Fe_{total}]$ molar ratio were prepared by melting in alumina or glassy carbon crucibles at various temperatures, and their magnetic properties were examined in detail. The iron phosphate glasses are converted into spin glass phases at low temperatures, as revealed by not only the magnetic aging and memory experiments but also the dynamic and static scaling analyses of the relaxation time and nonlinear magnetic susceptibility. Also, magnetic specific heat measurements suggest that the short-range magnetic correlation emerges

near the temperature at which magnetic susceptibility deviates from the Curie-Weiss law, and the correlation length gradually grows as the temperature is decreased. The last part of this secsion describes the dependence of magnetic parameters including the spin freezing temperature, T_f, and Weiss temperature, θ_W, on the glass compositions and oxidation states of iron ions in the glasses. In particular, it is found that the value of $|\theta_W|/T_f$, which is a measure of magnetic frustration proposed for geometrically frustrated magnetic materials [18], becomes lower with an decrease in $[Fe^{3+}]/[Fe_{total}]$ ratio. The suppression of magnetic frustration is discussed in terms of the strong single-ion anisotropy of Fe^{2+} ions which are more anisotropic than Fe^{3+} ions.

1.2.2 Experimental procedure

Glasses with nominal compositions of $x Fe_2O_3 \cdot (100-x)P_2O_5$ (x = 33, 37, 40 and 45, in mol%) were prepared from reagent grade Fe_2O_3 powder and H_3PO_4 aqueous solution by using a conventional melt-quenching method. After appropriate amounts of the starting materials were mixed thoroughly, the mixture was heated at 180°C to evaporate H_2O and then melted at T_m=X°C (X=1200, 1350, and 1500) for 30 min in an alumina crucible. The melt was poured onto a stainless steel plate and cooled in air. The samples are denoted as xFe(100-x)PX for convenience sake; for instance, 33Fe67P1200 denotes that the mixture with the nominal composition of $33Fe_2O_3 \cdot 67P_2O_5$ (mol%) was melted at 1200°C. The as-quenched glass was pulverized, and then remelted in a glassy carbon crucible placed in an alumina crucible with an alumina lid at 1200 °C for 30 min in air. The melt was quenched as well. The samples melted in glassy carbon crucible are denoted as xFe(100-x)PC ((x = 33, 37, and 40, in mol%). The amorphous nature of the samples was confirmed by X-ray diffraction analysis with CuK_α radiation. ^{57}Fe Mössbauer spectroscopy was carried out at room temperature employing ^{57}Co in metallic Rh as a γ-ray source so as to estimate valence states and coordination

environments for iron ions in the glasses. The velocity scale was calibrated by using a spectrum of α-Fe measured at room temperature. The temperature dependence of dc and ac susceptibility was determined by using a Quantum Design SQUID (superconducting quantum interference device) magnetometer (model MPMS-XL). Specific heat was measured by a thermal relaxation method in zero magnetic field using a commercial calorimeter (Quantum Design, model PPMS).

1.2.3 Results and discussion

1.2.3.1 ^{57}Fe Mössbauer spectroscopy

The ^{57}Fe Mössbauer spectra for 33Fe67P*X* glasses are illustrated in Fig. 1.10. These spectra are explainable in terms of the superposition of paramagnetic doublets attributable to Fe^{2+} and Fe^{3+} ions. It is reasonable to presume that the absorption area ratio of paramagnetic doublets of Fe^{2+} and Fe^{3+} ions corresponds to their existing ratio. Table 1.4 summarizes the fraction of Fe^{3+} ions in the total number of Fe ions, $[Fe^{3+}]/[Fe_{total}]$, along with the values of Mössbauer parameters, i.e., isomer shift (IS) and quadrupole splitting (QS) for all the samples. These values were obtained by fitting two symmetric Lorenzians to each of the paramagnetic doublets obtained experimentally. Irrespective of the value of x, $[Fe^{3+}]/[Fe_{total}]$ decreases with increasing the temperature of melting, T_m. This result is in good agreement with those reported previously [19]. A doublet of Fe^{3+} ion is not observed in the spectra of the glasses melted in glassy carbon crucibles. No systematic changes are found for IS and QS when x and T_m is varied. The values of IS and QS for the Fe^{3+} and Fe^{2+} ions (IS=0.37-0.40 mm/s and QS=0.83-0.90 mm/s for Fe^{3+}; IS=1.18-1.24 mm/s and QS=2.17-2.29 mm/s for Fe^{2+}) indicate that both the Fe^{3+} and Fe^{2+} ions occupy the octahedral sites surrounded by O^{2-} ions in the glasses.

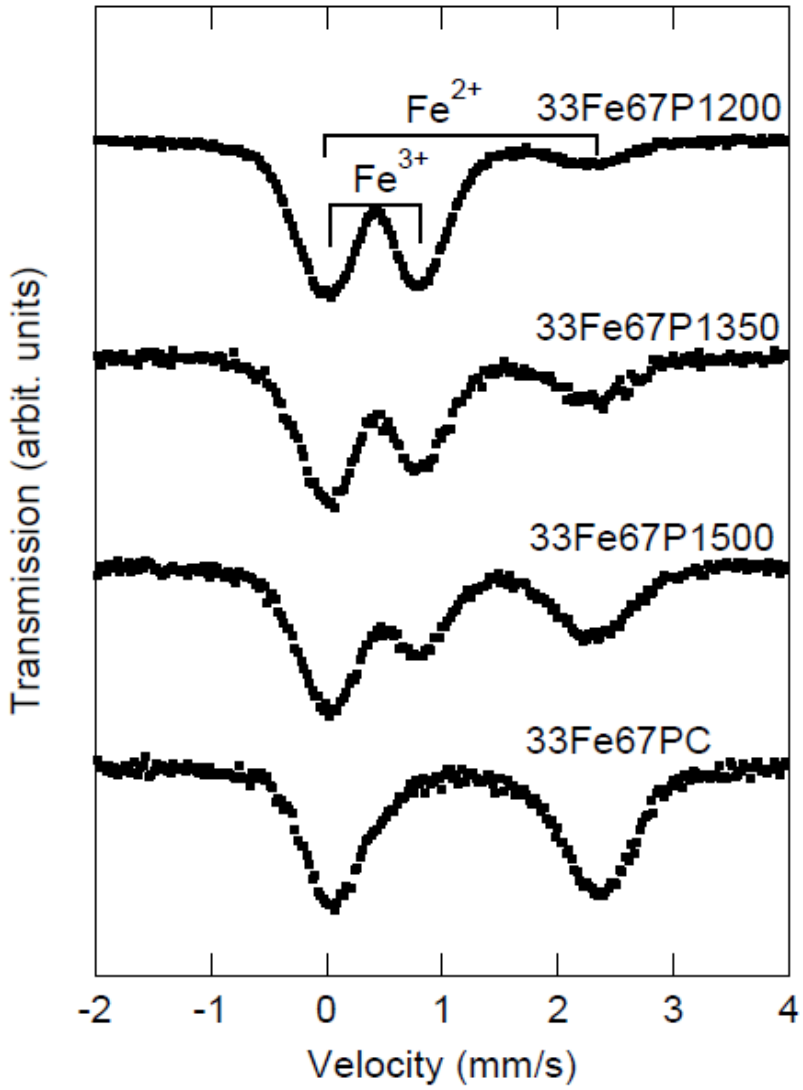

Figure 1.10: ^{57}Fe Mössbauer spectra of 33Fe67P*X* glasses with *X* = 1200, 1350, 1500, and C measured at room temperature. The fraction of Fe^{3+} ions in the total number of Fe ions, $[Fe^{3+}]/[Fe_{total}]$, along with the values of Mössbauer parameters, i.e., isomer shift (IS) and quadrupole splitting (QS) are summarized in Table 1.4 for all the samples.

Table 1.4: The parameters derived from the Mössbauer spectra and the temperature dependence of dc magnetic susceptibility for *x*Fe(100-*x*)P*X*.

Sample	Fe^{2+}		Fe^{3+}		$[Fe^{3+}]$	T_f	θ_W/K	*f*	M_B	M_B^{theory}
	IS/mm/s	QS/mm/s	IS/mm/s	QS/mm/s	/$[Fe_{total}]$	/K				
33Fe67P1200	1.24	2.17	0.40	0.84	0.84	4.3	-34.8	8.1	5.9	5.8
33Fe67P1350	1.20	2.24	0.40	0.84	0.63	4.5	-29.6	6.6	5.9	5.5
33Fe67P1500	1.20	2.22	0.40	0.85	0.39	4.3	-23.5	5.5	5.4	5.3
33Fe67PC	1.20	2.27	-	-	0.00	2.2	-8.6	3.9	5.6	4.8
37Fe63P1200	1.22	2.22	0.38	0.87	0.83	5.6	-45.9	8.2	5.8	5.7
37Fe63P1350	1.20	2.24	0.39	0.85	0.60	5.2	-33.4	6.4	5.7	5.5
37Fe63P1500	1.19	2.23	0.39	0.83	0.39	4.8	-25.4	5.3	5.4	5.3
37Fe63PC	1.20	2.29	-	-	0.00	2.6	-9.0	3.4	5.4	4.8
40Fe60P1200	1.21	2.17	0.37	0.89	0.83	6.2	-54.3	8.8	5.8	5.7
40Fe60P1350	1.19	2.25	0.39	0.87	0.57	6.1	-37.7	6.2	5.6	5.5
40Fe60P1500	1.20	2.22	0.38	0.88	0.38	5.5	-27.2	5.0	5.4	5.3
40Fe60PC	1.20	2.26	-	-	0.00	3.1	-11.6	3.7	5.2	4.8
45Fe55P1200	1.18	2.24	0.37	0.90	0.80	7.8	-71.9	9.2	5.8	5.7
45Fe55P1350	1.19	2.27	0.39	0.90	0.54	7.6	-51.9	6.8	5.6	5.5
45Fe55P1500	1.18	2.29	0.40	0.85	0.34	6.9	-36.0	5.2	5.4	5.2

1.2.3.2 The temperature dependence of dc magnetic susceptibility

Figures 1.11(a) and (b) show the temperature dependence of dc susceptibility $\chi(T)$ and its reciprocal $\chi^{-1}(T)$ for xFe(100-x)P1200 glasses, respectively. The inset of Fig. 1.11(a) depicts an enlarged view of the low temperature region between 2 and 10 K. The measurements were performed for both field cooling (FC) and zero-field cooling (ZFC) processes with a magnetic field of H = 50 Oe applied. The $\chi(T)$ curves for FC and ZFC are different from each other below the spin freezing temperature, T_f, at which the $\chi(T)$ curve for ZFC exhibits a maximum. The spin freezing temperature for all the glass samples is listed in Table 1.4. The $\chi(T)$ curves for FC are kept almost constant below T_f. This behavior is similar to that of typical spin glasses [20]. A linear relation between $\chi^{-1}(T)$ and T at high temperatures reveals that these glasses are paramagnetic in the high temperature region; the linear part is describable in terms of the following Curie-Weiss law:

$$\frac{1}{\chi} = \frac{3k_B(T-\theta_W)}{NM_B^{\,2}\mu_B^{\,2}}, \qquad (1.12)$$

where θ_W is the Weiss temperature, N the number of magnetic ions per unit mass, μ_B the Bohr magneton, M_B the effective number of Bohr magnetons, and k_B the Boltzmann constant. The dashed lines in Fig. 1.11(b) present the fitting Eq. (1.12) to the experimental data of $\chi^{-1}(T)$ at temperatures from 100 to 300 K. The parameters of M_B and θ_W evaluated by the fitting are summarized in Table 1.4. The value of M_B is slightly higher than M_B^{cal}, calculated by considering the valence states of iron ions and the spin moments for the high-spin states. This result indicates that nonzero unquenched orbital moments contribute to the magnetic moments. The negative values of θ_W indicate that the antiferromagnetic interaction is dominant among magnetic moments in the present glasses.

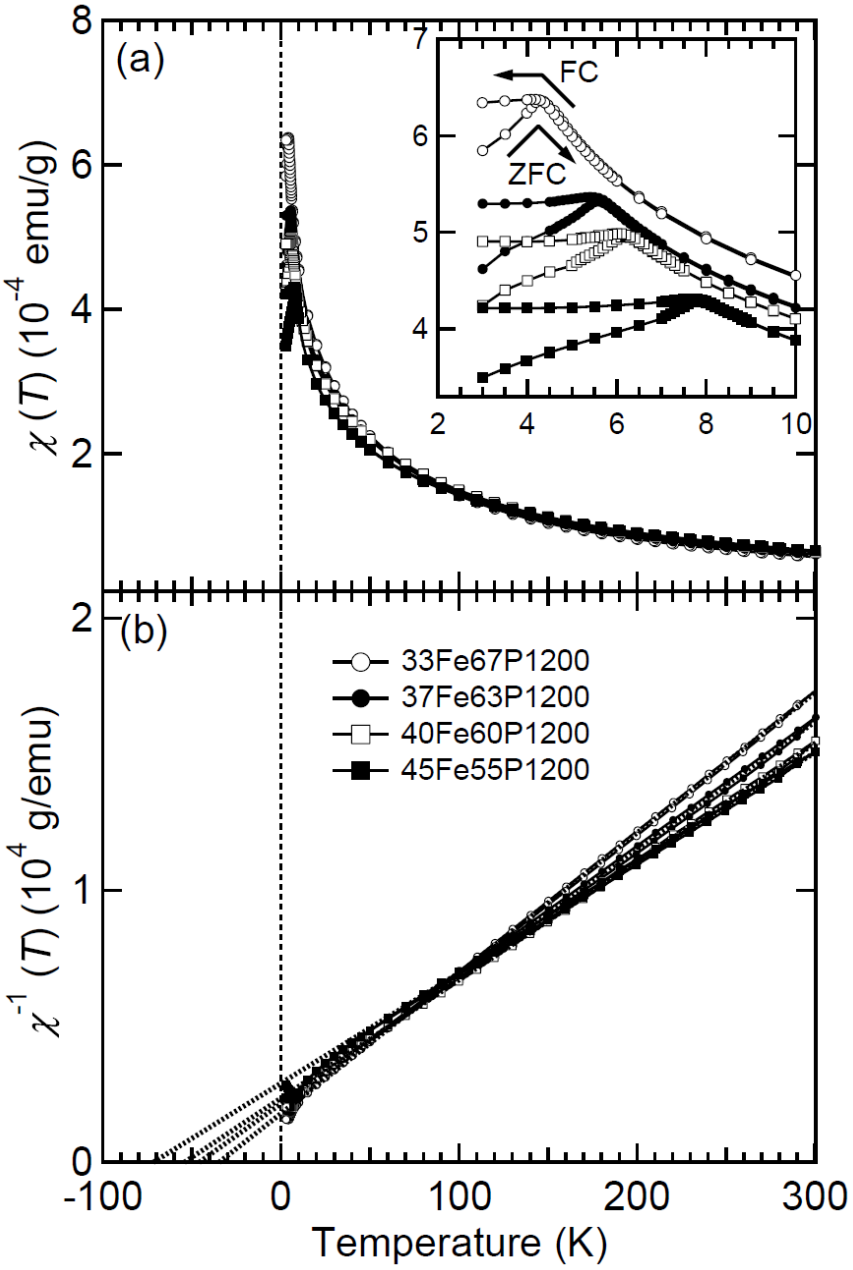

Figure 1.11: Temperature dependence of (a) dc magnetic susceptibility $\chi(T)$ and (b) its inverse $\chi^{-1}(T)$ for the xFe(100-x)P1200 glasses with x = 33, 37, 40 and 45 measured at H_{dc}=50 Oe. The broken lines indicate the fit of the experimental data at high temperatures to Eq. (1.12).

1.2.3.3 Dynamical scaling analysis

Figure 1.12 depicts the temperature dependence of real part of ac susceptibility obtained by zero-field cooling for 45Fe55P1200 glass. The amplitude of ac magnetic field was kept to be 3 Oe and the ac frequency was varied from 0.3 to 1000 Hz. As can be seen in Fig. 1.12, the frequency-dependent spin-freezing temperature $T_f(f)$, defined as a temperature at which the real part of ac susceptibility manifests a maximum, shifts to a higher temperature side with an increase in f. According to the dynamic scaling hypothesis, provided that this system exhibits a conventional critical slowing down toward the transition temperature T_c, the temperature variation of relaxation time $\tau = f^{-1}$ is described by

$$\tau = \tau_0 \left(\frac{T_f(f) - T_c}{T_c} \right)^{-zv} \qquad (1.13)$$

where zv is the dynamic exponent and τ_0 is a spin flipping time. In the present case, the best fitting of Eq. (1.13) to the experimental data yields zv= 11.0, T_c = 7.5 K, and τ_0 = 2.1×10^{-13} s, as shown in the inset of Fig. 1.12. The values of zv= 11.0 and τ_0 = 2.1×10^{-13} s are in good agreement with those reported for conventional atomic spin glasses [see Table 1.3 and Ref. 21 and 22]. For $20Fe_2O_3\cdot80TeO_2$ glass, zv= 10 and τ_0 = 1.0×10^{-13} s were obtained in Section 1.1. The results of this analysis imply the occurrence of phase transition from a paramagnet to an atomic spin glass in the present iron phosphate glass. The similar measurements and analyses have been performed for 33Fe67P1200, 33Fe67P1500, 33Fe67PC, 40Fe60PC, and 45Fe55P1500; the values of zv, T_c, and τ_0 obtained by the analysis by Eq. (1.13) are summarized in Table 1.5.

1.2.3.4 Static scaling analysis of nonlinear susceptibility

In order to reinforce the presence of spin glass transition in the iron phosphate glass system, a scaling analysis of static nonlinear susceptibility has been carried out

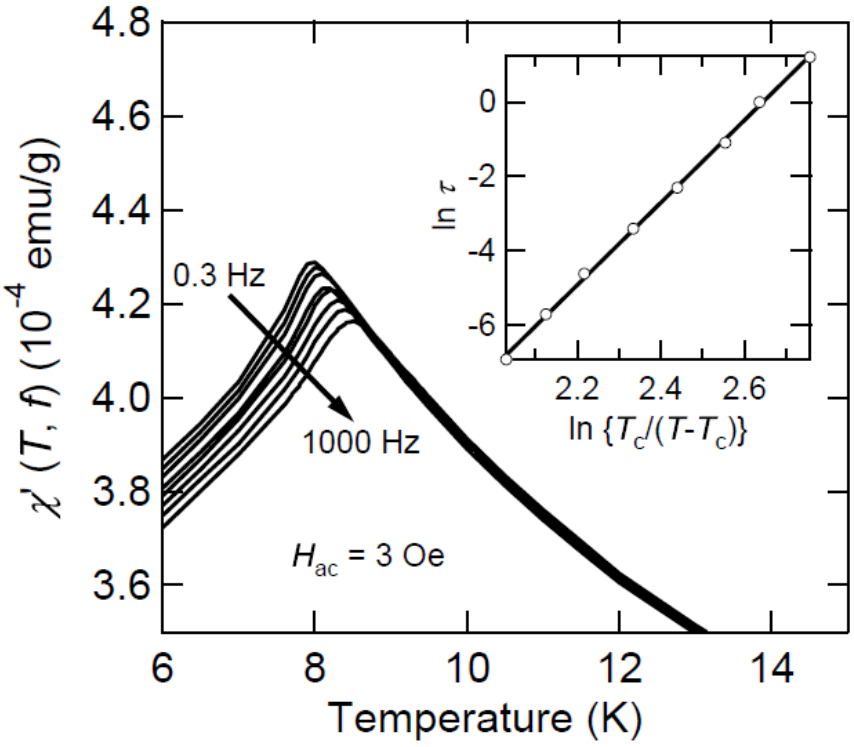

Figure 1.12: Temperature dependence of real part of ac susceptibility $\chi'(T)$ for 45Fe55P1200 glass at H_{ac}=3 Oe. The frequency f is 0.3, 1, 3, 10, 30, 100, 300 and 1000 Hz (from top to bottom). The inset illustrates the relationship between maximum relaxation time τ and spin freezing temperature $T_f(f)$ in analysis of critical slowing down analysis. The solid line shows the best fit of the experimental data to Eq. (1.13).

Table 1.5: Dynamic critical exponent $z\nu$, microscopic relaxation time τ_0 and critical temperature T_c obtained by the scaling analysis on critical slowing down.

	$z\nu$	τ_0/s	T_c/K
33Fe67P1200	12.5	1.0×10^{-12}	4.0
33Fe67P1500	12.9	1.5×10^{-9}	3.8
33Fe67PC	10.4	6.2×10^{-6}	1.9
45Fe55P1200	11.0	2.1×10^{-13}	7.5
45Fe55P1500	11.4	1.3×10^{-10}	6.5
40Fe60PC	11.5	8.0×10^{-7}	2.7

for 45Fe55P1200 glass. The analysis is based on the data concerning the temperature dependence of FC magnetization measured at various magnetic fields. Expanding $M(T, H)$ in terms of odd powers of H in the temperature region of $T > T_f$ leads to

$$M(T, H) = \chi_0(T)H - \chi_2(T)H^3 + \chi_4(T)H^5 - \ldots, \quad (1.14)$$

where $\chi_0(T)$ is the linear susceptibility in the limit of $H \rightarrow 0$. The static nonlinear susceptibility $\chi_{NL}(T, H)$ is defined as follows:

$$\chi_{NL}(T, H) = M(T, H)/H - \chi_0(T) = -\chi_2(T)H^2 + \chi_4(T)H^4 - \ldots . \quad (1.15)$$

The temperature dependence of $\chi_{NL}(T, H)$ for 45Fe55P1200 glass at varied magnetic fields is shown in the inset of Fig. 1.13, where $\chi_0(T)$ is taken as the dc susceptibility measured at the smallest dc magnetic field in this experiment, i.e., 20 Oe. It is found that $\chi_{NL}(T, H)$ exhibits a maximum at around T_f. A similar behavior was also seen in an insulating spin glass such as $Zn_{0.1}Mn_{0.9}In_2Te_4$ [23]. It is known that the scaling analyses developed for empirical description of paramagnet-ferromagnet phase

transitions provide consistent results when applied to paramagnet-spin glass transitions. The analysis has confirmed the scaling equation [24],

$$\chi_{NL} = -t^{\beta}\Phi\left(\frac{H^2}{t^{\beta+\gamma}}\right) \qquad (1.16)$$

where $t = (T-T_c)/T_c$ is the reduced temperature and β and γ are the critical exponents. The universal curve resulting from the experimental data at $T > T_f$ is depicted as a log-log scale plot in Fig. 1.13. All the data can be suited on a single curve with T_c=7.8 K, β=0.9 and γ=3.6. The universal scaling curve covers several orders of magnitude along both vertical and horizontal axes. The critical exponents obtained are in good agreement with those reported for other spin glasses [23,25,26]. At temperatures sufficiently higher than T_c (bottom left part of the curve), the slope approaches 1 as expected. As T approaches T_c from the higher temperature region (top right part of the curve), the slope tends to be the proper asymptotic value $\beta/(\beta+\gamma)$ [18,20,21]. The static scaling analysis of nonlinear susceptibility provides additional evidence for the presence of spin glass transition in the iron phosphate glasses.

1.2.3.5 ZFC memory effects

The magnetic aging and memory effects, which are characteristic of spin glasses, have been examined for 45Fe55P1200 glass to confirm the spin glass behavior. The zero-field cooling memory experiment proposed by Mathieu *et al* [2] has been performed. In this protocol, the system is cooled in zero magnetic field from a temperature higher than T_f with or without an intermittent stop at a stopping temperature T_s situated below the transition temperature. The $\chi(T)$ curve is recorded during subsequent heating in a measuring magnetic field. Sasaki *et al*. have demonstrated theoretically and experimentally that a memory is imprinted during the aging in the absence of magnetic field only for spin glasses and strongly interacting

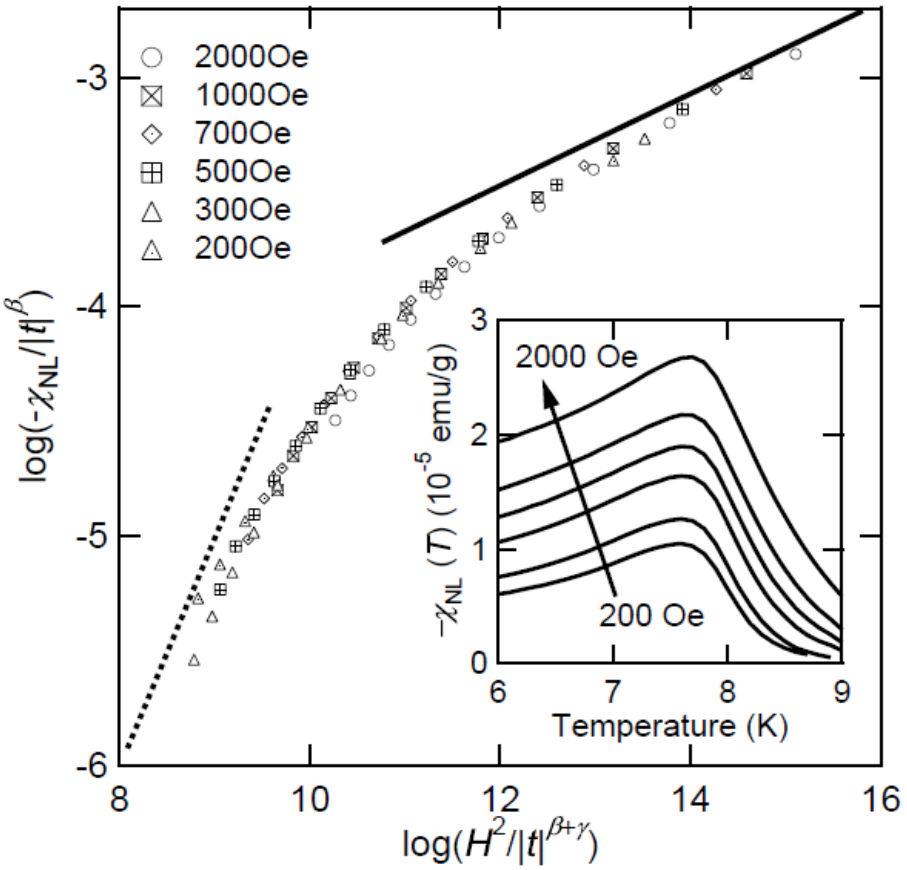

Figure 1.13: Nonlinear susceptibility $\chi_{NL}(T, H)$ for 45Fe55P1200 analyzed according to the universal scaling function of Eq. (1.16). The solid and broken lines represent the asymptotic limit of the experimental data to the $\beta/(\beta+\gamma)$ value and unity for $T \rightarrow T_f$ and $T \rightarrow \infty$, respectively. The inset shows $\chi_{NL}(T, H)$ plotted for T.

nanoparticles systems or superspin glasses, but not for non-interacting superparamagnets [27]. Hence, the observation of this memory effects warrants the cooperative spin dynamics.

In the present case, the glass sample was cooled at a rate of 0.2 K/min from a temperature well above T_f = 7.9 K to the stopping temperature T_s, which was lower than T_f, and was kept at T_s for 3 h. Here, T_s was selected to be 4, 5 and 6 K. After the stop for 3 h, the glass sample was recooled to 3 K at a rate of 0.2 K/min. Subsequently, a magnetic field of 50 Oe was applied and $\chi(T_s, T)$ was measured on heating at a rate of 0.2 K/min. As a reference, $\chi_{ref}(T)$ was determined by measuring the temperature dependence of zero-field cooled susceptibility without any intermittent stops. Figure 1.14 shows the results. The $\chi(T_s, T)$ curves coincide with the $\chi_{ref}(T)$ curve in a temperature range well below T_s. The $\chi(T_s, T)$ curves deviate downward from the $\chi_{ref}(T)$ curve as the temperature becomes close to T_s. As the temperature increases in a range above T_s, the $\chi(T_s, T)$ curves rapidly approach the $\chi_{ref}(T)$ curve, and eventually merge with the $\chi_{ref}(T)$. The difference between $\chi(T_s, T)$ and $\chi_{ref}(T)$ as a function temperature is also illustrated in Fig. 1.14. The effect of aging at T_s is reflected by the dip at around T_s. The experimental results definitely suggest that the magnetic phase adopted by the present glass at very low temperatures is a spin glass.

1.2.3.6 Magnetic specific heat

Magnetic specific heat, C_{mag}, has been explored for 33Fe67P1200 and 33Fe67P1500 glasses to obtain more detailed information about the phase transition in the glasses. By assuming that the specific heat of $33Ga_2O_3 \cdot 67P_2O_5$ (mol%) glass is identical with the contribution of phonons to the specific heat of the 33Fe67P*X* glasses, C_{mag} has been evaluated by subtracting the contribution of phonons from the total specific heat. The inset of Fig. 1.15(a) shows the temperature dependence of C_{mag} per 1 mol of iron ions in the low temperature regime. A very broad peak of C_{mag} is

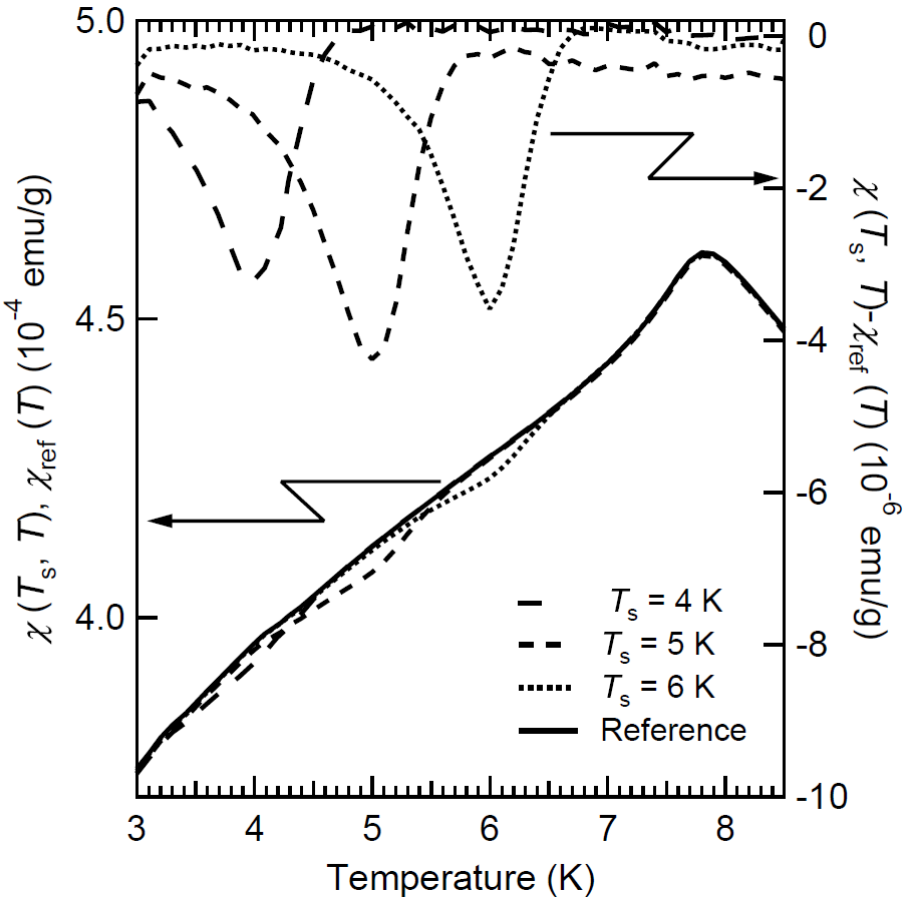

Figure 1.14: Temperature dependence of dc susceptibility measured on heating after zero-field cooling with and without an intermittent stop at T_s. The difference between $\chi(T\text{s}, T)$ and $\chi_{ref}(T)$ is illustrated as well.

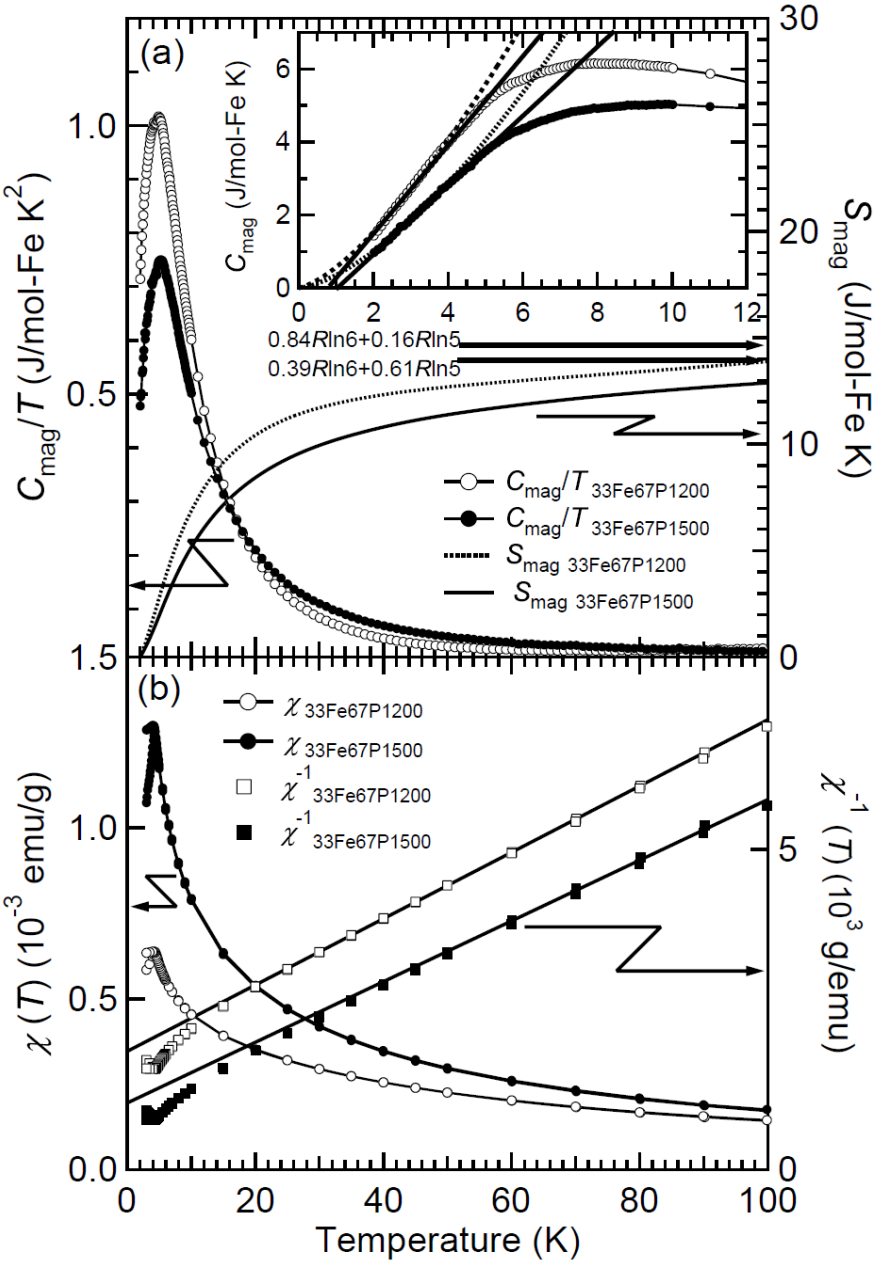

Figure 1.15: Temperature dependence of (a) magnetic specific heat divided by temperature C_{mag}/T and entropy S_{mag} and (b) dc magnetic susceptibility $\chi(T)$ and its reciprocal $\chi^{-1}(T)$ for 33Fe67PX with X = 1200 and 1500. The inset of Fig. 6(a) illustrates the enlarged view of C_{mag} in the low temperature region. The solid and dashed lines are guides to the eyes.

observed at 8 K and 10 K corresponding to $1.9T_f$ and $2.3T_f$ for 33Fe67P1200 and 33Fe67P1500, respectively. At low temperatures well below the peak temperature, C_{mag} exhibits a linear behavior with a positive intercept on the temperature axis [See the solid lines]. Similar behavior is observed in conventional spin glasses [28,29]. The alternative view is that C_M is proportional to T^{α} with $\alpha = 1.5$ and 1.6 for 33Fe67P1200 and 33Fe67P1500 at low temperatures, respectively [See the dashed curves]. In general, $C_{mag} \propto T^{1.5}$ is expected for spin wave excitation of ferromagnets. However, the $T^{1.5}$ dependence of C_{mag} is reported for some magnets which exhibit spin glass behavior such as $Yb_2Mn_2O_7$ and $Na_{0.70}MnO_2$ [30-32]. The quantities, C_{mag}/T, and the magnetic entropy, S_{mag}, calculated by integrating C_{mag}/T for T, are plotted as a function of T in Fig. 1.15(a). Figure 1.15(b) illustrates temperature dependence of $\chi(T)$ and $\chi^{-1}(T)$ for the present glasses. In high temperature regime, C_{mag}/T equals zero and $\chi^{-1}(T)$ shows the Curie-Weiss behavior. With lowering temperature, $\chi(T)$ starts to deviate from the Curie-Weiss law, accompanied by the onset of C_{mag}/T. This indicates that the short-range correlation emerges at temperatures higher by an order of magnitude than the transition temperatures. At high temperatures, the magnetic entropy reaches a value estimated from the degree of freedom of spins by considering the valence states of iron ions; $0.84R\ln6+0.16R\ln5 = 14.7$ and $0.39R\ln6+0.61R\ln5 = 14.0$ for 33Fe67P1200 and 33Fe67P1500, respectively, where R is the gas constant.

1.2.3.7 Magnetic frustration and single-ion anisotropy

As demonstrated above, the iron phosphate glasses are converted into spin glass phases at low temperatures, like the iron tellurite glasses in which all the iron ions are present as a trivalent state as shown in Section 1.1. Now let us consider the effects of the composition and the valence states of iron ions on magnetic parameters such as the spin freezing temperature and Weiss temperature. According to the mean field theory, the transition temperature is expected to be approximately proportional to NM_B^2, as is the case for θ_W. In the present case, x is directly related to N. The value of

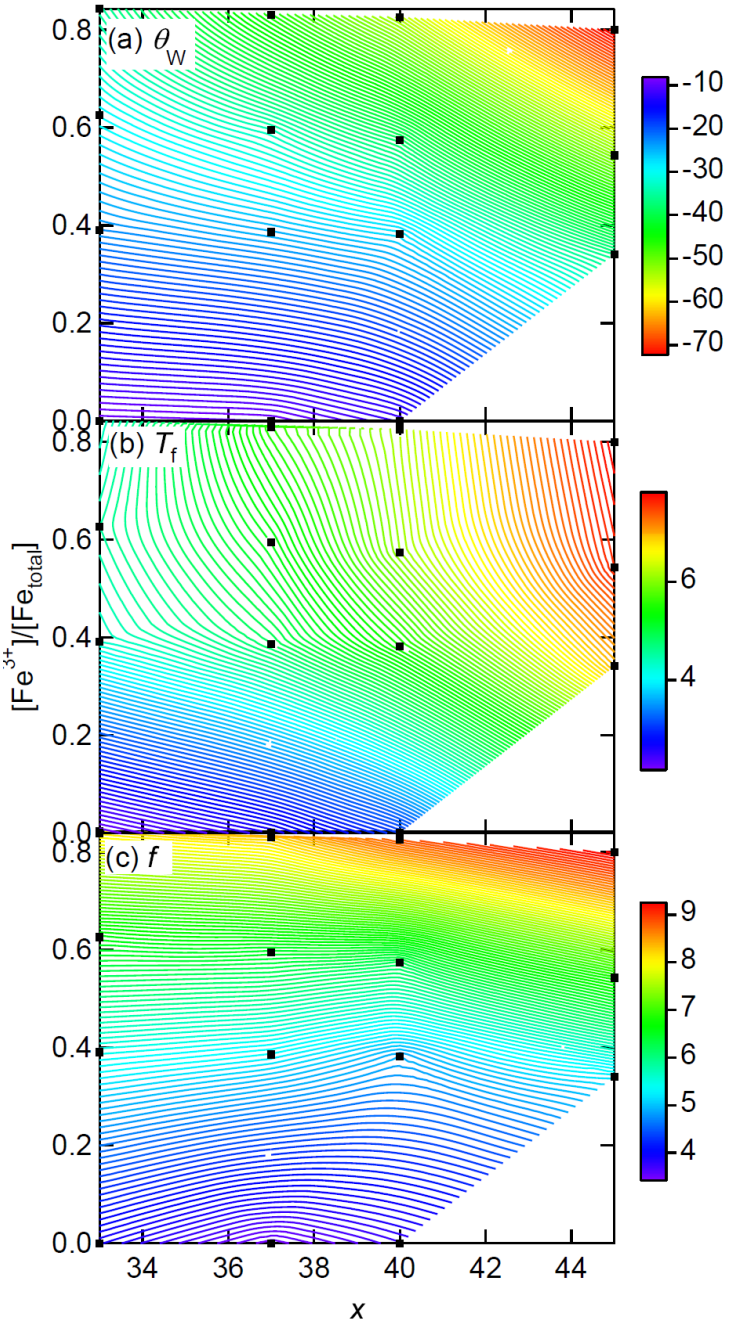

Figure 1.16: Depicted as a counter plot is the dependence of Weiss temperature θ_W, spin freezing temperature T_f and magnitude of magnetic frustration f on the ratio of iron ions per all cations in molar percent x and the ratio of Fe^{3+} ions per total iron ions $[Fe^{3+}]/[Fe_{total}]$. Closed circles show observational points.

$[Fe^{3+}]/[Fe_{total}]$ are related to M_B; the Fe^{2+} and Fe^{3+} ions have the electron configurations of $3d^6$ and $3d^5$ in high-spin states, leading to S=2 and S=5/2, respectively. Figures 1.16(a) and (b) illustrate counter plots of θ_W and T_f on the x-$[Fe^{3+}]/[Fe_{total}]$ planes, respectively. As can be seen in Fig. 1.16(a), the value of $|\theta_W|$, which reflects the strength of effective interactions among magnetic moments, becomes larger with increasing x or $[Fe^{3+}]/[Fe_{total}]$; the higher $|\theta_W|$ is found in the right upper part of Fig. 1.16(a). On the other hand, the variation of T_f on the x-$[Fe^{3+}]/[Fe_{total}]$ plane is rather different from that of $|\theta_W|$: T_f tends to be higher with an increase in x while it just slightly depends on $[Fe^{3+}]/[Fe_{total}]$, as shown in Fig. 1.16(b).

Here, it is worth introducing the parameter $f = |\theta_W|/T_f$. The parameter f is regarded as an empirical measure of magnetic frustration: a large value of f means a strong frustration, as discussed for a number of geometrically frustrated magnets [18]. The counter plot of f on the x-$[Fe^{3+}]/[Fe_{total}]$ plane is shown in Fig. 1.16(c). It should be noted that f approximately depends only on $[Fe^{3+}]/[Fe_{total}]$, and f becomes higher when $[Fe^{3+}]/[Fe_{total}]$ is increased. This behavior is consistent with the fact that almost all the geometrical frustrated magnets with $f > 10$ contain highly isotropic ions such as S-state ions like Fe^{3+} and Mn^{2+} as well as transition metal ions with fully quenched orbital moments like Cr^{3+} [18,33]. When magnetic ions such as Fe^{2+} and Co^{2+} have a finite orbital angular momentum, single-ion anisotropy arises from crystal field effects and spin-orbital coupling [34,35]. Assuming that the exchange interaction is isotropic, i.e. Heisenberg-like, the single-ion anisotropy is introduced into the Hamiltonian as follows:

$$H = -\sum_{(i,j)} J_{ij} S_i \cdot S_j + \sum_i D_i \left(S_i^{\,Z}\right)^2, \qquad (1.17)$$

where J_{ij} is the exchange coupling constant between the sites i and j, S_i, the spin operator at the site i, D_i the single-ion anisotropy constant at the site i, and S_i^Z the component of spin operator along the direction of the easy axis or perpendicular to the easy plane at the site i. The single-ion anisotropy term stimulates the spin freezing,

thereby resulting in the suppression of magnetic frustration. There is no orbital angular momentum due to the spin-orbit coupling in the presence of a crystal field for Fe^{3+} ions as long as they are in a high-spin $3d^5$ state. So, the effects of single-ion anisotropy are expected to be stronger for Fe^{2+} ions than for Fe^{3+} ions. Besides, the single-ion anisotropy influences the spin dynamics, as discussed in molecular magnets [36,37]. If the author assumes the uniaxial single-ion anisotropy for Fe^{2+} ions, the temperature dependence of microscopic relaxation time of Fe^{2+} ions is expected to be modified by incorporating the single-ion anisotropy as the thermal activation energy as follows [36, 37]:

$$\tau_{0i}(T) = \tau_0 \exp\left(\frac{|D_i|S_i^{\,2}}{k_B T}\right). \qquad (1.18)$$

Actually, lithium iron phosphate ($LiFePO_4$) has the single-ion anisotropy with easy axis. As seen in Table 1.5, τ_0 becomes longer with a decrease in $[Fe^{3+}]/[Fe_{total}]$. However, it is found to be difficult to analyze the temperature dependence of τ of 33Fe67PC and 40Fe60PC using the equation obtained by combining Eqs. (1.13) and (1.18), partly because D_i has a wide distribution depending on the Fe^{2+} site due to the random structure of glasses. The dependence of f and τ_0 on $[Fe^{3+}]/[Fe_{total}]$ is qualitatively explained by the single-ion anisotropy of Fe^{2+} ions.

1.2.4 Conclusion

In this section, the magnetic properties of mixed valence iron phosphate glasses have been investigated. The scaling analyses of relaxation time and nonlinear susceptibility yield critical exponents similar to those reported for conventional spin glasses, indicating the presence of spin glass transition at low temperatures. The observation of magnetic aging and memory effects reinforce the spin glass nature of the

present glasses. The experimental data of magnetic specific heat reveal that the deviation of magnetic susceptibility from Curie-Weiss behavior means the emergence of short-range correlation in the present glasses. The magnitude of magnetic frustration is strongly dependent of the valence states of iron ions in the glasses. The magnetic frustration is suppressed by the single-ion anisotropy effects of the Fe^{2+} ions less isotropic than the Fe^{3+} ions.

References in Section 1.2

[1] V. Cannella and J. A. Mydosh, *Phys. Rev. B* **6**, 4220 (1972).

[2] R. Mathieu, P. Jönsson, D. N. H. Nam, and P. Nordblad, *Phys. Rev. B* **63**, 092401 (2001).

[3] K. Jonason, E. Vincent, J. Hammann, J. P. Bouchaud, and P. Nordblad, *Phys. Rev. Lett.* **81**, 3243 (1998).

[4] L. W. Bernardi, H. Yoshino, K. Hukushima, H. Takayama, A. Tobo and A. Ito, *Phys. Rev. Lett.* **86**, 720 (2001).

[5] S. Miyashita and E. Vincent, *Eur. Phys. J. B* **22**, 203 (2001).

[6] P. E. Jönsson, R. Mathieu, P. Nordblad, H. Yoshino, H. A. Katori, and A. Ito, *Phys. Rev. B* **70**, 174402 (2004).

[7] J. J. Hopfield, *Proc. Natl. Acad. Sci. USA* **79**, 2554 (1982).

[8] J. A. Mydosh, *Spin glasses: an Experimental Introduction* (Taylor &Francis Ltd., London, 1993).

[9] R. A. Verhelst, R. W. Kline, A. M. de Graaf and H. O. Hooper, *Phys. Rev. B* **11**, 4427 (1975).

[10] J. Ferre, J. Pommier, J. P. Renard, and K. Knorr, *J. Phys. C: Solid State phys.* **13**, 3697 (1980).

[11] A. Ito, E. Torikai, H. Yamauchi, and Y. Shono, *J. Phys. C: Solid State phys.* **15**, 2759 (1982).

[12] J. P. Sanchez and J. M. Friedt, *J. Physique* **43**, 1707 (1982).

[13] J. P. Sanchez, J. M. Friedt, R. Horne, and A. J. Van Duyneveldt, *J. Phys. C* **17**, 127 (1984).

[14] P. Beauvillain, C. Dupas, J. P. Renard, and P. Veillet, *Phys. Rev. B* **29**, 4086 (1984)

[15] C. Dupas, J. P. Renard, G. Fonteneau, and J. Lucas, *J. Magn. Magn. Mater.* **27**, 152 (1982)

[16] F. A. Wedgwood and A. C. Wright, *J. Non-Cryst. Solids* **21**, 95 (1976).

[17] J. L. Shaw, A. C. Wright, R. N. Sinclair, G. K. Marasinghe, D. Holland, M. R. Lees, and C. R. Scales, *J. Non-Cryst. Solids* **345&346**, 245 (2004).

[18] A. P. Ramirez, *Annu. Rev. Mater. Sci.* **24**, 453 (1994).

[19] M. Karabulut, G. K. Marasinghe, C. S. Ray, D. E. Day, G. D. Waddill, C. H. Booth, P. G. Allen, J. J. Bucher, D. L Caulder, and D. K. Shuh, *J. Non-Cryst. Solids* **306**, 182 (2002).

[20] S. Nagata, P. H. Keesom, and H. R. Harrison, *Phys. Rev. B* **19**, 1633 (1979).

[21] K. Gunnarsson, P. Svedlindh, P. Nordblad, L. Lundgren, H. Aruga, and A. Ito, *Phys. Rev. Lett.* **61**, 754 (1988).

[22] P. Nordblad, *J. Phys.: Condens. Mater*. **16**, 715 (2004).

[23] G. F. Goya and V. Sagredo, *Phys. Rev. B* **64**, 235208 (2001).

[24] M. Suzuki, *Prog. Theor. Phys.* **58**, 1151 (1977).

[25] P. Beauvillain, C. Chappert, J. P. Renard, and J. Seiden, *J. Magn. Magn. Mater.* **54-57**, 127 (1986).

[26] A. Mauger, J. Ferre, and P. Beauvillain, *Phys. Rev. B* **40**, 862 (1989).

[27] M. Sasaki, P. E. Jönsson, H. Takayama, and H. Mamiya, *Phys. Rev. B* **71**, 104405 (2005).

[28] L. E. Wenger and P. H. Keesom, *Phys. Rev. B* **13**, 4053 (1976).

[29] G. W. Hunter, L. E. Wenger, and W. D. Wallace, *Phys. Rev. B* **36**, 5750 (1987).

[30] J. E. Greedan, N. P. Raju, A. Maignan, Ch. Simon, J. S. Pedersen, A. M. Niraimathi, E. Gmelin, and M. A. Subramanian, *Phys. Rev. B* **54**, 7189 (1996).

[31] L. B. Luo, Y. G. Zhao, G. M. Zhang, S. M. Guo, Z. Li, and J. L. Luo, *Phys. Rev. B* **75**, 125115 (2007).

[32] N. A. Chernova, J. K. Ngala, P. Y. Zavalij, and M. S. Whittingham, *Phys. Rev. B* **75**, 014402 (2007).

[33] I. S. Hagemann, P. G. Khalifah, A. P. Ramirez, and R. J. Cava, *Phys. Rev. B* **62**, 771 (2000).

[34] J. Li, V. O. Garlea, J. L. Zarestky, and D. Vaknin, *Phys. Rev. B* **73**, 024410 (2006).

[35] G. Liang, K. Park, J. Li, R. E. Benson, D. Vaknin, J. T. Markert, and M. C. Croft, *Phys. Rev. B* **77**, 064414 (2008).

[36] C. Coulon, R. Clérac, L. Lecren, W. Wernsdorfer, and H. Miyasaka, *Phys. Rev. B* **69**, 132408 (2004).

[37] M. Mito, H. Deguchi, T. Tajiri, S. Takagi, M. Yamashita, and H. Miyasaka, *Phys. Rev. B* **72**, 144421 (2005).

Section 1.3 Anomalous magnetic transition of Fe_2O_3-Bi_2O_3-B_2O_3 system

1.3.1 Introduction

Magnetic oxide glasses can be regarded as a system in which the magnetic moments localized at cations are randomly distributed in the insulating host glass structure. Short-range antiferromagnetic superexchange interactions are usually dominant in magnetic oxide glasses [1,2]. Due to the random distribution of magnetic ions and the antiferromagnetic interactions, magnetic frustrations occur in the configuration of magnetic moments: the antiferromagnetic interaction between two nearest-neighboring ions can be altered into ferromagnetic coupling by an additional magnetic ion present nearby the two ions. Therefore, most of magnetic oxide glasses satisfy the prerequisite for the spin glass transition: randomness and frustration [3]. Actually, the freezing of randomly oriented magnetic moments was observed at very low temperatures in the magnetic oxide glasses containing a sufficiently large amount of 3*d* transition metal ions such as Fe, Mn, and Co ions [1,2]. In Sections 1.1 and 1.2, the author have indicated that binary iron tellurite and phosphate glasses manifest unique properties relevant to the spin dynamics including magnetic aging and memory effects as well as critical slowing down. These properties are similar to those observed in the canonical spin glasses such as the *Au*-Fe alloys, similarly to conventional spin glasses.

As mentioned in General Introduction as well as Sections 1.1 and 1.2, magnetic oxide glasses often exhibit transitions like those of spin glasses. On the other hand, 'ferromagnetic' behavior even at room temperature has been reported in some amorphous oxides containing Fe_2O_3 and Bi_2O_3 such as Fe_2O_3-Bi_2O_3-ZnO [4], Fe_2O_3-Bi_2O_3-CaO [5], Fe_2O_3-Bi_2O_3-Li_2O [6,7], and Fe_2O_3-Bi_2O_3-CuO [8] systems in

the late eighties and early nineties. Nakamura *et al*. [9] concluded that the ferromagnetic behavior in the Fe_2O_3-Bi_2O_3-CaO and Fe_2O_3-Bi_2O_3-Li_2O systems was attributed to some ferrimagnetic nanocrystalline phases embedded in the amorphous matrix, although the lattice images of the regions they regarded as the nanocrystals in their transmission electron micrographs are not so clear. It should be noted that these iron-containing amorphous oxides do not exhibit any hyperfine sextet splittings in their Mössbauer spectra at room temperature, evidently suggesting that the ferromagnetic order does not extend over a long range, but is restricted within a localized region.

This section describes experimental results in detail about magnetic and structural properties for $x$$Fe_2O_3$·(80.0-$x$)$Bi_2O_3$·20.0$B_2O_3$ (mol%) bulk glasses with $18.2 \leq x \leq 40.0$. The magnetic behavior of $x$$Fe_2O_3$·(80.0-$x$)$Bi_2O_3$·20.0$B_2O_3$ glasses is describable in terms of the spin glass transition due to individual magnetic moments of Fe^{3+} ions and/or small spin clusters as well as the glassy behavior of magnetic clusters where the spins of Fe^{3+} ions are locally frozen in very small regions; the glass of $x = 18.2$ consists of a spin glass phase at low temperatures, while the contribution of magnetic clusters to the magnetic properties becomes more significant with an increase in the content of Fe_2O_3, x. The coexistence of spin glass phase and magnetic clusters exhibiting the superspin glass-like behavior is clearly reflected by the double transitions observed in the temperature dependence of ac susceptibility. Detailed experiments on the 32.0Fe_2O_3·48.0Bi_2O_3·20.0B_2O_3 glass reveal that the magnetic clusters are mainly amorphous and that very few clusters are attributed to nanocrystals. The magnetic structure of the present glass system is unprecedented for the magnetic oxide glass systems in a sense that both a spin glass phase and magnetic clusters exhibiting a collective superspin glass-like freezing coexist in a single glass matrix.

1.3.2 Experimental procedure

Glasses whose nominal compositions were represented by $x$$Fe_2O_3$·(80.0-$x$)$Bi_2O_3$·20.0$B_2O_3$ in mol% ($18.2 \leq x \leq 40.0$), hereafter denoted as xFeBiB for the convenience, were prepared from reagent grade Fe_2O_3, Bi_2O_3, and B_2O_3 powders by using a conventional melt-quenching method. Appropriate amounts of the starting materials were mixed thoroughly and the mixture was melted at 1150 °C for 1 h in a platinum crucible. The melt was poured onto a stainless steel plate and cooled in air. In order to explore the structural properties of the resultant glasses, X-ray diffraction (XRD) patterns were recorded by using CuK_α radiation, and plane-view transmission electron microscope (TEM) observations were performed. ^{57}Fe Mössbauer spectroscopy was carried out at room temperature employing a ^{57}Co in metallic Rh as a γ-ray source so as to estimate the valence states and coordination environments of Fe ions in the glasses. The velocity scale was calibrated by using the spectrum of α-Fe measured at room temperature. Magnetic properties including magnetic aging and memory effects and exchange bias effect were examined by using a superconducting quantum interference device (SQUID) magnetometer.

1.3.3 Results and discussion

1.3.3.1 X-ray diffraction and TEM observation

Figure 1.17 illustrates XRD patterns for 18.2FeBiB, 30.0FeBiB, 32.0FeBiB and 40.0FeBiB. The XRD diagram for 18.2FeBiB manifests only halo pattern, suggesting that this sample is amorphous from a point of view of XRD. Only halo patterns seem to appear in the XRD diagrams of 30.0FeBiB and 32.0FeBiB at a glance, although a careful look at these patterns reveals that very weak diffraction lines attributed to α-Fe_2O_3 are present at about 2θ=61.5 and 63.6 ° [see the inset of Fig.1.17]. The low

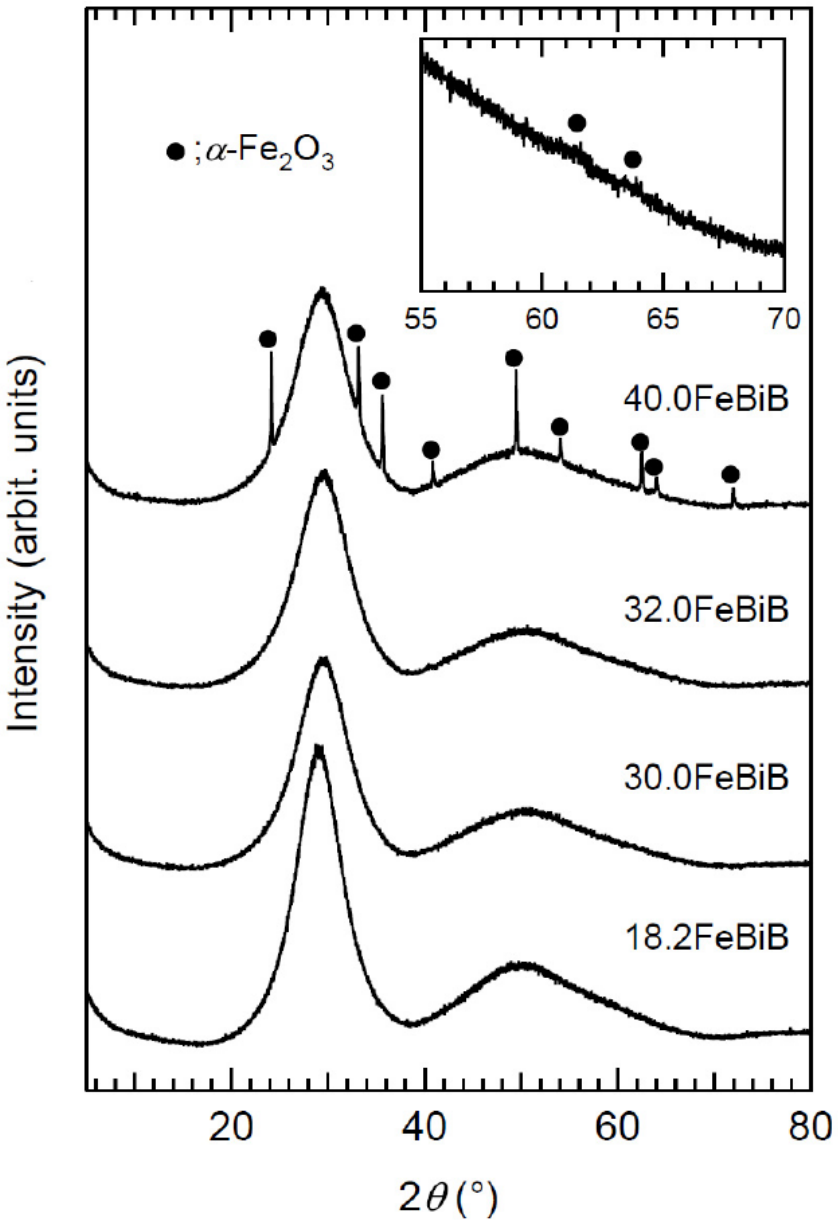

Figure 1.17: X-ray diffraction patterns of 18.2FeBiB, 30.0FeBiB, 32.0FeBiB and 40.0FeBiB. The inset illustrates magnification of the XRD pattern for 32.0FeBiB in the range of 2θ=55°~70°.

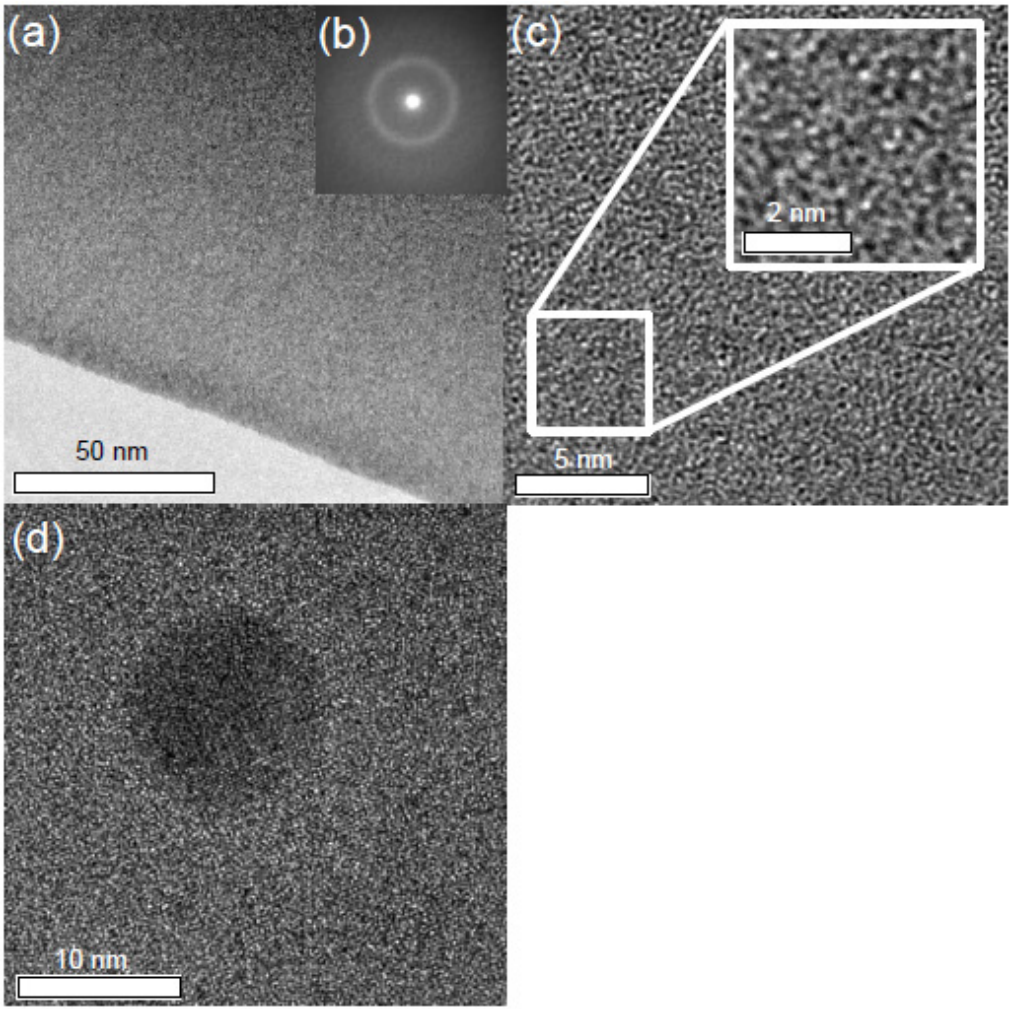

Figure 1.18: (a) TEM image and (b) selected area electron diffraction pattern of a typical region of 32.0FeBiB, and TEM image of (c) an amorphous region of 32.0FeBiB and (d) a nanocrystalline phase precipitated in the amorphous matrix.

intensity of these peaks indicates that the amount of α-Fe_2O_3 crystalline phases precipitated in these glasses is very small. Actually, TEM observation for 32.0FeBiB indicates that almost all the regions observed consist of an amorphous phase as shown in Figs. 1.18(a), (b) and (c). Only one crystalline phase of about 10 nm were observed in the plane-view observation by which an area of about 10 μm^2 was explored over the sample [Fig. 1.18(d)]. The XRD pattern for 40.0FeBiB clearly depicts the diffraction lines corresponding to α-Fe_2O_3 in addition to the halo pattern. The glass forming region of the present system obtained in this study is found to be smaller than those reported previously [10]. The amount of α-Fe_2O_3 precipitated is apt to increase with increasing the value of x, as expected.

1.3.3.2 ^{57}Fe Mössbauer spectroscopy

The ^{57}Fe Mössbauer spectra for xFeBiB are shown in Fig. 1.19. The spectra for the xFeBiB samples with x<40.0 manifest a paramagnetic doublet attributable to Fe^{3+} ion, while absorption peaks due to Fe^{2+} ion are not observed. The spectrum for 40.0FeBiB clearly shows a hyperfine sextet as well as a paramagnetic doublet attributable to Fe^{3+} ion. The peak positions of hyperfine sextet are identified as those of α-Fe_2O_3, being consistent with the result of XRD. The values of isomer shift for the paramagnetic Fe^{3+} ions are about 0.32 mm/s regardless of the value of x, suggesting that the Fe^{3+} ions mainly lie on the tetrahedral sites surrounded by O^{2-} ions in the present glasses in contrast to those in α-Fe_2O_3 where Fe^{3+} ions occupy the octahedral sites.

1.3.3.3 Temperature dependence of dc susceptibility

In Fig. 1.20, the dependence of dc susceptibility on temperature is illustrated for xFeBiB with varied x values. Both field cooling (FC) and zero field cooling (ZFC) were performed with the magnetic field H_{dc} of 50 Oe applied. The temperature dependence of dc susceptibility for 18.2FeBiB is similar to those observed in spin

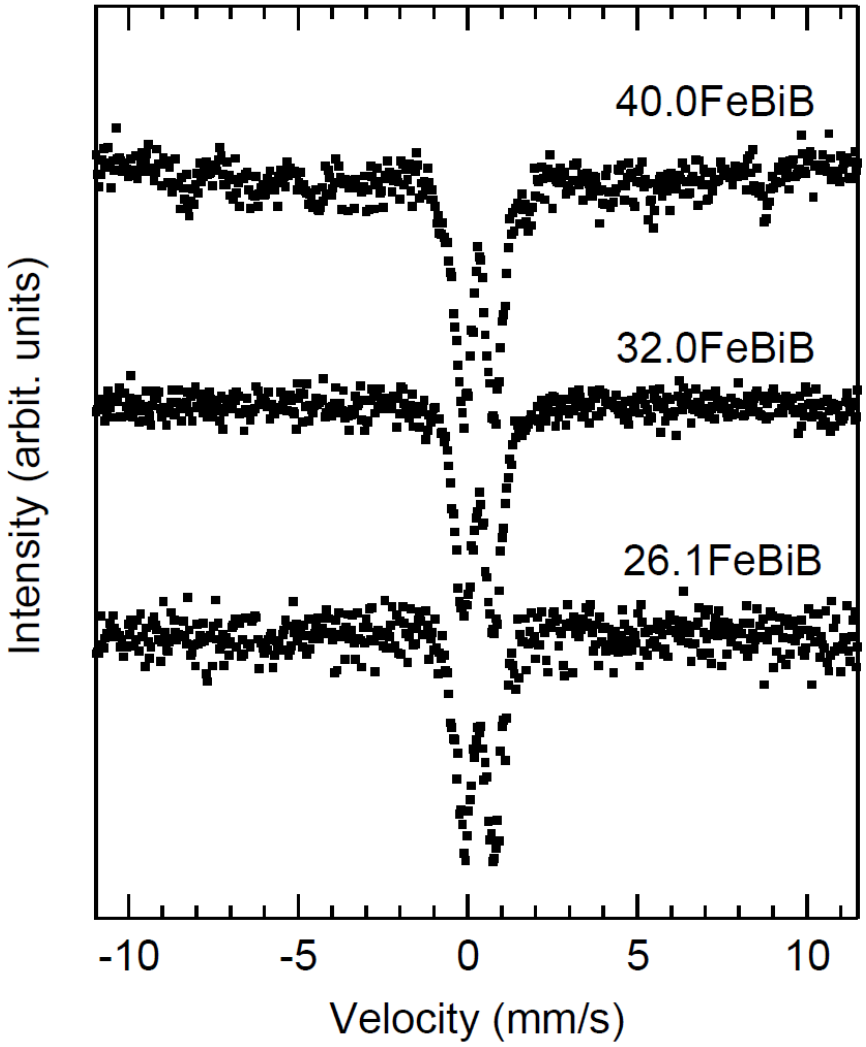

Figure 1.19: ^{57}Fe Mössbauer spectra of 26.1FeBiB, 32.0FeBiB and 40.0FeBiB at room temperature.

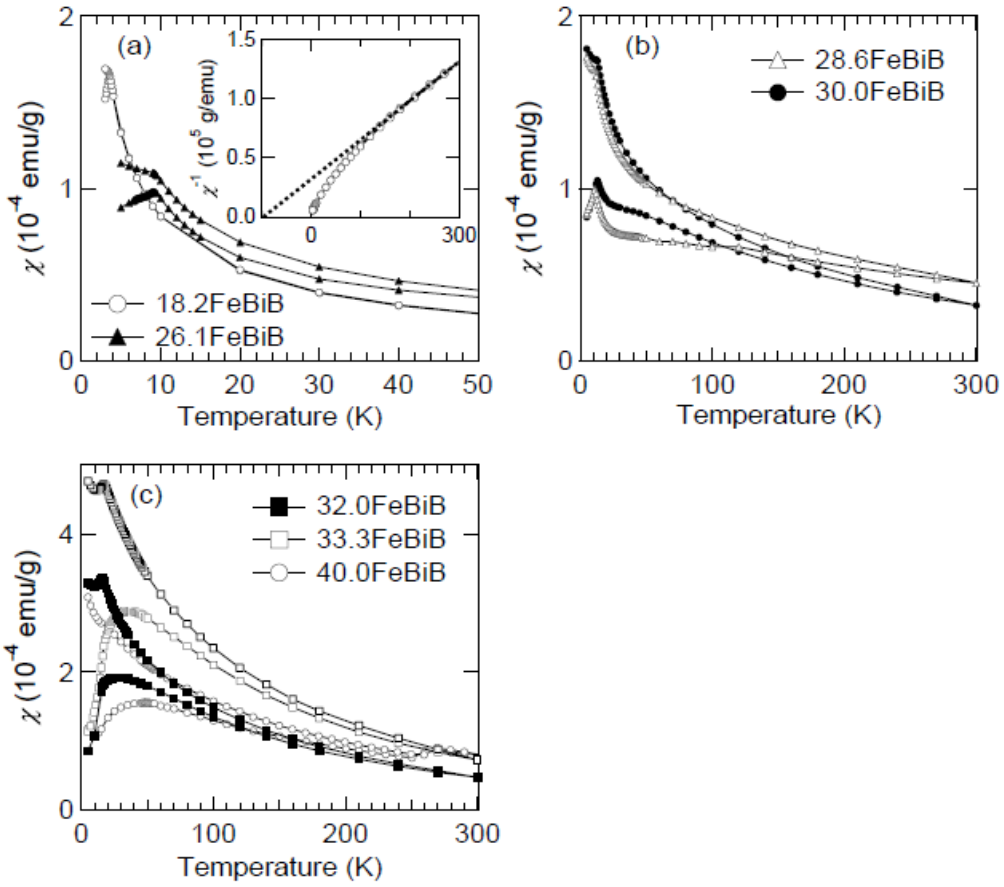

Figure 1.20: Temperature dependence of ZFC and FC dc susceptibilities for the *x*FeBiB with (a) *x*=18.2, 26.1, (b) 28.6, 30.0, (c) 32.0, 33.3 and 40.0 measured at H_{dc}=50 Oe. The inset of Fig. 1.20(a) shows the temperature dependence of inverse dc susceptibility for 18.2FeBiB glass. The broken line presents the fit of the experimental data to Eq. (1.19).

glasses; the susceptibility for ZFC shows the cusp-like maximum at T_{cZFC}=3.5 K and the susceptibility for FC deviates from that for ZFC below T_{cZFC} [see Fig. 1.20(a)]. This kind of behavior is also seen in other magnetic oxide glasses such as the Fe_2O_3-TeO_2 system, as shown in Section 1.1. The inset of Fig. 1.20(a) depicts the inverse dc susceptibility as a function of temperature for 18.2FeBiB. The linear relationship at high temperatures reveals that the glass is paramagnetic in the high temperature region; the linear part is describable in terms of the following Curie-Weiss law,

$$\frac{1}{\chi} = \frac{3k_B(T-\theta)}{NM_B{}^2\mu_B{}^2}, \qquad (1.19)$$

where χ is the dc susceptibility, T is the temperature, θ is the Weiss temperature, N is the number of magnetic ions per unit mass, μ_B is the Bohr magneton, M_B is the effective number of Bohr magnetons, and k_B is the Boltzmann constant. The dashed line represents the best fit of Eq. (1.19) to the experimental data with M_B=4.7 and θ_W=-97 K. The value of M_B is significantly smaller than that expected from the spin-only value of Fe^{3+} ion, i.e., 5.9. This implies that a part of magnetic moments of the Fe^{3+} ions form spin clusters at high temperatures near the room temperature. The negative value of θ_W means that the antiferromagnetic interaction is dominant among the Fe^{3+} ions in the glass. The ratio of $|\theta_W|$ to the Néel temperature or the spin glass transition temperature is regarded as a measure of magnetic frustration, i.e., a large ratio means a strong frustration, as discussed for a number of geometrically frustrated magnets [11]. In the present case, $|\theta_W|/T_{cZFC}$=28 is much larger than unity. A similar result was obtained for the Fe_2O_3-TeO_2 glasses, for which $|\theta_W|/T_{cZFC}$=16 [see Section 1.1]. In oxide glasses, the antiferromagnetic superexchange interactions via oxide ions are predominant among the magnetic ions. A combination of these interactions with the random distribution of magnetic ions leads to the magnetic frustration which suppresses the magnetic transition toward lower temperatures.

In contrast to the sharp cusp observed for 18.2FeBiB, the ZFC susceptibilities for *x*FeBiB with *x*=32.0, 33.3 and 40.0 exhibit rather broad peaks at T_{pZFC}=28, 36 and 50 K, respectively [see Fig. 1.20(c)]. It is noticeable that the ZFC and FC susceptibilities depart from each other just below 300 K, the highest measurement temperature in the present experiments. Such behavior implies the presence of magnetic clusters similar to that observed in many magnetic nanoparticles systems with a wide distribution of particle size. A monotonous increase in T_{pZFC} with increasing *x* indicates that the higher the value of *x*, the larger the average volume of magnetic clusters in *x*FeBiB. The ZFC susceptibility at T_{pZFC} for 40.0FeBiB is lower than those for 32.0FeBiB and 33.3FeBiB. This fact is attributed to the precipitation of α-Fe_2O_3 as clearly detected by the XRD measurement and the Mössbauer spectroscopy for 40.0FeBiB. This is also confirmed from Fig. 1.20(c), where the ZFC and FC susceptibilities for 40.0FeBiB show a dip in the temperature range from 270 to 250 K, suggesting that the magnetic behavior of 40.0FeBiB is significantly influenced by the α-Fe_2O_3 crystal which has the magnetic anomaly called Morin point at 250 K [12]. Therefore, the amount of Fe^{3+} ions present in the antiferromagnetic α-Fe_2O_3 phase is larger in 40.0FeBiB than in 32.0FeBiB and 33.3FeBiB, leading to the smaller ZFC susceptibility at T_{pZFC}. A close look at the FC susceptibility curves for 32.0FeBiB and 33.3FeBiB reveals that cusp-like maxima are observed at T_{cFC}=15 and 17 K, respectively. For both samples, T_{cFC} is lower than T_{pZFC}. As discussed later, T_{cFC} is thought to be a spin glass transition temperature.

As shown in Fig. 1.20(b), the susceptibility curves for 26.1FeBiB, 28.6FeBiB and 30.0FeBiB seem to be explained in terms of the coexistence of spin glass phase and magnetic clusters, the former and the latter of which are observed in 18.2FeBiB and 32.0FeBiB, respectively [see Figs. 1.20(a) and (c)]. The ZFC susceptibilities for 26.1FeBiB, 28.6FeBiB and 30.0FeBiB manifest cusp-like maxima at T_{cZFC}=9, 11 and 13 K, respectively, and the susceptibilities in the FC run separate from those in the ZFC run at temperatures much higher than T_{cZFC}.

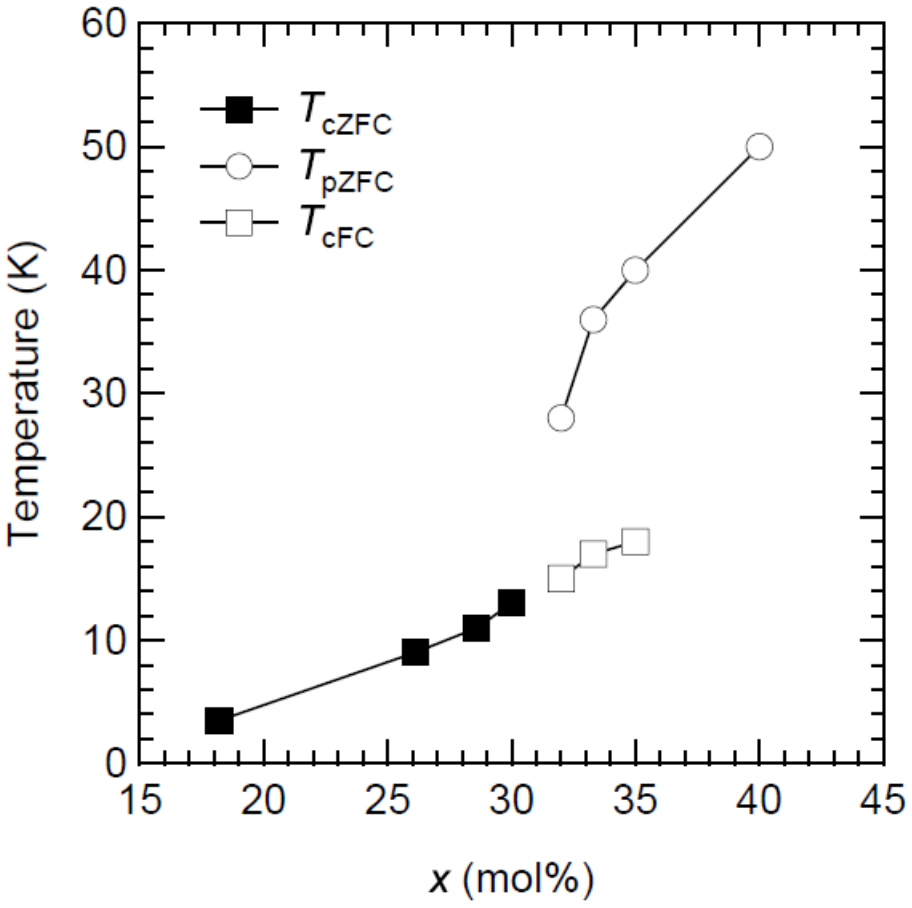

Figure 1.21: Variation of T_{cZFC}, T_{pZFC} and T_{cFC} with Fe_2O_3 content, x. The definitions of these temperature parameters are denoted in the text.

Figure 1.21 illustrates the relationship between T_{cZFC}, T_{pZFC} and T_{cFC} and the content of Fe_2O_3, x. All the characteristic temperatures monotonically increase as x is increased. It is noteworthy that T_{cZFC} and T_{cFC} appear to lie on the same curve although these two characteristic temperatures were evaluated through the different procedures. This suggests that T_{cZFC} and T_{cFC} arise from the same origin, that is, the spin glass transition.

1.3.3.4 Temperature dependence of ac susceptibility

In order to elucidate the spin dynamics for the present glasses, the ac susceptibilities as a function of temperature were examined for 18.2FeBiB and 32.0FeBiB. The amplitude of ac magnetic field H_{ac} was kept to be 3 Oe and the ac frequency f was varied in the range from 0.3 to 1000 Hz. Figure 1.22 shows the temperature dependence of the real part of ac susceptibilitiy for 18.2FeBiB. As can be seen, the frequency-dependent spin-freezing temperature $T_f(f)$, defined as a temperature at which the real part of ac susceptibility manifests a maximum, shifts to a higher temperature side with increasing f. It is thought that $T_f(f)$ corresponds to T_{cZFC} in the dc susceptibility for 18.2FeBiB. Figures 1.23(a) and (b) depict the temperature dependence of the real and imaginary parts of ac susceptibilities for 32.0FeBiB, respectively. A systematic shift of the broad peak is obvious in Fig. 1.23(a). This peak stems from the same origin as T_{pZFC} in Fig. 1.20(c). In addition, a close inspection reveals that a shoulder and another peak appear in the real and imaginary parts of ac susceptibilities for 32.0FeBiB, respectively, in the temperature range lower than $T_f(f)$ [see the inset of Fig. 1.23(b)]. This corresponds to the cusp-like maximum at T_{cFC}=15 K in the FC curve of dc susceptibility [see Fig. 1.20(c)].

The relative shift of $T_f(f)$ per decade of f, i.e., $\Psi=(\Delta T_f/ T_f)/\Delta(\log f)$ [14], for the real part of ac susceptibility was determined to be 0.029 and 0.085 for 18.2FeBiB and 32.0 FeBiB, respectively. The former value is in the range of those obtained for the spin glasses, i.e., $\sim 10^{-3}$-10^{-2}, while the latter value is in an intermediate range between the

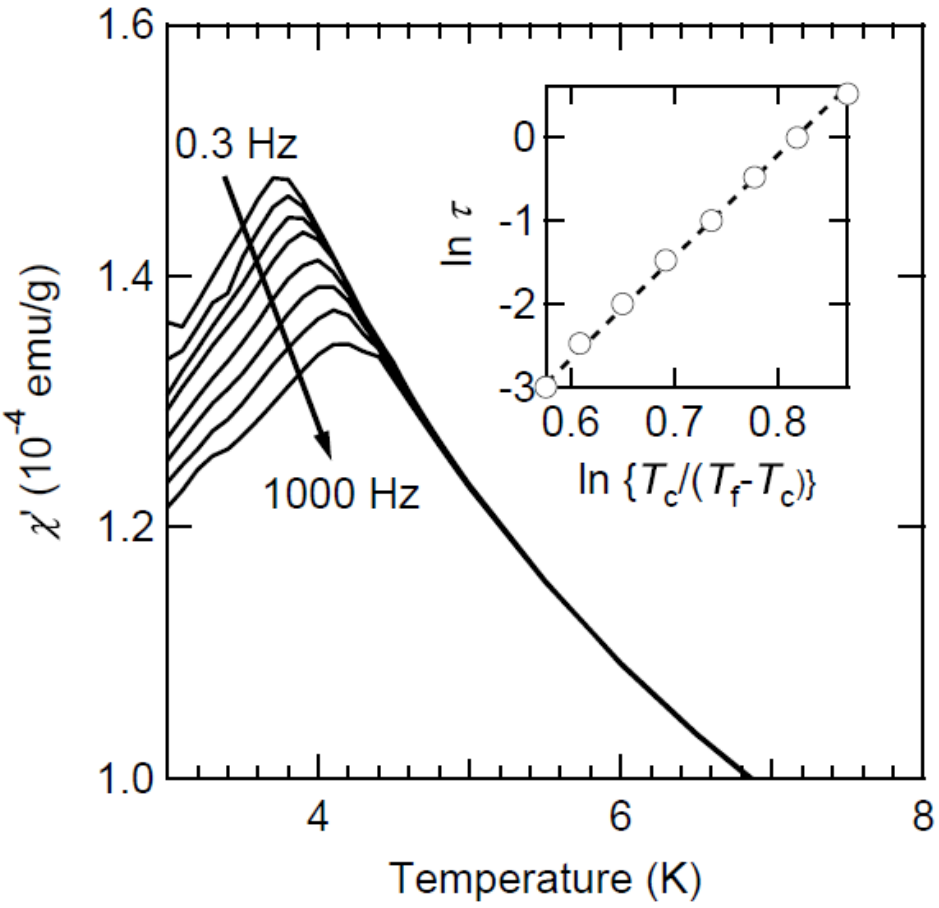

Figure 1.22: Temperature dependence of real part of ac susceptibility for 18.2FeBiB glass at H_{ac}=3 Oe. The frequency f is 0.3, 1, 3, 10, 30, 100, 300 and 1000 Hz (from top to bottom). The inset illustrates the relationship between maximum relaxation time τ and spin freezing temperature $T_f(f)$ based on the critical slowing down analysis. The broken line shows the result of analysis by Eq. (1.20).

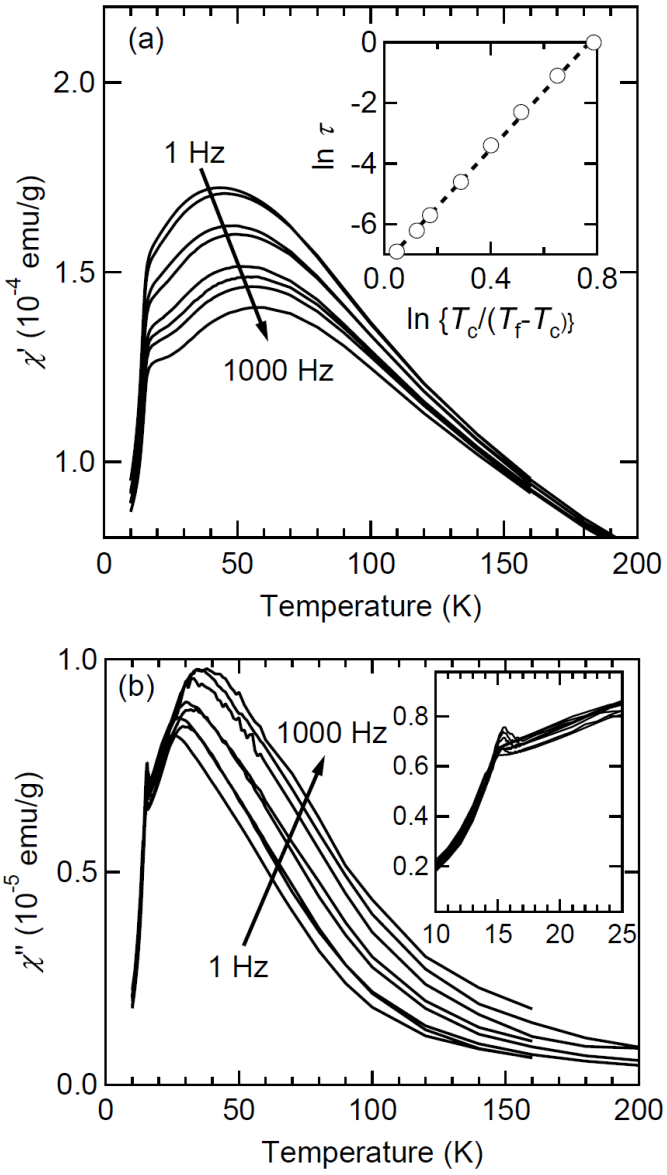

Figure 1.23. Temperature dependence of (a) real and (b) imaginary parts of ac susceptibility for 32.0FeBiB at H_{ac}=3 Oe. The frequency f is 1, 3, 10, 30, 100, 300, 500 and 1000 Hz (from top to bottom in (a) and vice versa in (b)). The inset of Fig. 1.23(a) illustrates the relationship between maximum relaxation time τ and spin freezing temperature $T_f(f)$ based on the critical slowing down analysis. The inset of Fig. 1.23(b) shows a magnified figure of temperature variation of imaginary part of ac susceptibility in the range from 10 to 25 K.

spin glasses and the superparamagnets, i.e., ~10^{-1} [3,13,14]. For the magnetic transition in the vicinity of T_{cFC}=15 K in 32.0FeBiB, it is difficult to evaluate the value of Ψ in the same way as mentioned above, because the real part of ac susceptibility does not exhibit a distinguishable peak but appears as a shoulder near T_{cFC}. However, Ψ=0.017 could be roughly determined by setting T_f equal to the peak temperature of out-of phase component. This value suggests that the transition near T_{cFC} is categorized into the spin glass transition.

The analysis of the data in terms of the power law,

$$\tau = \tau_0 \left(\frac{T_f(f) - T_c}{T_c} \right)^{-z\nu}, \qquad (1.20)$$

based on the dynamic scaling hypothesis yields $z\nu$=11.9, T_C=3.3 K and τ_0=1.6×10^{-10}s for 18.2FeBiB and $z\nu$=9.5, T_C=30 K and τ_0=6.6×10^{-4}s for 32.0FeBiB. The value of $z\nu$ for 18.2FeBiB is comparable with the typical values of canonical spin glasses [15,16] while τ_0 is slightly longer than the spin flip time of individual magnetic moments belonging to atoms or ions, i.e., 10^{-13}~10^{-12} s, implying that small spin clusters are involved in the spin glass transition of 18.2FeBiB. On the other hand, the value of τ_0=6.6×10^{-4}s for 32.0FeBiB is similar to but somewhat larger than those reported for strongly interacting nanoparticles systems and superspin glasses, for which τ_0~10^{-6}s [15,17]. The larger value of τ_0 (=$10^{-4.7}$) was reported for Fe_xC_{1-x} (x~0.2-0.3) nanoparticles dispersed in xylene with the volume fraction of 5 vol.%, suggesting that the behavior was attributed to a mixture of collective and single-particle dynamics [17]. It was proposed that the strong inter-particle interactions arising from the regions where the number density of the particles is higher than its average may enhance the local correlation length and render the relaxation time longer than expected from the volume fraction of particles when a homogeneous dispersion is assumed. In 32.0FeBiB, both cooperative and non-cooperative characteristics are also seen: the former appears in the magnetic aging and memory effects as observed in the strongly interacting

nanoparticles systems and superspin glasses (shown below), and the latter is reflected by the absence of plateau of the FC susceptibility below T_{pZFC} as observed in the non-interacting superparamagnets. Therefore, in the present case, the local correlation of magnetic clusters can contribute to the larger value of τ_0.

The Vogel-Fulcher empirical law is described as follows:

$$\tau = \tau_0 \exp\left(\frac{E_a}{k_B (T - T_0)} \right), \qquad (1.21)$$

where E_a and T_0 are the fitting parameters associated with energy and temperature. The physical meanings of these parameters are not completely clear although it is suggested that E_a and T_0 present activation energy of magnetic clusters and inter-cluster interaction or a true transition temperature, respectively. Fitting the experimental data to Eq. (1.21) yields the parameter values of τ_0=1.0×10^{-7}s, E_a/k_B =320 K and T_0=25 K. On the other hand, the analysis by using the Arrhenius law:

$$\tau = \tau_0 \exp\left(\frac{E_a}{k_B T} \right), \qquad (1.22)$$

results in the fitting parameters of τ_0=1.3×10^{-12}s and E_a/k_B =1200 K. The activation energy seems to be too large. It is clear that the Arrhenius law, which deals with the relaxation of non-interactive magnetic clusters, fails to explain the temperature dependence of relaxation time for 32.0FeBiB although the validness of the analysis by the Voger-Fulcher law is not discussed here. This fact implies the existence of inter-cluster interactions in 32.0FeBiB.

1.3.3.5 ZFC memory effects

To get an insight into the nature of magnetically ordered phase of 32.0FeBiB, the zero-field cooling memory experiment proposed by Mathieu *et al* [18] has been performed. In this experiment, the system is cooled in zero magnetic field from high

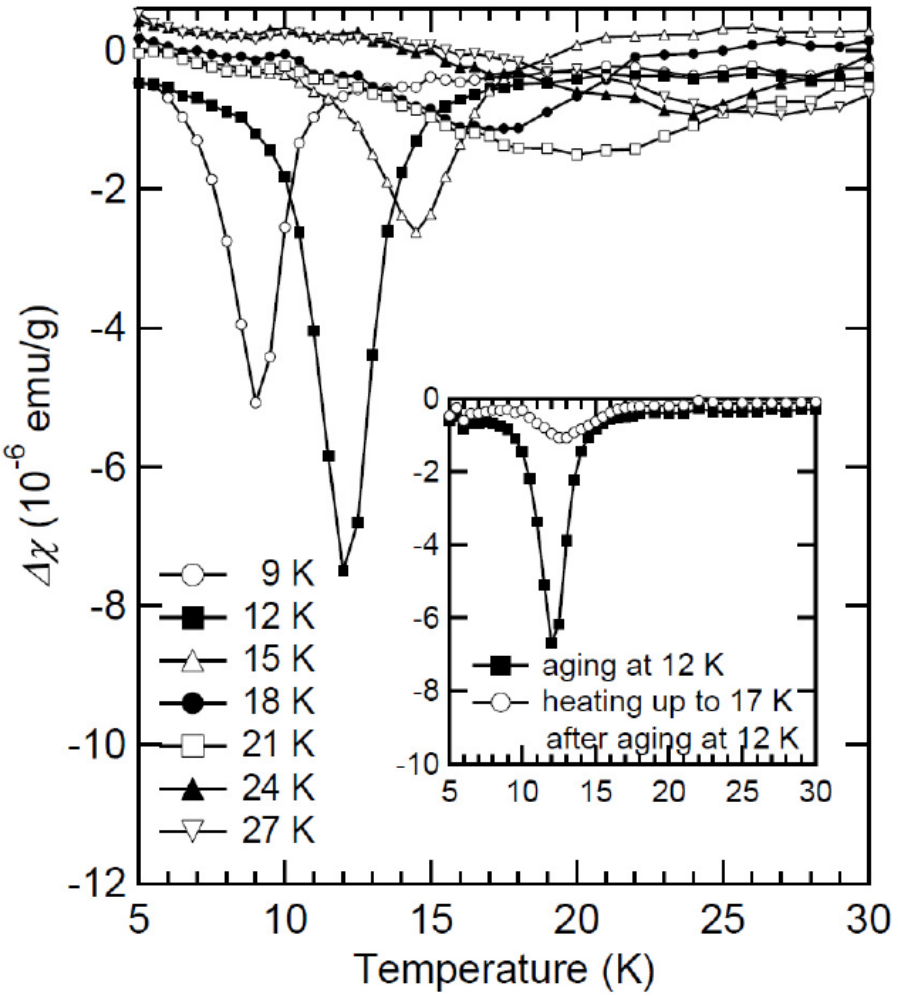

Figure 1.24: Temperature variation of the difference in susceptibility for 32.0FeBiB between with and without aging for 3 h at each of stopping temperatures. The susceptibilities were measured on heating after zero-field cooling with or without the aging. The inset shows the temperature dependence of the difference in susceptibility between with and without aging for 3 h at 12 K (closed squares). The open circles denote the aging at 12 K and subsequent heating to 17 K.

temperature with or without a long stop at a specific temperature T_s situated below the transition temperature. The $\chi(T)$ curve is recorded during the subsequent heating in a measuring magnetic field. Sasaki *et al*. [19] have demonstrated that a memory is imprinted during the aging in the absence of magnetic field only for spin glasses and strongly interacting nanoparticles systems or superspin glasses, but not for non-interacting superparamagnets. Hence, the observation of the memory effect is the confirmation of cooperative spin dynamics [14,19-25].

The stopping temperatures (T_s) are set to be 9 to 27 K at intervals of 3 K. The differences in $\chi(T)$ between with and without the long stop are plotted in Fig. 1.24 for varied T_s. The memory effect is clearly seen as the dip at T_s. As T_s becomes lower than 15 K, the memory dip becomes much narrower and deeper. Although it is difficult to discuss this phenomenon quantitatively, the memory dips observed under the condition that T_s>15 K are reasonably ascribed to the superspin glass-like freezing of magnetic clusters, while those at T_s<15 K are due to the spin glass phase which emerges below about 15 K. The observation of the memory dip at T_s>15 K clearly rules out the occurrence of two-step phase transition of a single magnetic component. This is because if one magnetic phase showed a two-step transition, the spin configuration grown by the aging at T_s>15 K would be forced to change into a completely different configuration state as the temperature was decreased below 15 K, and as a result, the memory effect would disappear. The ZFC memory experiment has been performed in order to verify that two magnetic phases coexist in the present system. The system was cooled down to 12 K (<T_{cFC}=15 K) at which it was aged for 3 h in zero magnetic field, and cooled down to 5 K after heating up to 17 K(>T_{cFC}=15 K). Subsequently, the magnetic field of 50 Oe was applied and $\chi(T)$ was measured on heating. The result is shown in the inset of Fig. 1.24. The aging effect imprinted at 12 K does not vanish completely after heating up to 17 K. This fact indicates that the dip observed at 12 K consists of two components at least and supports the idea that the system does not undergo any two-step magnetic phase transitions.

One question remains whether the magnetic clusters are identified as the crystalline phase of α-Fe_2O_3 detected by the XRD and TEM. Clusters composed of other crystalline phases such as γ-Fe_2O_3 and Fe_3O_4 are also possible. As far as magnetic nanoparticles systems are concerned, the memory effect imprinted during the aging in zero field has been observed only for those with the numbur density of the nanoparticles being very large. For instance, in $Co_{80}Fe_{20}/Al_2O_3$ multilayer system [20], no ZFC memory effects were observed for the thin film even when the volume fraction of magnetic phase was as high as 14 vol.%, where CoFe particles with the average diameter of about 1.8 nm were precipitated inside the Al_2O_3 matrix and the separation between the particles was about 10 nm. In the present case, the volume fraction of the crystalline phase detected by the XRD measurement and the TEM observation is so small that the magnetic clusters exhibiting the collective dynamics including the ZFC memory effect can not be ascribed to the crystalline phase. The origin of magnetic clusters in the present system is conjectured as follows. Some Fe ion-rich regions are produced in the amorphous matrix during the process of melt-quenching, since the driving force to form α-Fe_2O_3 brings about certain microscopic concentration fluctuation of Fe ions, and some parts of such regions are frozen as amorphous clusters before the crystallization into α-Fe_2O_3. The regions enriched with Fe^{3+} ions in the amorphous matrix are responsible for the superspin glass transition. The other regions in the amorphous matrix undergo the spin glass transition at low temperatures. The magnetic clusters present as the amorphous phase can lead to the superspin glass freezing assisted by the strong intercluster interactions even at room temperature as depicted in Fig. 1.20. A similar phenomenon was reported for amorphous oxides with high Fe^{3+} ion concentration such as amorphous Fe_2O_3, in which the superspin glass like behavior was observed even at room temperature [26].

1.3.3.6 Exchange bias-like effect

An exchange bias effect is peculiar to an interface between two magnetic phases such as ferromagnet/antiferromagnet and ferromagnet/spin glass [27-32]. The exchange bias is a shift of magnetic hysteresis loop when the system containing such magnetic interfaces is cooled down in an external magnetic field from a certain temperature below the Curie temperature to a temperature below the Néel temperature or the spin freezing temperature. At the interface, the magnetic moments of antiferromagnets or spin glasses are coupled with those of ferromagnets oriented in the direction of external magnetic field, leading to a unidirectional anisotropy along the magnetic field. Also, the exchange interactions at the interfaces usually enhance the coercivity of ferromagnets. Recently, the exchange bias has been measured to confirm the interface exchange coupling in magnetically phase-separated manganites and cobaltates [27,28]. The exchange bias measurements have been performed for 32.0FeBiB, which is composed of two magnetic components, i.e., the spin glass and the magnetic clusters exhibiting superspin glass transition. In this case, the term 'exchange bias-like effects' instead of 'exchange bias effects' should be used because this section deals with not the conventional ferromagnetic hysteresis loops but magnetic hysteresis cycles within the non-ergodic low temperature region peculiar to the spin glasses. In the present experiments, the magnetic field dependence of magnetization was measured after cooling in the magnetic field of 0.5 T from 300 K to the measurement temperature. The magnetization measurements were performed in the magnetic field of -3 to 3 T. In this system, in contrast to the ferromagnet/spin glass systems often studied for the exchange bias effects, the magnetization is not saturated even in high magnetic fields. So, the highest measurement magnetic field was set to be 3 T, where the hysteresis loops are completely closed at any temperatures, and the cooling field was set to be 0.5 T much lower than 3 T. Figure 1.25(a) shows the dependence of magnetization on magnetic field at 5 K. The central region of Fig. 1.25(a) is magnified in Fig. 1.25(b). It is found that the magnetic hysteresis loop shifts

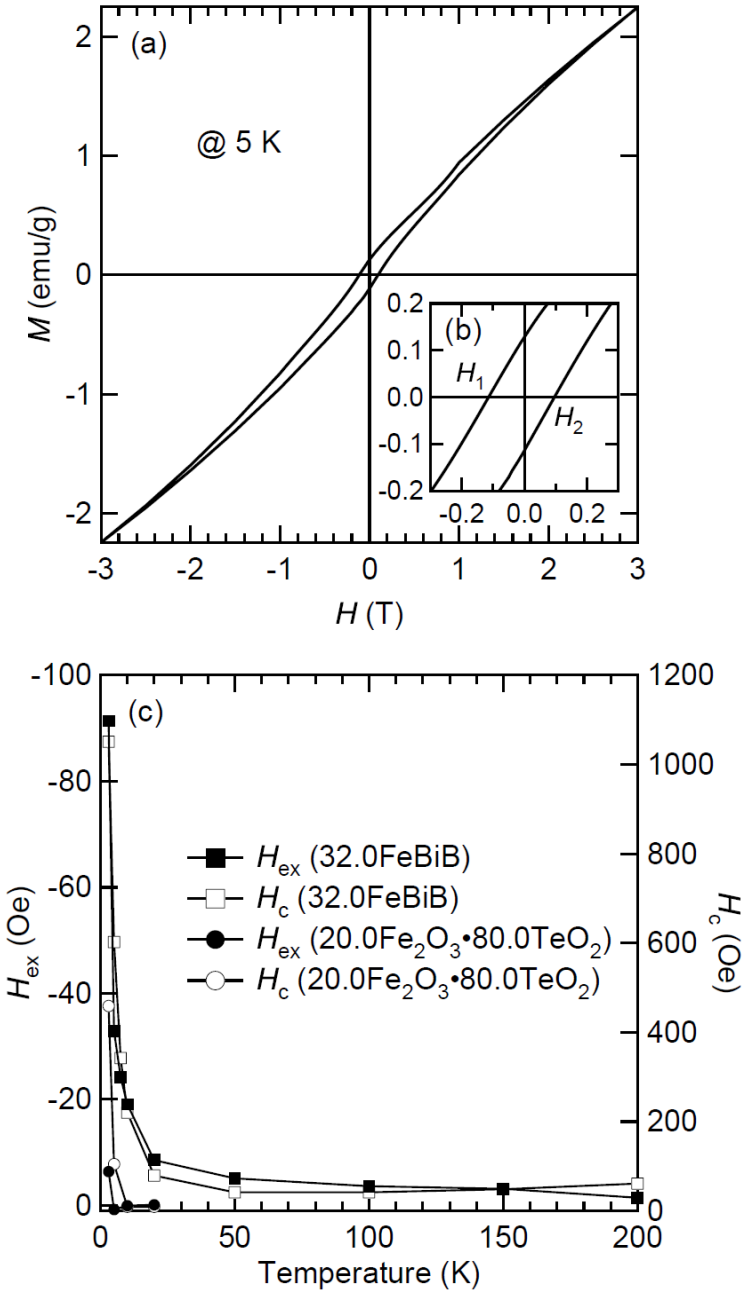

Figure. 1.25: (a) Variation of magnetization with magnetic field measured for 32.0FeBiB at 5 K. (b) Enlarged view of the central region of Fig. 9(a). (c) Temperature dependence of exchange bias field, H_{ex} (closed square and circle) and coercive field, H_c (opened square and circle) for 32.0FeBiB and $20Fe_2O_3{\cdot}80TeO_2$ glass.

along the field axis. The coercive field H_c and the exchange bias-like field H_{ex} are defined as $(H_2-H_1)/2$ and $(H_2+H_1)/2$, respectively, where H_1 and H_2 are the negative and positive magnetic fields at which the magnetization is equal to zero, as shown in Fig. 1.25(b). H_{ex} and H_c are plotted against temperature in Fig. 1.25(c). H_{ex} shows very small but non-zero values above T_{cFC}=15 K at which the spin glass transition takes place, and increases drastically below 15 K. H_c exhibits the temperature dependence similar to that of H_{ex}. The magnitude of the exchange bias-like field becomes larger as the superspin glass-like freezing of magnetic clusters gradually proceeds with a decrease in the temperature. The enhancement of exchange anisotropy and coercive force presumably indicates the emergence of the interface exchange coupling between the magnetic clusters and the spin glass phase. The metastable alignment of superspins formed under the FC condition is thought to exert a positive internal magnetic field onto the atomic spin glass phase. However, the finite values of H_{ex} may be explainable in terms of the fact that the exchange bias-like effect is one of the intrinsic properties of spin glasses and related materials such as cluster spin glasses and superspin glasses [29]. Both possibilities must be discussed. As a reference of the intrinsic exchange bias-like effect in a simple amorphous oxide spin glass, the exchange bias-like effect was examined by the same procedure for the $20.0Fe_2O_3 \cdot 80.0TeO_2$ (mol%), which exhibits the spin glass transition at T_g=9 K as described in Section 1.1. For the $20.0Fe_2O_3 \cdot 80.0TeO_2$ glass, H_{ex} is actually equal to zero above 5 K (=0.6T_g) and H_{ex}=-6 Oe and H_c=459 Oe are obtained at 3 K (=0.3T_g), as shown in Fig. 1.25(c). In the case of 32.0FeBiB, the abrupt rise of H_{ex} is observed just below T_{cFC}, and the amplitude of H_{ex} at 5 K (=0.3T_{cFC}) for 32.0FeBiB is five times larger than that at 3 K (=0.3T_g) for the $20.0Fe_2O_3 \cdot 80.0TeO_2$ glass. Therefore, the temperature dependence of H_{ex} for 32.0FeBiB is not well explained simply in terms of the inherent nature of spin glass phase emerging at T_{cFC}. The present glass can be regarded as one of the exchange bias-like systems possessing no clear structural interfaces as confirmed by the TEM observation but having interfaces among the magnetic phases.

1.3.4 Conclusion

For the $x$$Fe_2O_3$·(80.0-$x$)$Bi_2O_3$·20.0$B_2O_3$ (mol%) glass system with $18.2 \leq x \leq 40.0$, the magnetic structure depends on the content of Fe_2O_3. The magnetic behavior of 18.2FeBiB is similar to that of the canonical spin glasses. In the cases that the content of Fe_2O_3 is above 26.1 mol%, the glasses are composed of two magnetic components, i.e., the spin glass phase and magnetic clusters manifesting the superspin glass transition. As the value of x increases, the contribution of magnetic clusters to the magnetic properties becomes more remarkable. The careful investigations including the ZFC memory experiments and the TEM observation for 32.0FeBiB suggest that the magnetic clusters strongly interact with each other to assist the occurrence of superspin glass transition and that the clusters are mainly present as an amorphous state. It is revealed from the measurements of exchange bias effect that the spin glass phase interplays with the magnetic clusters to form the exchange anisotropy field after the field cooling. Compared with the magnetic oxide glass systems reported so far, the present glass system has novel magnetic structure in a sense that there exist two magnetic ordered phases interacting with each other.

References in Section 1.3

[1] R. A. Verhelst, R. W. Kline, A. M. de Graaf and H. O. Hooper, *Phys. Rev. B* **11**, 4427 (1975).

[2] F. A. Wedgwood and A. C. Wright, *J. Non-Cryst. Solids* **21**, 95 (1976).

[3] J. A. Mydosh, *Spin glasses: an Experimental Introduction* (Taylor &Francis Ltd., London, 1993).

[4] N. Ota, M. Okubo and S. Masuda, *J. Magn. Magn. Mater.* **54-57**, 293 (1986).

[5] S. Nakamura and N. Ichinose, *J. Non-Cryst. Solids* **95&96**, 849 (1987).

[6] S. Nakamura and N. Ichinose, *Jpn. J. Appl. Phys.* **28**, 984 (1989).

[7] J. Chen, S. Cheney and G. Srinivasan, *J. Appl. Phys.* **75**, 6828 (1994).

[8] S. Soeya, S. Nakamura and N. Ichinose, *J. Appl. Phys.* **68**, 2875 (1990).

[9] S. Nakamura, Y. Hirotsu and N. Ichinose, *Jpn. J. Appl. Phys*. **30**, L844 (1991).

[10] H. H. Qiu, T. Ito and H. Sakata, *Mater. Chem. Phys.* **58**, 243 (1999).

[11] A. P. Ramirez, *Annu. Rev. Mater. Sci.* **24**, 453 (1994).

[12] F. J. Morin, *Phys. Rev.* **78**, 819 (1950).

[13] B. Antic, G. F. Goya, H. R. Rechenberg, V. Kusigerski, N. Jovic and M. Mitric, *J. Phys.: Condens. Mater.* **16**, 651 (2004).

[14] S. Sahoo, O. Petracic, W. Kleemann, S. Stappert, G. Dumpich, P. Nordblad, S. Cardoso and P. P. Freitas, *Appl. Phys. Lett.* **82**, 4116 (2003).

[15] C. Djurberg, P. Svedlindh, P. Nordblad, M. F. Hansen, F. Bodker and S. Morup, *Phys. Rev. Lett.* **79**, 5154 (1997).

[16] K. Gunnarsson, P. Svedlindh, P. Nordblad, L. Lundgren, H. Aruga and A. Ito, *Phys. Rev. Lett.* **61**, 754 (1988).

[17] M. F. Hansen, P. E. Jönsson, P. Nordblad and P. Svedlindh, *J. Phys.: Condens. Mater.* **14**, 4901 (2002).

[18] R. Mathieu, P. Jönsson, D. N. H. Nam and P. Nordblad, *Phys. Rev. B* **63**, 092401 (2001).

[19] M. Sasaki, P. E. Jönsson, H. Takayama and H. Mamiya, *Phys. Rev. B* **71**, 104405 (2005).

[20] Xi Chen, S. Bedanta, O. Petracic, W. Kleemann, S. Sahoo, S. Cardoso and P. P. Freitas, *Phys. Rev. B* **72**, 214436 (2005).

[21] S. Sahoo, O. Petracic, W. Kleemann, P. Nordblad, S. Cardoso and P. P. Freitas, *Phys. Rev. B* **67**, 214422 (2003).

[22] O. Cador, F. Grasset, H. Haneda and J. Etourneau, *J. Magn. Magn. Mater.* **268**, 232 (2004).

[23] C. R. Sankar and P. A. Joy, *Phys. Rev. B* **72**, 132407 (2005).

[24] J. Du, B. Zhang, R. K. Zheng and X. X. Zhang, *Phys. Rev. B* **75**, 014415 (2007).

[25] Sunil Nair, A. K. Nigam, A. V. Narlikar, D. Prabhakaran and A. Boothroyd, *Phys. Rev. B* **74**, 132407 (2006).

[26] K. Shafi, A. Ulman, X. Yan, N. Yang, C. Estournès, H. White and M. Rafailovich, *Lngmuir* **17**, 5093 (2001).

[27] D. Niebieskikwiat and M. B. Salamon, *Phys. Rev. B* **72**, 174422 (2005).

[28] Y. K. Tang, Y. Sun and Z. H. Cheng, *Phys. Rev. B* **73**, 174419 (2006).

[29] J. Nogués and I. K. Schuller, *J. Magn. Magn. Mater.* **192**, 203 (1999).

[30] L. Del Bianco, D. Fiorani, A. M. Testa, E. Bonetti and L. Signorini, *Phys. Rev. B* **70**, 052401 (2004).

[31] M. Ali, P. Adie, C. H. Marrows, D. Greig, B. J. Hickey and R. L. Stamps, *Nature Mater.* **6**, 70 (2007).

[32] B. Martínez, X. Obradors, L. Balcells, A. Rouanet and C. Monty, *Phys. Rev. Lett.* **80**, 181 (1998).

CHAPTER 2: Magnetic properties of amorphous Fe_2O_3-R_2O_3 (R = La, Gd and Tb) thin films fabricated by sputtering method

2.1 Introduction

Magnetic oxide glasses are regarded as a system in which magnetic moments localized at cations are randomly distributed in a glass structure. In oxide glasses, negative superexchange interactions via oxide ions are dominant between magnetic moments [1-3]. It may be naturally speculated that magnetic moments necessarily experience a frustrated situation, because such a magnetic structure that keeps all localized pairs of magnetic moments antiferromagnetic is not stable in an amorphous structure. Thus, it is expected that magnetic oxide glasses exhibit spin glass behavior since both frustration and randomness are the definitive factors to induce spin glasses [4].

Some researchers have reported the magnetic properties of the magnetic oxide glasses since the observation of the magnetic anomaly in the CoO-Al_2O_3-SiO_2 and MnO-Al_2O_3-SiO_2 glass systems by Verhelst *et al* [1-3,5-8]. The temperature dependence of not only dc and ac magnetic susceptibilities but Mössbauer spectra and specific heat was explored in order to clarify the mechanism of magnetic transitions of oxide glasses [1,2,5-8]. The spin freezing behavior of the magnetic oxide glasses is similar to that observed in spin glasses. Sections 1.1 and 1.2 have reported that the binary iron tellurite and phosphate glasses manifest properties relevant to spin dynamics including magnetic aging and memory effects as well as critical slowing down similar to those observed in canonical spin glasses.

The systematic research on magnetic properties of simple binary oxide glass systems is instructive for comprehensive understanding of mechanism of magnetic transitions in magnetic oxide glasses. However, systems and compositions to form binary oxide glasses containing a large amount of magnetic ions such 3*d* transition

metal ions are restricted. Confined to iron-based glasses, only the iron tellurite and phosphate glasses can be easily prepared by conventional melt quenching method using stainless sheets. The glasses containing a high concentration of iron oxide such as Fe_2O_3-CaO, Fe_2O_3-SrO, Fe_2O_3-BaO, Fe_2O_3-PbO and Fe_2O_3-Bi_2O_3 were reported to be fabricated by rapidly quenching of melt using a twin-roller [9-11].

In this chapter, the amorphous oxide thin films of Fe_2O_3-R_2O_3 (R = La, Gd and Tb) have been prepared on silica glass substrates by using a radio frequency (rf) sputtering method, which provides a quenching rate higher than a conventional melt quenching method, and the magnetic properties of the resultant thin films have been investigated. The Fe_2O_3-La_2O_3 films are regarded as a system in which magnetic iron ions are dispersed in a nonmagnetic matrix like Fe_2O_3-TeO_2 and Fe_2O_3-P_2O_5 systems. On the other hand, it is worth noting that all cations are magnetic ions in Fe_2O_3-Gd_2O_3 and Fe_2O_3-Tb_2O_3 systems. Subsequently, it has been found that the Fe_2O_3-La_2O_3 films exhibit magnetic properties peculiar to spin glasses. The temperature dependence of magnetic susceptibility, $\chi(T)$, in zero field cooling (ZFC) shows a cusp as observed in spin glasses, and the $\chi(T)$ curves in ZFC and field cooling (FC) deviate from each other below the cusp temperature. Magnetic aging and memory effects have been observed in ZFC protocol proposed by Mathieu *et al*, [11] indicating the presence of spin glass phase in the films. For the Fe_2O_3-Gd_2O_3 and Fe_2O_3-Tb_2O_3 films, the $\chi(T)$ curve in the ZFC process does not show a maximum. However, the magnetic aging effects have been observed below the temperature at which the discrepancy between the $\chi(T)$ curves for ZFC and FC appears. This fact implies that the magnetic moments of iron ions take part in the formation of a spin glass state, while those belonging to rare-earth ions remain in a paramagnetic state even at very low temperature.

2.2 Experimental procedure

Amorphous oxide thin films of Fe_2O_3-R_2O_3 (R = La, Gd and Tb) systems were prepared by utilizing a radio frequency (rf) sputtering method (ULVAC RFS-200). Sputtering targets with prescribed compositions listed in Table 2.1 were prepared from Fe_2O_3, La_2O_3, Gd_2O_3 and Tb_4O_7 powders as starting materials. The mixed powders were compacted with a mould made of copper and then used as a target. Thin films were deposited on a silica glass substrate under conditions that the rf power was 100 W, the atmosphere was a mixture of 67% O_2 and 33% Ar, and the gas pressure was 1.5 $\times 10^{-2}$ Torr. Silica glass substrates with the typical dimensions of 20 × 20 × 0.5 mm^3 were used for the x-ray diffraction (XRD) and energy dispersion of x-ray spectroscopy (EDS) measurements. On the other hand, the glass substrates used for the magnetic measurements have the typical dimension of 5 × 100 × 0.5 mm^3, and the thin films were deposited only on the central portion of the substrates with the area of 5 × 10 mm^2 in order to exclude the diamagnetic contribution of the substrates.

The compositions of the sputtered films were estimated by EDS [see Table 2.1]. The compositional analysis by Rutherford backscattering spectroscopy using 2.0 MeV He^+ led to almost the same result as that by EDS analysis. The deposited thin films were subjected to XRD analysis with a Cu K_α radiation (Rigaku RINT2500) in order to confirm that the thin films were amorphous. The observation in transmission electron microscope (TEM) was performed for thin films with composition of $81Fe_2O_3 \cdot 19La_2O_3$ (mol%).

Magnetic properties of the thin films were examined by using a superconducting quantum interference device magnetometer (Quantum Design MPMS-XL). Temperature dependence of dc magnetic susceptibility under zero field cooling (ZFC) and field cooling (FC) conditions was measured with a magnetic field of 1000 and 50 Oe applied for the Fe_2O_3-La_2O_3 and Fe_2O_3-R_2O_3 (R = Gd and Tb) systems, respectively.

Table 2.1: The compositions of thin films evaluated by EDS and the nominal compositions of targets for Fe_2O_3-R_2O_3 (R = La, Gd and Tb). Spin freezing temperatures are also shown.

Oxide system	The composition of thin films evaluated by EDS	The composition of sputtering target	T_f/K
Fe_2O_3-La_2O_3	$58Fe_2O_3 \cdot 42La_2O_3$	$62.5Fe_2O_3 \cdot 37.5La_2O_3$	42
	$64Fe_2O_3 \cdot 36La_2O_3$	$70.0Fe_2O_3 \cdot 30.0La_2O_3$	50
	$68Fe_2O_3 \cdot 32La_2O_3$	$75.0Fe_2O_3 \cdot 25.0La_2O_3$	60
	$76Fe_2O_3 \cdot 24La_2O_3$	$80.0Fe_2O_3 \cdot 20.0La_2O_3$	70
	$81Fe_2O_3 \cdot 19La_2O_3$	$83.3Fe_2O_3 \cdot 16.7La_2O_3$	76
Fe_2O_3-Gd_2O_3	$54Fe_2O_3 \cdot 46Gd_2O_3$	$62.5Fe_2O_3 \cdot 37.5Gd_2O_3$	35
	$64Fe_2O_3 \cdot 36Gd_2O_3$	$70.0Fe_2O_3 \cdot 30.0Gd_2O_3$	45
Fe_2O_3-Tb_2O_3	$50Fe_2O_3 \cdot 50Tb_2O_3$	$62.5Fe_2O_3 \cdot 37.5Tb_2O_3$	45
	$64Fe_2O_3 \cdot 36Tb_2O_3$	$70.0Fe_2O_3 \cdot 30.0Tb_2O_3$	45

The measurements of magnetic aging and memory effects were performed by applying a magnetic field of 1000 Oe.

2.3 Results and discussion

2.3.1 X-ray diffraction and TEM observation

Figure 2.1 illustrates the representative XRD patterns for the Fe_2O_3-La_2O_3 thin films prepared by the sputtering method. All of the films exhibit only halo pattern in their XRD diagrams. The XRD patterns do not manifest any diffraction lines attributed to crystalline phases, indicating that these films are amorphous from a point of view of XRD. The halo patterns centered at around $2\theta = 21°$ and 31° are assigned to the silica glass substrate and thin films, respectively. The cross-sectional TEM image is shown in Fig. 2.2 for the $81Fe_2O_3 \cdot 19La_2O_3$ thin film, and reveals that the film does not possess any crystalline phases. Similarly, no diffraction lines are observed in the XRD patterns for the Fe_2O_3-Gd_2O_3 and Fe_2O_3-Tb_2O_3 films.

2.3.2 Temperature dependence of dc susceptibility

Figures 2.3(a) and (b) depict $\chi(T)$ and reciprocal dc magnetic susceptibility, $\chi^{-1}(T)$, for some of the Fe_2O_3-La_2O_3 thin films. The $\chi(T)$ curve in ZFC exhibits a cusp at 70 K for the $76Fe_2O_3 \cdot 24La_2O_3$ film, and the $\chi(T)$ curves in ZFC and FC deviate from each other at the cusp temperature. This behavior is similar to that observed in typical spin glasses. The spin freezing temperature becomes higher with an increase in the concentration of iron oxide. A linear dependence of $\chi^{-1}(T)$ on T at high temperatures reveals that these films are paramagnetic in the high temperature region; the linear part is describable in terms of the Curie-Weiss law:

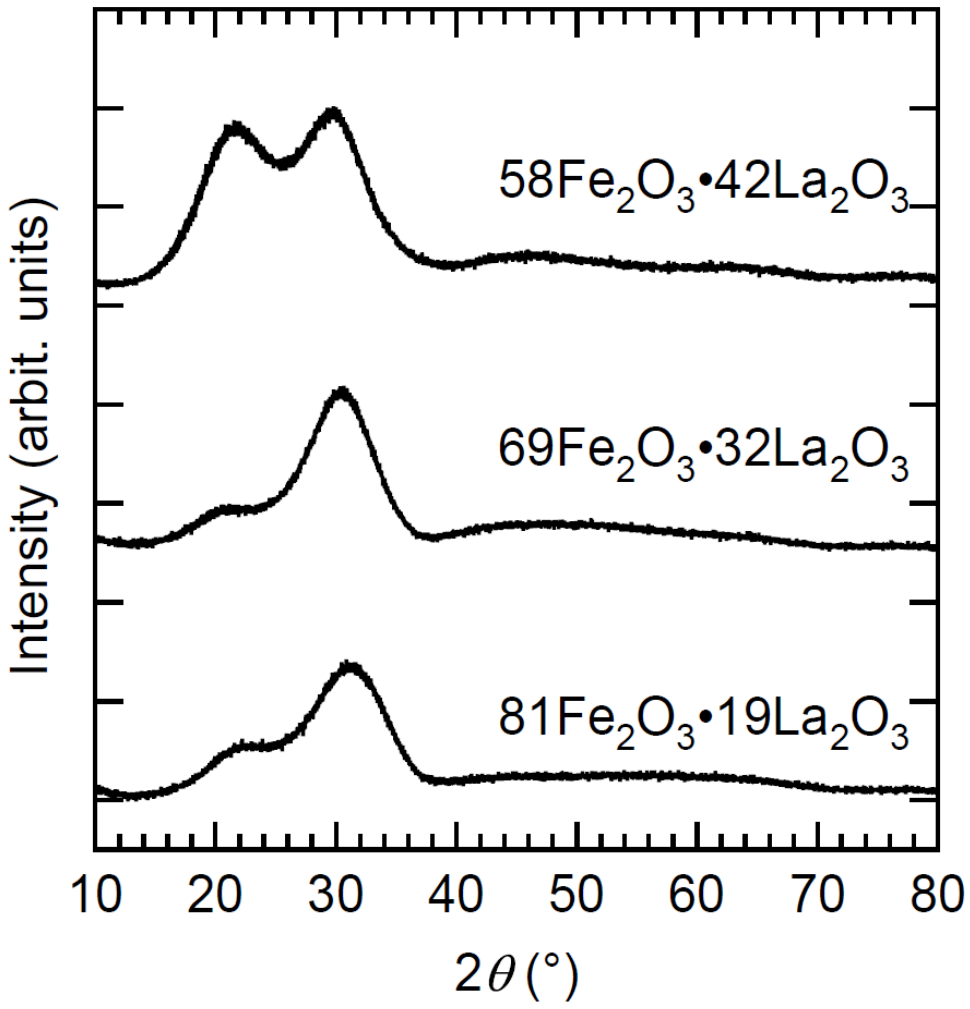

Figure 2.1: X-ray diffraction patterns for the Fe_2O_3-La_2O_3 thin films prepared by sputtering method.

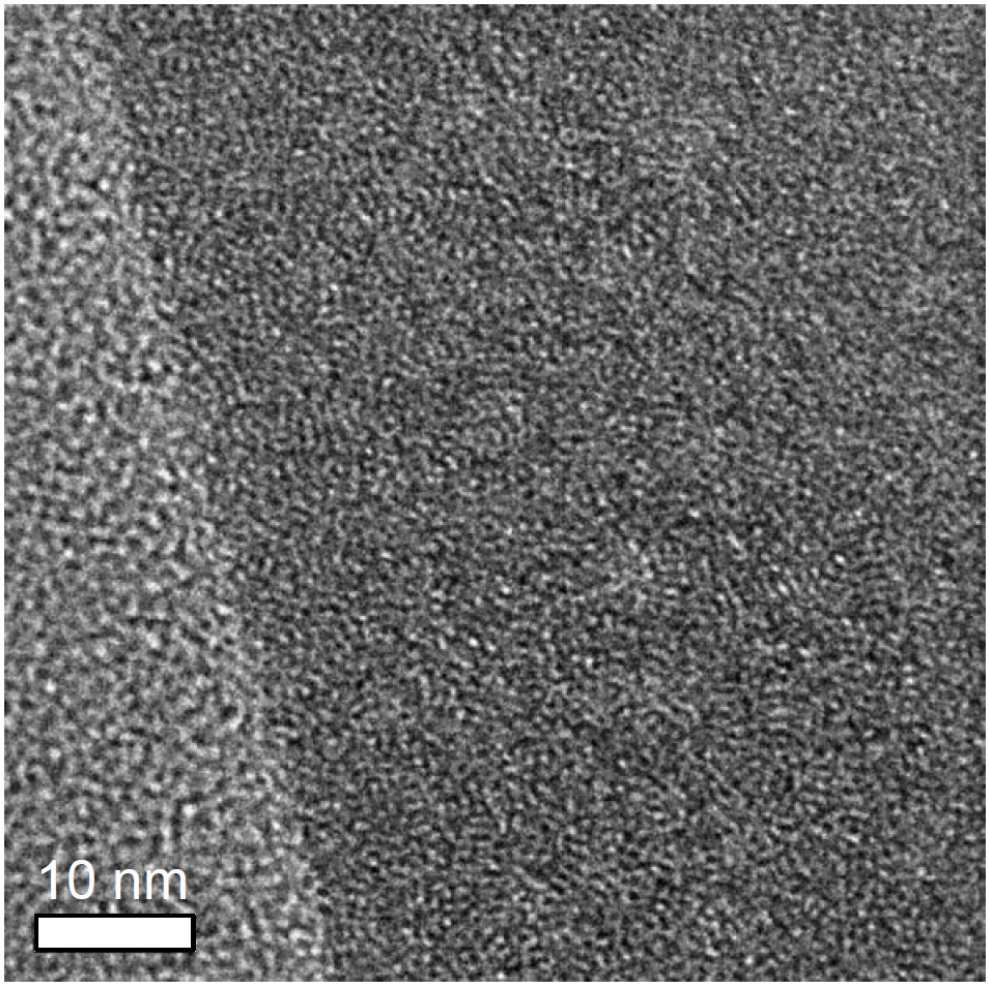

Figure 2.2: The cross-sectional TEM image of $81Fe_2O_3 \cdot 19La_2O_3$ thin film. The blight and dark regions in the left and right sides present the silica glass substrate and the film, respectively.

$$\chi^{-1} = \frac{3k_B((T-\theta_W)}{NM_B{}^2\mu_B{}^2} \qquad (2.1)$$

where θ_W is the Weiss temperature, N the number of magnetic ions per unit mass, μ_B the Bohr magneton, M_B the effective number of Bohr magnetons and k_B the Boltzmann constant. The dashed lines were drawn by using Eq. (2.1) to fit to experimental data of $\chi^{-1}(T)$ in the high temperature regime. It is hard to evaluate the value of M_B precisely because of the difficulty in measuring the weight of the films correctly. The negative value of θ_W means that the antiferromagnetic interaction is dominant among the magnetic moments in the films.

The $\chi(T)$ and $\chi^{-1}(T)$ curves for the Fe_2O_3-Gd_2O_3 thin films are illustrated in Figs. 2.4(a) and (b), respectively. The inset of Fig. 2.4(a) shows an enlarged view of low temperature region. The $\chi(T)$ curves in the ZFC process increase monotonously with a decrease in temperature and exhibit no peak, in contrast to those for the Fe_2O_3-La_2O_3 thin films [see Fig. 2.3(a)]. The discrepancy between the $\chi(T)$ curves under the ZFC and FC conditions is observed below 40 K and 50 K for the $54Fe_2O_3 \cdot 46Gd_2O_3$ and $64Fe_2O_3 \cdot 36Gd_2O_3$ films, respectively [see the inset of Fig. 2.4(a)]. As demonstrated below, the discrepancy corresponds to the spin glass transition. In Fig. 2.4(b), $\chi^{-1}(T)$ is linearly dependent on T in the high temperature regime. The Fe_2O_3-Tb_2O_3 thin films exhibit the temperature dependent magnetic susceptibility similar to that of the Fe_2O_3-Gd_2O_3 thin films (not shown).

In order to understand the nature of low-temperature magnetic phase of Fe_2O_3-Gd_2O_3 system in detail, the zero-field cooling memory experiment proposed by Mathieu *et al* [12] has been performed for the $54Fe_2O_3 \cdot 46Gd_2O_3$ film. In this protocol, the film is cooled in the absence of magnetic field from high temperature with or without an intermittent stop at a stopping temperature T_s set below the spin freezing temperature. The $\chi(T)$ curve is recorded during subsequent heating in a measuring magnetic field. Sasaki *et al*. demonstrated that a memory is imprinted during aging in

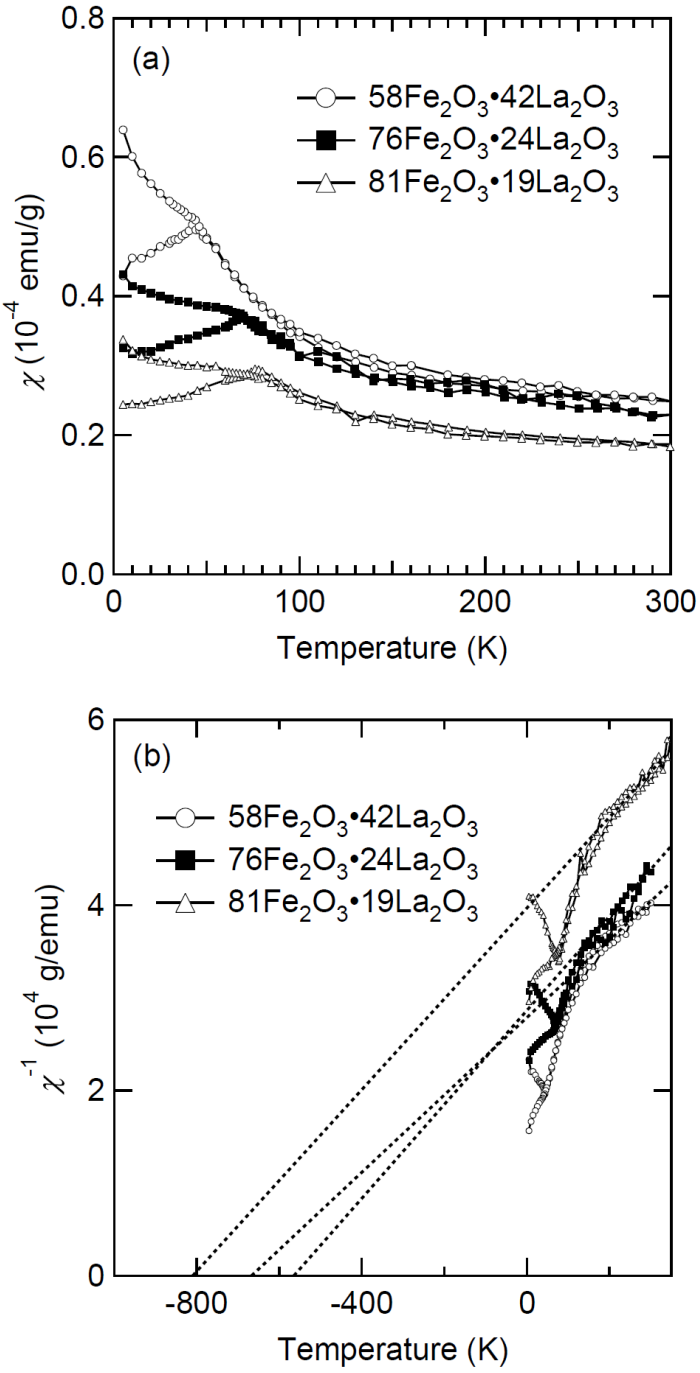

Figure 2.3: Temperature dependence of (a) magnetic susceptibility and (b) inverse magnetic susceptibility for the thin films of the Fe_2O_3-La_2O_3 system. The dotted lines in Fig. 2.3(b) correspond to the Curie-Weiss law described by Eq. (2.1).

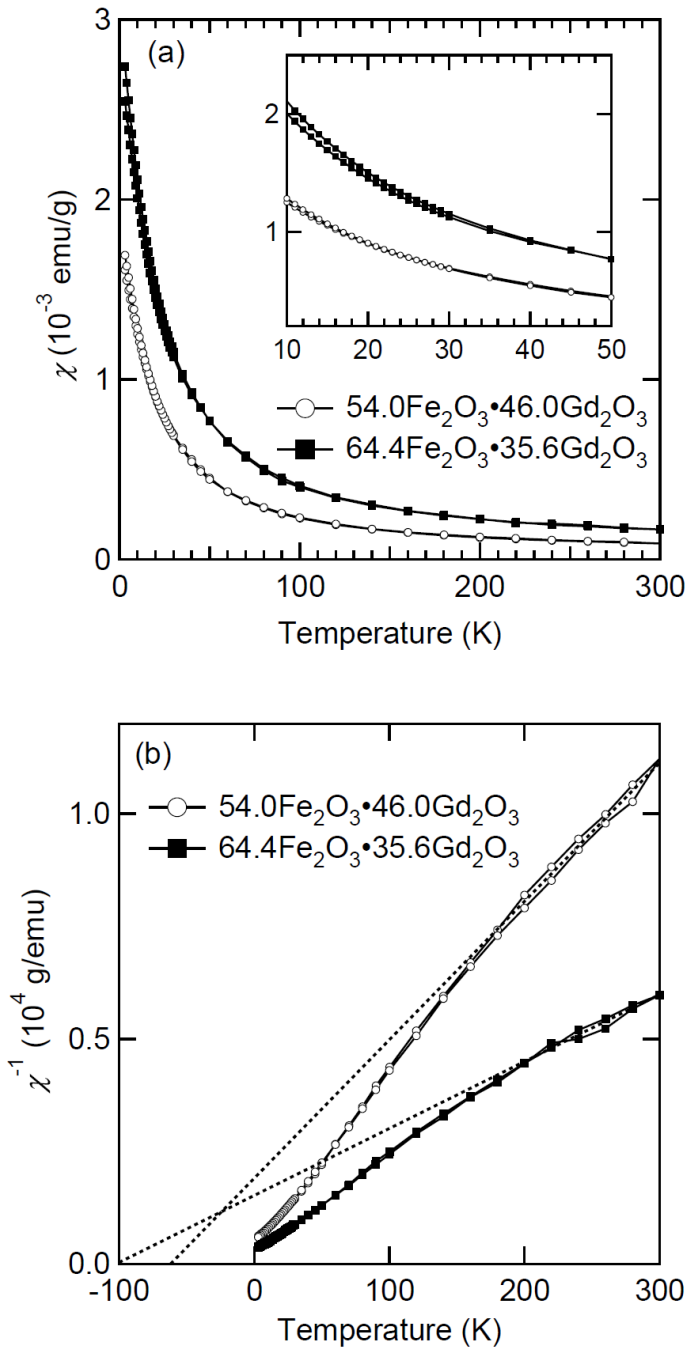

Figure 2.4: Temperature dependence of (a) magnetic susceptibility and (b) inverse magnetic susceptibility for the thin films of the Fe_2O_3-Gd_2O_3 system. The inset of Fig. 2.4(a) shows an enlarged view of low temperature regime. The dashed lines in Fig 2.4(b)correspond to the Curie-Weiss law described by Eq. (2.1).

the absence of magnetic field only for spin glasses and strongly interacting nanoparticles systems or superspin glasses, but not for non-interacting superparamagnets [13]. Hence, the observation of this memory effects indicates cooperative spin dynamics.

2.3.3 ZFC memory effects

Figure 2.5(a) shows $\chi(T)$ measured by applying a magnetic field of 1000 Oe on heating after cooling with and without aging at T_s = 20, 30 and 40 K for 7 h. The difference in $\chi(T)$ between with and without aging is plotted in Fig. 2.5(b) for a series of T_s. A memory effect is clearly found as a dip at T_s if T_s = 20 and 30 K, while no memory dip is observed if T_s = 40 K, indicating that the spin glass phase emerges at a temperature between 30 and 40 K. This result suggests that the discrepancy of $\chi(T)$ between ZFC and FC processes below 35 K corresponds to the occurrence of spin glass transition. These magnetic aging and memory effects can be observed for the $68Fe_2O_3{\cdot}32La_2O_3$ in the condition that T_s = 50 and 60 K (not shown). On the other hand, aging at T_s = 70 K does not imprint a memory dip. It is thought that a spin glass transition takes place when the temperature is decreased from 70 to 60 K, consistent with the fact that $\chi(T)$ under the ZFC condition exhibits a peak at around 60 K.

2.3.4 The nature of the low-temperature magnetically ordered phase

The nature of magnetically ordered phases of the Fe_2O_3-R_2O_3 (R = Gd and Tb) films remains unclear; $\chi(T)$ in ZFC increases monotonically with a decrease in temperature like a paramagnet although the magnetic aging and memory effects relevant to spin glasses are observed below the temperature at which $\chi(T)$'s in the ZFC and FC processes deviate from each other. In Fig. 2.6, the variation of spin freezing temperature, T_f, with the concentration of Fe_2O_3 is shown for Fe_2O_3-R_2O_3 (R = La, Gd and Tb) sputtered thin films and Fe_2O_3-TeO_2 bulk glasses. For the case of the Fe_2O_3-Gd_2O_3 and Fe_2O_3-Tb_2O_3 thin films, a temperature below which $\chi(T)$'s in ZFC

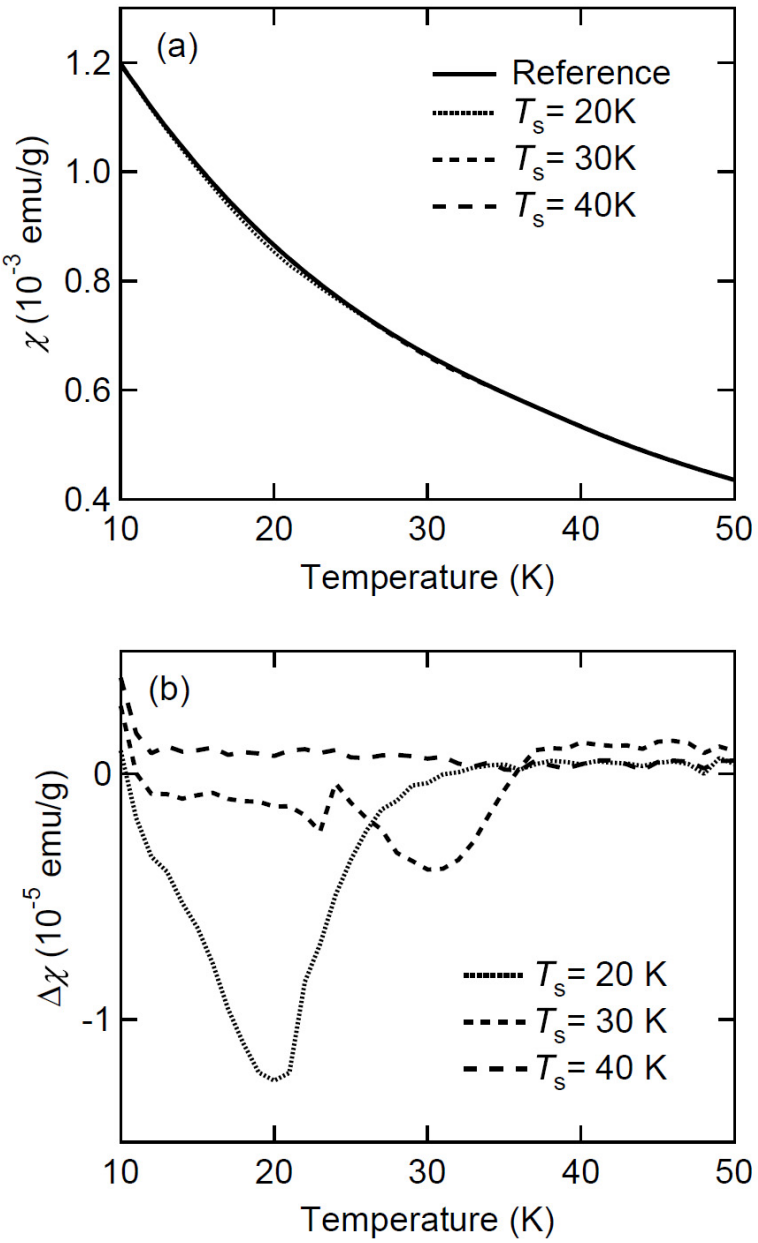

Figure 2.5: The temperature dependence of dc susceptibility, $\chi(T)$, measured on heating after zero-field cooling with an intermittent stop at T_s, is shown in Fig. 2.5(a). As a reference, temperature dependent susceptibility in ZFC process, $\chi_{ref}(T)$, is also shown. Figure 2.5(b) illustrates the difference between $\chi(T)$ and $\chi_{ref}(T)$, $\Delta\chi(T)$, for a series of T_s.

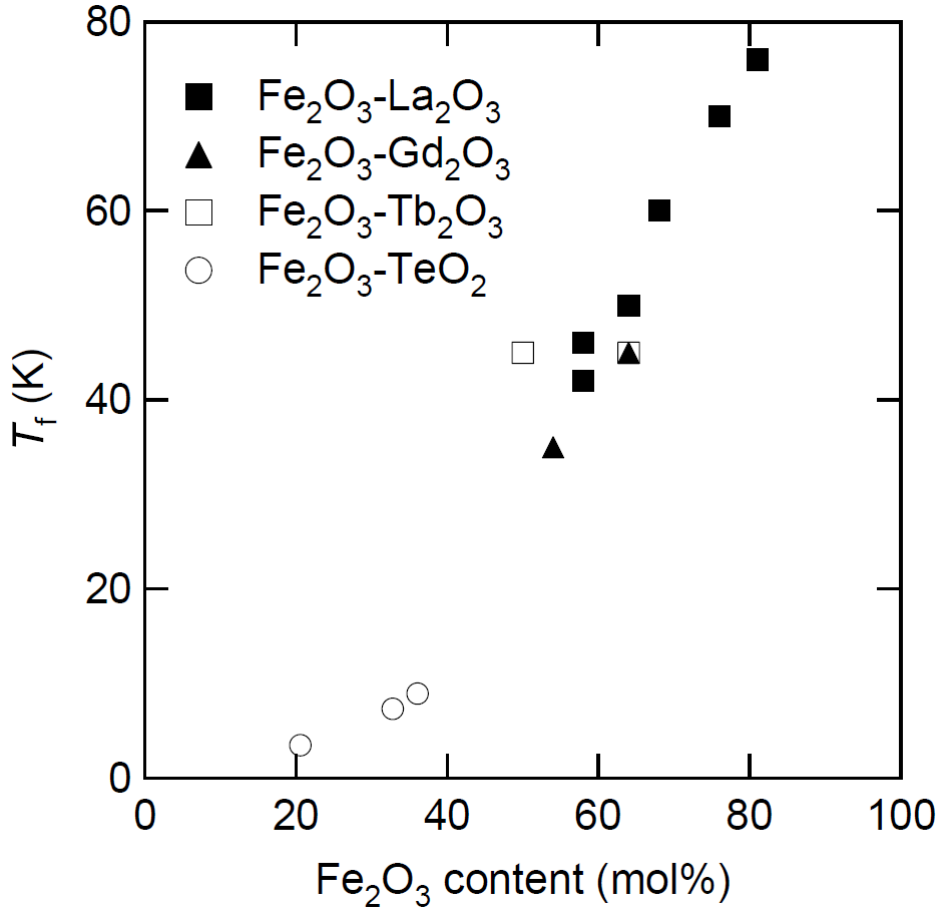

Figure 2.6: Relationship between spin freezing temperature, T_f, and Fe_2O_3 content for Fe_2O_3-R_2O_3 (R = La, Gd and Tb) sputtered thin films and Fe_2O_3-TeO_2 bulk glasses.

and FC are different from each other is regarded as T_f. Figure 2.6 indicates that T_f is strongly associated with the content of Fe_2O_3. In other words, the concentration of rare-earth ions seems to have no significant influence on T_f, implying that the magnetic moments of rare-earth ions do not take part in the spin freezing process at T_f. It is deduced that the magnetic moments of iron ions give rise to a spin glass state, while those of rare-earth ions remain to be paramagnetic even at low temperatures. The magnetic behavior of the Fe_2O_3-Gd_2O_3 and Fe_2O_3-Tb_2O_3 thin films can be explainable in terms of a superposition of the spin glass phase composed of the magnetic moments of iron ions and the paramagnetism of those of rare-earth ions.

2.4 Conclusion

The amorphous Fe_2O_3-R_2O_3 (R = La, Gd and Tb) thin films have been fabricated via an rf sputtering method and investigated magnetic properties including magnetic aging and memory effects for the films. The Fe_2O_3-La_2O_3 thin films exhibit magnetic behavior typical of spin glasses. In Fe_2O_3-R_2O_3 (R = Gd and Tb) systems, the magnetic moments due to iron ions form a spin glass phase while those of gadolinium and terbium ions remain to be included in a paramagnetic phase.

References in Chapter 2

[1] R. A. Verhelst, R. W. Kline, A. M. de Graaf and H. O. Hooper, *Phys. Rev. B* **11**, 4427 (1975).

[2] J. L. Shaw, A. C. Wright, R. N. Sinclair, G. K. Marasinghe, D. Holland, M. R. Lees, and C. R. Scales, *J. Non-Cryst. Solids*, 345&346 (2004) 245.

[3] F. A. Wedgwood and A. C. Wright, *J. Non-Cryst. Solids* **21**, 95 (1976).

[4] J. A. Mydosh, *Spin glasses: an Experimental Introduction* (Taylor &Francis Ltd., London, 1993).

[5] P. Beauvillain, C. Dupas, J. P. Renard, and P. Veillet, *Phys. Rev. B* **29**, 4086 (1984).

[6] J. P. Sanchez and J. M. Friedt, *J. Physique* **43**, 1707 (1982).

[7] A. Ito, E. Torikai, H. Yamauchi, and Y. Syono, *J. Phys. C: Solid State phys.* **15**, 2759 (1982).

[8] G. W. Hunter, L. E. Wenger, and W. D. Wallance, *Phys. Rev. B* **36**, 5750 (1987).

[9] K. Tanaka, K. Hirao, and N. Soga, *J. Appl. Phys*. **69**, 7752 (1991).

[10] K. Tanaka, Ph. D Thesis (1990).

[11] S. Nakamura, S. Soeya, and M. Tanaka, *J. Appl. Phys*. **74**, 5652 (1993).

[12] R. Mathieu, P. Jönsson, D. N. H. Nam and P. Nordblad, *Phys. Rev. B* **63**, 092401 (2001).

[13] M. Sasaki, P. E. Jönsson, H. Takayama and H. Mamiya, *Phys. Rev. B* **71**, 104405 (2005).

CHAPTER 3: Ferromagnetic properties of Eu^{2+}-based bulk oxide glasses

3.1 Introduction

Amorphous oxide magnets, where the magnetic cations are randomly distributed in the three-dimensional disordered network, have attracted considerable attention as an example of an insulating spin glass (SG). Due to the insulating properties, their magnetic properties are dominated by short-range superexchange interactions via oxide ions. This is in contrast to canonical SGs, where the long-range Ruderman-Kittel-Kasuya-Yoshida interactions via conduction electrons play an important role for the SG ordering [1]. According to the Kanamori-Goodenough rule, the sign and strength of superexchange interactions depend on the sorts of magnetic cations and the angles of *M*-O-*M* where *M* is a magnetic cation and O is an oxide ion in insulating oxides [2,3]. For the most cases of the same sort of magnetic ions, the nature of superexchange interactions changes from antiferromagnetic (AFM) to ferromagnetic (FM) when the angle of *M*-O-*M* is varied from 180° to 90°. Therefore, the sign of superexchange interactions should have a wide distribution in amorphous materials as well as the strength. In most of magnetic oxide glasses, AFM interactions are dominant over FM interactions, as experimentally revealed by the negative Weiss temperature (θ_W) [4-8]. This fact reflects the openness of glass structure: magnetic oxide glasses favor the AFM interactions characteristic of the angles of *M*-O-*M*=180°. The random distribution of magnetic ions and the prevailing AFM interactions between them inevitably causes magnetic frustration of geometrical origin in the alignment of magnetic moments. One can naturally speculate that oxide glasses with AFM interactions undergo a SG transition due to the combination of randomness and frustration. Actually, most oxide glasses with a high content of magnetic ions exhibit a paramagnetic (PM)-SG transition at a low temperature of several Kelvins [4-12].

About thirty years ago, however, Shoenes *et al*. reported the positive value of θ_W (=+1 K) for the binary europium silicate glass in which Eu^{2+} ions account for 27 mol% of whole cations [13]. This result indicates the FM interaction is dominant in this glass. It is quite unusual for an oxide glass to exhibit the positive value of θ_W. Unfortunately, no magnetic transition was observed down to 1.5 K, which is the lowest measurement temperature. Despite of this fascinating discovery, the magnetic properties of Eu^{2+}-containing oxide glasses have not been investigated extensively since then. Here, three questions remain to be clarified: (i) whether the FM interactions are essential to the nature of Eu^{2+} ions, that is, whether the dominance of FM interactions is common in any oxide glasses with Eu^{2+} ions, (ii) what the origin of the FM interactions is, and (iii) what the magnetically ordered state is. In this letter, in order to clarify these questions, we have fabricated bulk oxide glasses possessing a series of the concentrations of Eu^{2+} ions in total cations, $[Eu^{2+}]$, of various systems, and carried out a comprehensive investigation of their magnetic properties using dc and ac magnetic susceptibility and specific heat. As a result, all the resultant glasses have positive values of θ_W independently of the kind of glass hosts, suggesting the universality of the FM nature of Eu^{2+} ions in oxide glasses. The magnitude of θ_W varies nonlinearly with $[Eu^{2+}]$, being contrary to the expectation from the molecular field theory. This is attributed to the enhancement of superexchange interactions due to an increase with the covalency of Eu-O bonds. The glasses with the high values of $[Eu^{2+}]$ exhibit a reentrant SG (RSG) transition at a low temperature of about 2 K. The RSG behavior suggests that the minor AFM interactions also exist, leading to magnetic frustrations due to the competition between the FM and AFM interactions.

3.2 Experimental procedure

Europium borate, aluminoborate, and aluminoborosilicate glasses were prepared by the melt quenching methods from reagent-grade Eu_2O_3, B_2O_3, Al_2O_3, and SiO_2 as starting materials. The raw materials were mixed thoroughly and melted in glassy carbon or graphite crucibles for 30-120 min under Ar(95)/H_2(5) (vol.%) atmosphere at 1400-1500 ˚C. The glass compositions, their notation, and preparation conditions are summarized in Table 3.1. The molten glasses were cooled slowly under N_2 atmosphere to room temperature. The amorphous nature of the glasses was confirmed by X-ray diffraction (XRD) using Cu $K\alpha$ radiation. ^{151}Eu Mössbauer effect measurements were performed at room temperature using 1.85 GBq $^{151}Sm_2O_3$ as the γ-ray source to investigate the chemical environment of Eu^{2+} ions. The measurements of magnetic properties including the temperature dependence of ac and dc magnetic susceptibilities and the magnetic field dependence of magnetization were carried out by using Quantum Design SQUID magnetometer. The specific heat measurement was performed by relaxation methods with Quantum Design Physical Properties Measurement System.

3.3 Results and discussion

3.3.1 Characterization

Figure 3.1(a) illustrates the XRD patterns of the 30EuB2, 53EuAlB, and 60EuAlBSi glasses. No diffraction peaks attributed to crystalline precipitation are observed in the XRD pattern. Instead, halo patterns typical of amorphous structure are observed. The ^{151}Eu Mössbauer spectra of these glasses are shown in Fig. 3.1(b). All the spectra are composed of two absorption bands at about -13 mm/s and 0 mm/s. The absorption bands are ascribed to Eu^{2+} and Eu^{3+} ions, respectively. The fraction of

Table 3.1: The composition, preparation condition, and notation are shown for the resultant glasses. The concentration of Eu^{2+} ions in the total cations, $[Eu^{2+}]$, the fraction of the number of Eu^{2+} ions in the total number of Eu ions, x, and the Weiss temperature, θ_W, obtained from the analysis by Eq. (2) are also shown. In the column of preparation condition, GS and GP denote glassy and graphite carbon crucibles, respectively.

Notation	Composition (mol%)	Condition	$[Eu^{2+}]$ (mol%)	x	θ_W (K)
25EuB1	$25.0EuO{\cdot}75.0B_2O_3$	GS, 1400°C, 30 min	10.9	0.73	0.13
25EuB2	$25.0EuO{\cdot}75.0B_2O_3$	GP, 1400°C, 60 min	14.3	1.00	0.26
30EuB1	$30.0EuO{\cdot}70.0B_2O_3$	GS, 1400°C, 30 min	15.6	0.89	0.28
30EuB2	$30.0EuO{\cdot}70.0B_2O_3$	GP, 1400°C, 60 min	17.6	1.00	0.36
40EuAlB	$40.0EuO{\cdot}10.0Al_2O_3{\cdot}50.0B_2O_3$	GS, 1450°C, 30 min	16.4	0.66	0.47
50EuAlB1	$50.0EuO{\cdot}10.0Al_2O_3{\cdot}40.0B_2O_3$	GS, 1450°C, 30 min	22.5	0.67	0.52
50EuAlB2	$50.0EuO{\cdot}10.0Al_2O_3{\cdot}40.0B_2O_3$	GP, 1450°C, 30 min	31.8	0.95	1.42
50EuAlB3	$50.0EuO{\cdot}10.0Al_2O_3{\cdot}40.0B_2O_3$	GP, 1450°C, 60 min	32.8	0.98	1.85
50EuAlB4	$50.0EuO{\cdot}20.0Al_2O_3{\cdot}30.0B_2O_3$	GP, 1500°C, 30 min	32.8	0.98	1.52
53EuAlB	$52.5EuO{\cdot}10.0Al_2O_3{\cdot}37.5B_2O_3$	GP, 1500°C, 60 min	35.3	0.99	1.89
47EuAlBSi	$46.7EuO{\cdot}13.3Al_2O_3{\cdot}13.3B_2O_3{\cdot}26.7SiO_2$	GP, 1500°C, 60 min	33.8	0.92	1.87
50EuAlBSi	$50.0EuO{\cdot}12.5Al_2O_3{\cdot}17.5B_2O_3{\cdot}20.0SiO_2$	GP, 1500°C, 60 min	36.2	0.94	1.98
55EuAlBSi	$55.0EuO{\cdot}10.0Al_2O_3{\cdot}15.0B_2O_3{\cdot}20.0SiO_2$	GP, 1500°C, 60 min	38.5	0.88	2.83
58EuAlBSi1	$58.0EuO{\cdot}12.0Al_2O_3{\cdot}20.0B_2O_3{\cdot}10.0SiO_2$	GP, 1500°C, 60 min	38.2	0.87	2.72
58EuAlBSi2	$58.0EuO{\cdot}12.0Al_2O_3{\cdot}20.0B_2O_3{\cdot}10.0SiO_2$	GP, 1450°C, 120 min	40.1	0.91	2.95
58EuAlBSi3	$58.0EuO{\cdot}12.0Al_2O_3{\cdot}20.0B_2O_3{\cdot}10.0SiO_2$	GP, 1500°C, 120 min	41.5	0.94	3.46
59EuAlBSi	$59.0EuO{\cdot}11.0Al_2O_3{\cdot}20.0B_2O_3{\cdot}10.0SiO_2$	GP, 1500°C, 120 min	43.5	0.97	3.57
60EuAlBSi	$60.0EuO{\cdot}11.0Al_2O_3{\cdot}19.5B_2O_3{\cdot}9.5SiO_2$	GP, 1500°C, 120 min	45.3	0.98	3.62

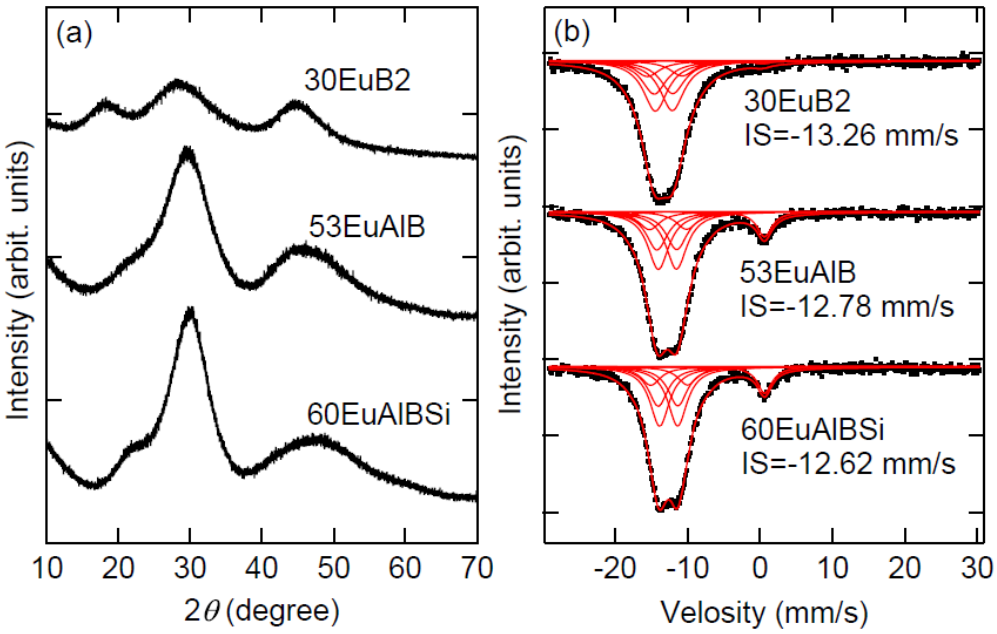

Figure 3.1: (a) X-ray diffraction patterns of the 30EuB2, 53EuAlB, and 60EuAlBSi glasses. (b) ^{151}Eu Mossbauer spectra of these glasses at room temperature. The values of isomer shift (IS) are also shown. The calculated spectra are illustrated as solid curves.

absorption area of Eu^{2+} ion in the total area of the Mössbauer spectrum is larger than 90 % for these glasses. This fact suggests that at least 90 % of Eu ions exist as divalent ions in these glasses, because the fraction of the number of Eu^{2+} ions is underestimated due to the difference in recoilless fraction between divalent and trivalent ions [14]. The absorption band due to Eu^{2+} was analyzed using a method developed by Shenoy and Dunlap [15]. Within the framework of their model, the absorption spectrum of Eu^{2+} is contributed to by the twelve transitions, of which the resonance energy and the transition intensity are dependent of isomer shift (IS), quadrupole interaction parameter, and asymmetric parameter, assuming that each transition is expressed as a single Lorentzian shape [16]. The absorption spectrum of Eu^{3+} was analyzed by a single Lorentzian curve because of the poor spectral resolution. The calculated Mössbauer spectra are described as solid curves in Fig. 3.1(b). The agreement between measured and calculated spectra is fairly good. The values of IS of Eu^{2+} ions obtained from this analysis are shown in Fig. 3.1(b). The value of IS of Eu^{2+} ions is a measure of the covalency of chemical bonds between divalent europium and oxide ions and the coordination number in oxide solids [16]. The IS values of Eu^{2+} ions in the present glasses are comparable to those of perovskite-type oxides $EuTiO_3$ (-12.5 mm/s) and $EuZrO_3$ (-13.1 mm/s) [16], indicating the average coordination number for Eu^{2+} ions is about 12 in these glasses. The values of IS increase with an increase in $[Eu^{2+}]$, implying that the glasses with higher values of $[Eu^{2+}]$ have more covalent Eu^{2+}-O bonds.

3.3.2 The estimation of Weiss temperature

Figure 3.2(a) depicts the temperature dependence of inverse dc magnetic susceptibility, $\chi^{-1}(T)$, for the 30EuB2, 53EuAlB, and 60EuAlBSi glasses. Both the measurements for zero-field cooling (ZFC) and field cooling (FC) processes were carried out using a magnetic field of 50 Oe. The $\chi^{-1}(T)$ curves exhibit a linear dependence at high temperatures as expected from Curie-Weiss law:

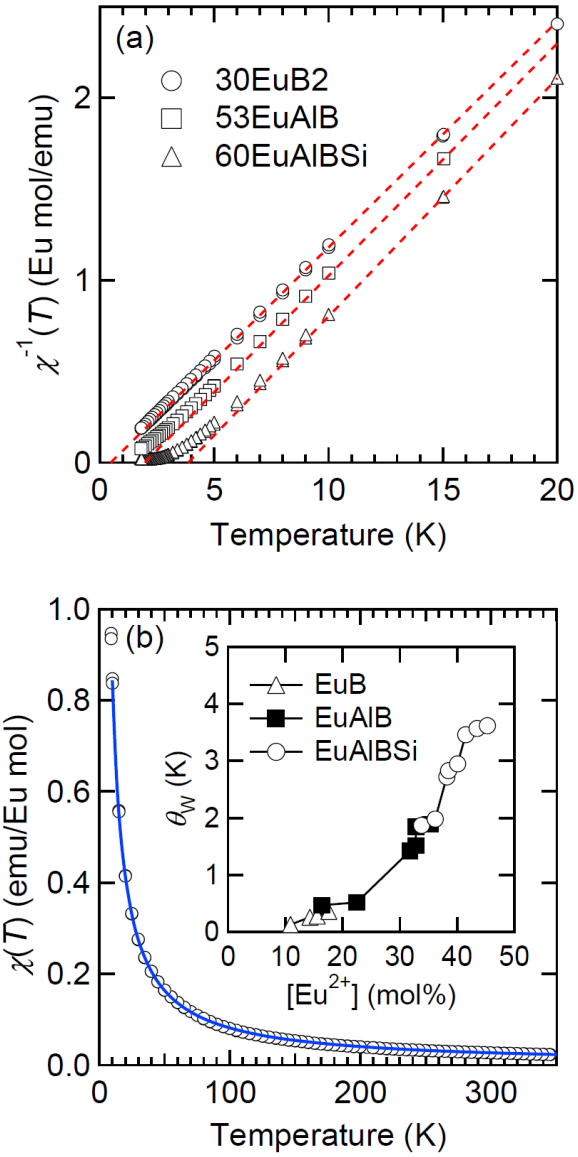

Figure 3.2: (a) The temperature dependence of inverse magnetic susceptibility, $\chi^{-1}(T)$, of the 30EuB2, 53EuAlB, and 60EuAlBSi glasses. The dashed lines are obtained by fitting Eq. (3.1) to the experimental data in the high temperature region. (b) The temperature-dependent magnetic susceptibility, $\chi(T)$, is shown. The solid curve is yielded by the fit of the experimental data to Eq. (3.2). In the inset, the Weiss temperature, θ_W, is plotted against the concentration of Eu^{2+} ions.

$$\chi^{-1} = \frac{3k_B}{NM_B{}^2}(T - \theta_W), \qquad (3.1)$$

where N is the number of magnetic ions per unit volume, M_B the effective magnetic moment, k_B the Boltzman constant, θ_W the Weiss temperature. This fact reveals that the glasses are PM at high temperatures. Figure 3.2(a) shows dashed lines obtained by fitting approximately the experimental data in the high temperature regime. The intercept on the temperature axis is found to be positive for the present glasses. This fact means that FM interactions are dominant between Eu^{2+} ions. The $\chi^{-1}(T)$ curves deviates from the dashed lines upward as temperature is lowered, indicating the emergence of short-range FM correlation at low temperatures. The linear approximation of $\chi^{-1}(T)$ based on Eq. (3.1) is a usual way of estimating the values of θ_W. In this case, the present glasses have a small amount of Eu^{3+} ions, which are non-magnetic in the ground state but have the net moment in the excited states. Accordingly, $\chi(T)$ per one molar amount of Eu ion is expressed taking into account both the contributions of Eu^{2+} and Eu^{3+} ions as follow:

$$\chi(T) = x \times \frac{N_A(7.94\mu_B)^2}{3k_B(T - T_W)} + (1-x) \times \frac{N_A \sum_{J=0}^{2}(2J+1)\exp(-E_J/k_BT)\left\{\frac{g_J\mu_B{}^2 J(J+1)}{3k_BT} + \alpha_J\right\}}{\sum_{J=0}^{2}(2J+1)\exp(-E_J/k_BT)}. \qquad (3.2)$$

Here, the first term represents Curie-Weiss paramagetism of Eu^{2+} ions and the second one Van Vleck paramagnetism of Eu^{3+} ions and Curie paramagnetism of the excited states of Eu^{3+} ions. The value x is the fraction of the number of Eu^{2+} ions in the total number of Eu ions, N_A the Avogadro number, μ_B the Bohr magneton. In the second term, g_J, E_J, and α_J are the g-factor, the energy, and the Van Vleck magnetic susceptibility of the excited state designated by the total angular momentum number J, respectively. For J more than 0, the difference between the energies of the J and J-1 states is given by $E_J - E_{J-1} = \lambda J$, where λ is the spin-orbital coupling constant. For Eu^{3+} ions, λ varies in the range of 320 to 370 cm^{-1} depending on the screening effect and

crystal field anisotropy [17]. In this analysis, we used λ=348 cm^{-1}, which is attained for a EuB_3O_6 crystalline material [17]. Figure 3.2(b) demonstrates the $\chi(T)$ versus T plot for the 30EuB2 glass. The solid curve in Fig. 3.2(b) represents the fitting curve obtained by using Eq. (3.2). The fitting is done very well. The analysis by Eq. (3.2) was performed in the temperature region higher than 10 K, where $\chi^{-1}(T)$ exhibits approximate linear dependence on temperature. The two fitting parameters, x and θ_W, are summarized in Table 3.1. All the present glasses have the positive values of θ_W, indicating that Eu^{2+} ions interplay ferromagnetically with each other in any glass system, in contrast to many oxide glasses including the other magnetic ions [4-8]. In the inset of Fig. 3.2(b), θ_W is plotted as a function of $[Eu^{2+}]$, which is given by multiplying the concentration of Eu ions in the total cations by the value of x. A monotonic increase of θ_W with $[Eu^{2+}]$ is observed. Within the molecular field approximation, θ_W is expected to be proportional to $[Eu^{2+}]$. However, the concentration dependence of θ_W is distinctly different from a linear increase. This discrepancy implies some factors contributing to the enhancement of interactions, as discussed later.

3.3.3 The nature of the magnetically ordered phase

Now we focus on the magnetic anomaly observed in the 60EuAlBSi glass at low temperatures. Figure 3.3(a) presents the temperature dependence of $\chi(T)$ for the 60EuAlBSi glass. At high temperatures, the glass exhibits a paramagnetic behavior similarly to the 30EuB2 glass. As seen in Fig. 3.2(a), the short-range FM correlation begins to form at about 10 K with lowering temperature. The inset of Fig. 3.3(a) shows the enlarged view of the low temperature region. The $\chi(T)$ curve exhibits a plateau-like behavior below 2.3 K; then, $\chi(T)$'s for the ZFC and FC processes deviate from each other below 2.2 K. The bifurcation of $\chi(T)$ for ZFC and FC is peculiar to SG. Besides, a magnetic aging and memory effect is observed at 2 K by using the protocol proposed by Mathieu *et al* (the data is not shown) [18]. This result indicates

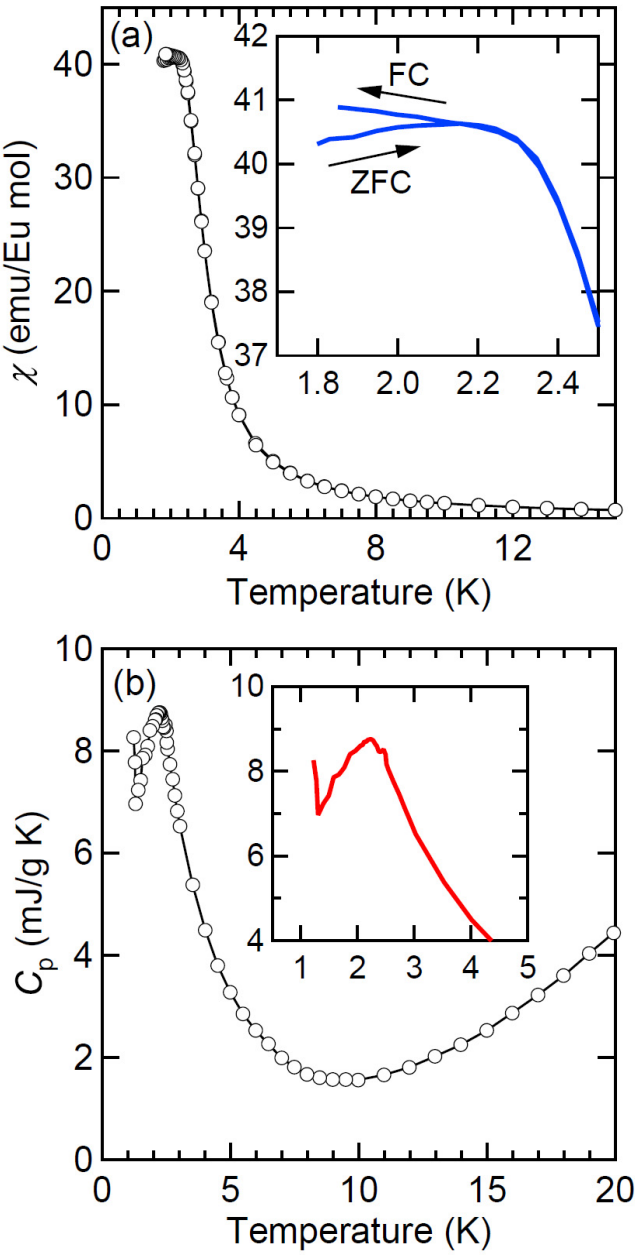

Figure 3.3: (a) The temperature dependence of magnetic susceptibility, $\chi(T)$, of the 60EuAlBSi glass. The inset shows the enlarged view of the low temperature region. (b) The specific heat, C_p, of the 60EuAlBSi glass is plotted as a function of temperature. The magnified view of the low temperature region is illustrated in the inset.

that the glass is in a SG state at 2 K [19]. However, the glass does not exhibit a sharp cusp like that observed in a conventional SG. The specific heat, C_p, of this glass as a function of temperature is illustrated in Fig. 3.3(b). The phonon contribution of C_p is dominant at high temperatures above 10 K. As temperature is decreased, the magnetic contribution of C_p increases below 10 K, which is in good agreement with the deviation of $\chi^{-1}(T)$ from a linear behavior. Then, a pronounced peak is observed near the magnetic anomaly temperature, indicating a three-dimensional magnetic ordering. At lower temperatures, C_p starts to increase with a decrease in temperature due to the nuclear contribution of Eu [20]. In a conventional SG, a magnetic specific heat shows neither peaks nor anomalies at a cusp temperature; a rounded peak is observed at temperatures sufficiently higher than a cusp temperature [1]. Therefore this magnetic anomaly is not attributed to a simple SG transition.

In Fig. 3.4(a) and (b), the temperature dependence of real and imaginary parts of ac susceptibility, $\chi'(T)$ and $\chi''(T)$, is shown for the 60EuAlBSi glass. The amplitude of ac magnetic field was 3 Oe. The $\chi'(T)$ curves exhibit a peak at temperatures from 2.2 to 2.3 K; besides, a shoulder-like behavior is observed below 2.2 K. This behavior is reflected as a two-step rise in $\chi''(T)$: on cooling, $\chi''(T)$ first increases abruptly at about 2.3 K, and exhibits the second rise at about 2.1 K after the slope becomes moderate once. These results indicate that the present glass exhibits the two-step magnetic transition. The spin freezing temperature, $T_f(f)$, at which $\chi'(T)$ exhibits a peak, shows a moderate dependence on frequency, while the frequency dependence of $\chi'(T)$ is pronounced below 2.2 K. The extent to which $T_f(f)$ become higher with an increase in the frequency, $\Delta T_f(f)/(T_f(f)\Delta \log f)$, is 0.0029 (see the inset of Fig. 3.4(a)). This value is significantly small compared to those obtained for canonical SGs such as *Cu*Mn (0.005) and *Au*Fe (0.010), and one order of magnitude smaller than those obtained for amorphous oxide spin glasses such as a cobalt aluminosilicate glass (0.06) [1]. Based on the dynamic scaling hypothesis, provided that this system exhibits a conventional critical slowing down toward the transition temperature T_c, the variation

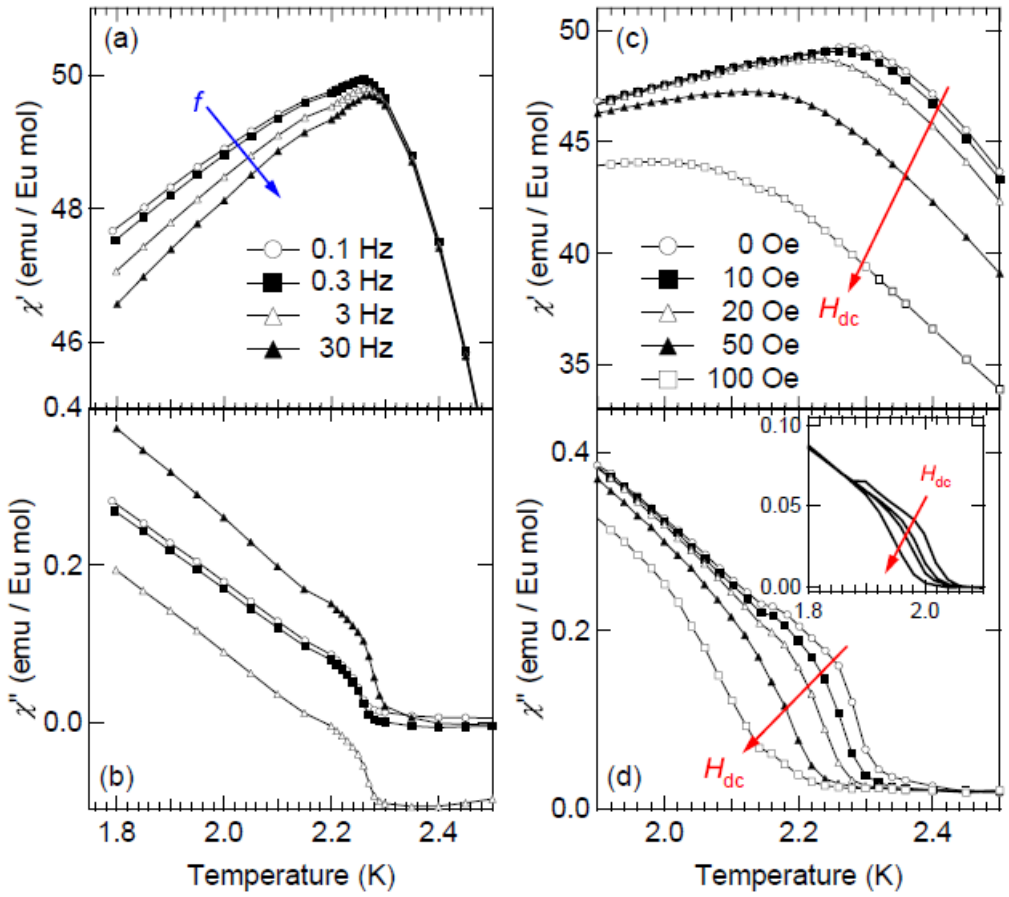

Figure 3.4: The real and imaginary parts, $\chi'(T)$ and $\chi''(T)$, of ac susceptibility measured at various frequencies are depicted as a function of temperature for of the 60EuAlBSi glass in Fig. 4(a) and (b), respectively. The frequency dependence of spin freezing temperature, $T_f(f)$, is illustrated in the inset of Fig. 4(a). Figure 4(c) and (d) show the temperature dependence of $\chi'(T)$ and $\chi''(T)$ measured under a series of superimposed dc magnetic fields. The inset of Fig. 4(d) shows $\chi''(T)$ of the 59EuAlBSi glass.

of maximum relaxation time, τ, with transition temperature is described by

$$\tau = \tau_0 \left(\frac{T_f(f) - T_c}{T_c} \right)^{-zv}, \qquad (3.3)$$

where zv is the dynamic exponent and τ_0 is a microscopic relaxation time. In the present case, the best fitting of Eq. (3.3) to the experimental data yields zv=17, T_c=2.2 K, and τ_0=3.2×10^{-30} s. The values of zv=17 and τ_0=3.2×10^{-30} s are not in any agreement with those reported for prototypes of spin glasses [21,22]. The results of this analysis also imply that this magnetic anomaly is not assigned a conventional SG transition.

In order to shed light on this magnetic anomaly, the dependence of ac susceptibility was measured superimposing dc magnetic field, H_{dc}. The frequency of ac magnetic field was 100 Hz, and H_{dc} was varied from 0 to 100 Oe. The $\chi'(T)$ and $\chi''(T)$ curves are shown in Fig. 3.4(c) and (d), respectively. There is suppression of both $\chi'(T)$ and $\chi''(T)$ with increasing H_{dc}. In particular, $\chi''(T)$ exhibits a decisive signature: the intensity of $\chi''(T)$ is suppressed prominently in the temperature region between 2.1 and 2.3 K on increasing H_{dc}. The higher temperature rise in $\chi''(T)$ is pronouncedly depressed while the lower temperature jump is slightly suppressed. This behavior is observed in many RSG systems. In RSGs, H_{dc} depresses the intensity of $\chi''(T)$ pronouncedly near the PM-FM transition temperature whereas there is rather weaker depression near the FM-SG transition temperature [23]. We infer that on lowering temperature the 60EuAlBSi glass reenters a SG phase as soon as it becomes a FM state at about 2.3 K. The similar behavior is also observed in the 59EuAlBSi glass (see the inset of Fig. 3.4(c)); the magnetic anomaly temperature is lower than that of the 60EuAlBSi glass. The systematic increase in the magnetic anomaly temperature with the value of [Eu^{2+}] implies that this anomaly is not ascribed to extrinsic factors such as the precipitation of FM crystalline materials.

3.3.4 The origin of ferromagnetic interaction

As demonstrated above, the positive magnetic interactions are dominant in the Eu^{2+}-containing oxide glasses irrespective of the sorts of glass host, and the glasses with high content of Eu^{2+} exhibit a RSG transition. However, the microscopic origin of the FM interactions still remains unclear. The FM exchange interactions and/or FM transitions have been found in various Eu^{2+}-based crystalline compounds [24-30]. The mechanism of FM interactions in Eu^{2+}-based materials have been analyzed both experimentally and theoretically since the discovery of a ferromagnet EuO [24]. Some competing interactions are considered to coexist [25]. The 4*f*-4*f* direct exchange interactions are rather weak because of the localized nature of 4*f* electronss. The indirect exchange mechanism via the overlap of 5*d* orbitals is suggested for the FM nearest-neighbor interactions in EuO, Eu_2TiO_4, and $Eu_3Ti_2O_7$ [26]. This mechanism includes a virtual intra-atomic 4*f*→5*d* electron transfer; accordingly, the crystal chemistry, i.e., crystal-field splitting of 5*d* orbitals is important for the strength of the interaction. This interaction is effective for the nearest-neighbor interaction in EuO, Eu_2TiO_4, and $Eu_3Ti_2O_7$, but not in $EuTiO_3$, since the formers have a relatively strong crystal-field splitting compared to the latter [26]. The local structures of Eu^{2+} ions in the present glasses are similar to that in $EuTiO_3$ in terms of the value of IS of Mössbauer spectra. So, this interaction is presumably ineffective for the present glasses. Kasuya reported that the second nearest-neighbor FM interaction in EuO is explainable by the third-order perturbation including the complicated processes [25]. This model is applicable to the configuration of the angle of Eu^{2+}-O^{2-}-Eu^{2+}=180° in general. It is reasonable to consider that the openness of glass structure bears an earmark of the FM 180° configuration. This exchange mechanism explains qualitatively the variation of θ_W with [Eu^{2+}] in the present glasses as follows. The processes in this mechanism involve the virtual inter-atomic O(2*p*)→Eu(5*d*) transfer. The covalency of Eu^{2+}-O bonds increases as [Eu^{2+}] is higher as mentioned above. The increase in the covalency of Eu^{2+}-O bonds means the enhancement of the

O(2*p*)→Eu(5*d*) transfer. Therefore, with increasing [Eu^{2+}], θ_W exhibits an increase than a linear one. On the other hand, the emergence of RSG phase indicates that, although the FM interactions predominate in this system, the negligible AFM interactions are also present. This distribution of the sign of magnetic interactions is thought to stem from the random structure of amorphous materials.

3.4 Conclusion

In conclusion, our experimental results reveal the dominance of FM interactions in the Eu^{2+}-based bulk oxide glasses. The origin of the FM interaction is explained in terms of the high order superexchange mechanism suggested by Kasuya. The present glasses exhibit a RSG behavior, indicating that the FM interactions are favored but the AFM ones are not negligible.

References in Chapter 3

[1] J. A. Mydosh, *Spin glasses: an Experimental Introduction* (Taylor &Francis Ltd., London, 1993).

[2] J. B. Goodenough, *Phys. Rev.* **100**, 564 (1955).

[3] J. Kanamori, *J. Phys. Chem. Solids* **10**, 87 (1959).

[4] R. A. Verhelst, R. W. Kline, A. M. de Graaf and H. O. Hooper, *Phys. Rev. B* **11**, 4427 (1975).

[5] J. L. Shaw, A. C. Wright, R. N. Sinclair, G. K. Marasinghe, D. Holland, M. R. Lees, and C. R. Scales, *J. Non-Cryst. Solids* **345&346**, 245 (2004).

[6] K. Tanaka, H. Akamatsu, S. Nakashima, and K. Fujita, *J. Non-Cryst. Solids* **354**, 1346 (2008).

[7] H. Akamatsu, K. Tanaka, K. Fujita, and S. Murai, *J. Phys. C*: *Condensed Matter* **20**, 235216 (2008).

[8] H. Akamatsu, K. Fujita, S. Murai, and K. Tanaka, *Appl. Phys. Lett.* **92**, 251908 (2008).

[9] P. Beauvillain, C. Dupas, J. P. Renard, and P. Veillet, *Phys. Rev. B* **29**, 4086 (1984).

[10] J. P. Sanchez, J. M. Friedt, R. Horne, and A. J. Van Duyneveldt, *J. Phys. C* **17**, 127 (1984).

[11] H. Akamatsu, K. Tanaka, K. Fujita, and S. Murai, *Phys. Rev. B* **74**, 012411 (2006).

[12] H. Akamatsu, K. Tanaka, K. Fujita, and S. Murai, *J. Magn. Magn. Mater.* **310**, 1506 (2007).

[13] J. Schoenes, E. Kaldis, W. Thöni, and P. Wachter, *Phys. Stat. sol.* **51**, 173 (1979).

[14] J. M. D. Coey, A. McEvoy, and M. W. Shafer, *J. Non-Cryst. Solids* **43**, 387 (1981).

[15] G. H. Shenoy and B. D. Dunlap, *Nucl. Instrum. Methods* **71**, 285 (1969).

[16] K. Fujita, K. Tanaka, K. Hirao, and N. Soga, *J. Am. Ceram. Soc.* **81**, 1845 (1998).

[17] K. Koteswara Rao, M. Vithal, and D. Ravinder, *J. Magn. Magn. Mater.* **253**, 65

(2002).

[18] R. Mathieu, P. Jönsson, D. N. H. Nam and P. Nordblad, *Phys. Rev. B* **63**, 092401 (2001).

[19] M. Sasaki, P. E. Jönsson, H. Takayama and H. Mamiya, *Phys. Rev. B* **71**, 104405 (2005).

[20] O. W. Dietrich, A. J. Henderson, and H. Meyer, *Phys. Rev. B* **12**, 2844 (1975).

[21] P, Nordblad, *J. Phys,:Condens. Matter.* **16**, S715 (2004).

[22] C. Djurberg, P. Svedlindh, P. Nordblad, M. F. Hansen, F. Bødker, and S. Morup, *Phys. Rev. Lett.* **79**, 5154 (1997).

[23] K. Jonason, J. Mattsson, and P. Nordblad, *Phys. Rev. B.* **53**, 6507 (1996).

[24] B. T. Matthias, R. M. Bozorth, and J. H. Van Vleck, *Phys .Rev. Lett.* **7**, 160 (1961).

[25] T. Kasuya, IBM J. Res. Dev. **14**, 214 (1970).

[26] C. L. Chien, S. Debenedetti, and F. D. S. Barros, *Phys. Rev. B.* **10**, 3913 (1974).

[27] T. R. McGuire, B. E. Argyle, M. W. Shafer, and J. S. Smart, *Appl. Phys. Lett.* **1**, 17 (1962).

[28] J. E. Greedan and G. J. McCarthy, *Mat. Res. Bull.* **7**, 531 (1972).

[29] M. W. Shafer, *J. Appl. Phys.* **36**, 1145 (1965).

[30] H. Hata, G. Adachi, J. Shiokawa, *Mat. Res. Bull.* **12**, 811 (1977).

CHAPTER 4: Magneto-optical properties of transparent divalent iron phosphate glasses

4.1 Introduction

In magnetic oxide glasses, the magnetic moments belonging to the cations such as 3*d* transition metal and 4*f* rare-earth ions are randomly distributed in the host glass structure. The mechanism of magnetic transition observed in oxide glasses has been experimentally investigated mainly based on the temperature dependence of dc and ac magnetic susceptibilities and ^{57}Fe Mössbauer spectrum [1-3]. Magnetic oxide glasses exhibit a wide variety of magnetic properties as shown in previous chapters.

Another interesting phenomenon associated with the magnetic oxide glasses lies in magneto-optical properties such as the Faraday effect. A great deal of attention has been paid to the Faraday effect of glasses containing 4*f* rare-earth ions such as Eu^{2+} and Tb^{3+} [4-8]. The glasses with high concentration of such rare-earth ions show rather high transmittance and large Faraday effect in the visible to ultraviolet wavelength region. These glasses can be applied as an optical isolator, an optical switch and an optical modulator working in such a short wavelength range. On the other hand, there exist few reports on the Faraday effect of glasses containing 3*d* transition metal ions, because the glasses bearing only a few molar percents of these ions often show intense absorption in the visible range. Nevertheless, in this chapter, phosphate glasses containing a large amount of Fe^{2+} ions, which are highly transparent in the wavelength range from 400 to 700 nm, have been prepared; their magnetic susceptibilities, optical absorption spectra, and Faraday rotation angles have been examined. Some iron phosphate glasses melted at various temperatures and under reducing conditions have been characterized so far [9-11], but there are no reports on iron phosphate glasses containing only Fe^{2+} ions, the concentration of which is as high as several tens percents

or so. Besides, although the reduction of Fe^{3+} into Fe^{2+} ions was completely achieved for an iron aluminosilicate glass system, the optical absorption and Faraday effect were not measured [2,3]. This chapter demonstrates that, in addition to the high transmittance in the visible range, the present phosphate glasses containing divalent iron ions exhibit large Faraday effect in the near-ultraviolet to blue range, which meets the emission from the blue laser diodes. The dependence of Faraday rotation angle on wavelength can be analyzed in terms of the Van Vleck-Hebb theory. This analysis leads to the effective transition probability comparable to those for the glasses containing rare-earth ions.

4.2 Experimental procedure

Glasses having xFeO·(100-x)P_2O_5 (mol%) [x = 50.0, 54.0, 57.1] compositions were prepared by a conventional melt quenching method using reagent grade Fe_2O_3 and H_3PO_4 aqueous solution as starting materials. Fe_2O_3 powder and H_3PO_4 aqueous solution were mixed and the mixture was heated at 180 °C to eliminate water. The mixture was then melted in an alumina crucible at 1200 °C for 30 min in air. The melt was poured onto a stainless steel plate to obtain glass, which showed black color due to the presence of Fe^{3+} ions. The resultant glass was pulverized, and the glass powder was remelted in a glassy carbon crucible placed in an alumina crucible with an alumina lid at 1200 °C for 30 min in air. The melt was quenched by being pressed with two stainless steel plates. The preparation methods of the present glasses are also described in section 1.2.2 (note that the glasses with x = 50.0, 54.0, and 57.1 correspond to xFe(100-x)PC with x = 33, 37, and 40, respectively.). Surprisingly, the glasses thus obtained were fairly transparent to the naked eye [see Fig. 4.2]. The as-quenched glasses were annealed at 460 to 480 °C for 3 h in an atmosphere of Ar (95 vol.%)/ H_2 (5 vol.%) to prevent the glasses from oxidation. X-ray diffraction analysis with Cu K_α

radiation confirmed the absence of crystalline phases in the glasses. Although phosphate glasses sometimes show relatively poor chemical durability, changes in appearance such as devitrification have not been observed for the present phosphate glasses even after they were set in air for more than 4 months. The glass samples were polished so that their thickness was 0.4 to 0.5 mm, and subjected to Faraday effect and optical absorption measurements. The Faraday effect measurements were performed at room temperature by using a commercial measurement system for Faraday and Kerr effects (JASCO, Model K-250). The wavelength was varied from 350 to 850 nm and the applied magnetic field was fixed to be 15 kOe. The optical absorption spectra were recorded using a spectrophotometer (JASCO, V-570). The transparent glasses were pulverized and subjected to ^{57}Fe Mössbauer effect and magnetic susceptibility measurements. The ^{57}Fe Mössbauer measurements were performed at room temperature by using ^{57}Co in metallic Rh as a γ-ray source. The magnetic susceptibility under zero-field cooling (ZFC) and field cooling (FC) conditions was measured in the temperature range from 2 to 300 K with the dc magnetic field of 50 Oe applied by utilizing a superconducting quantum interference device (SQUID) magnetometer (Quantum Design, model MPMS-XL).

4.3 Results and discussion

4.3.1 ^{57}Fe Mössbauer spectroscopy

The ^{57}Fe Mössbauer spectra of the glasses are depicted in Fig. 4.1. All the spectra are composed of a paramagnetic doublet attributable to Fe^{2+} ions; absorption peaks ascribed to Fe^{3+} ions are barely observed in all the spectra. The Mössbauer spectra of glasses prepared by melting only in air indicate that more than 80% of iron ions are present as Fe^{3+} in the glasses [see Table 1.4]. The remelting in a glassy carbon crucible could reduce almost all the Fe^{3+} ions into Fe^{2+} ions. This technique is

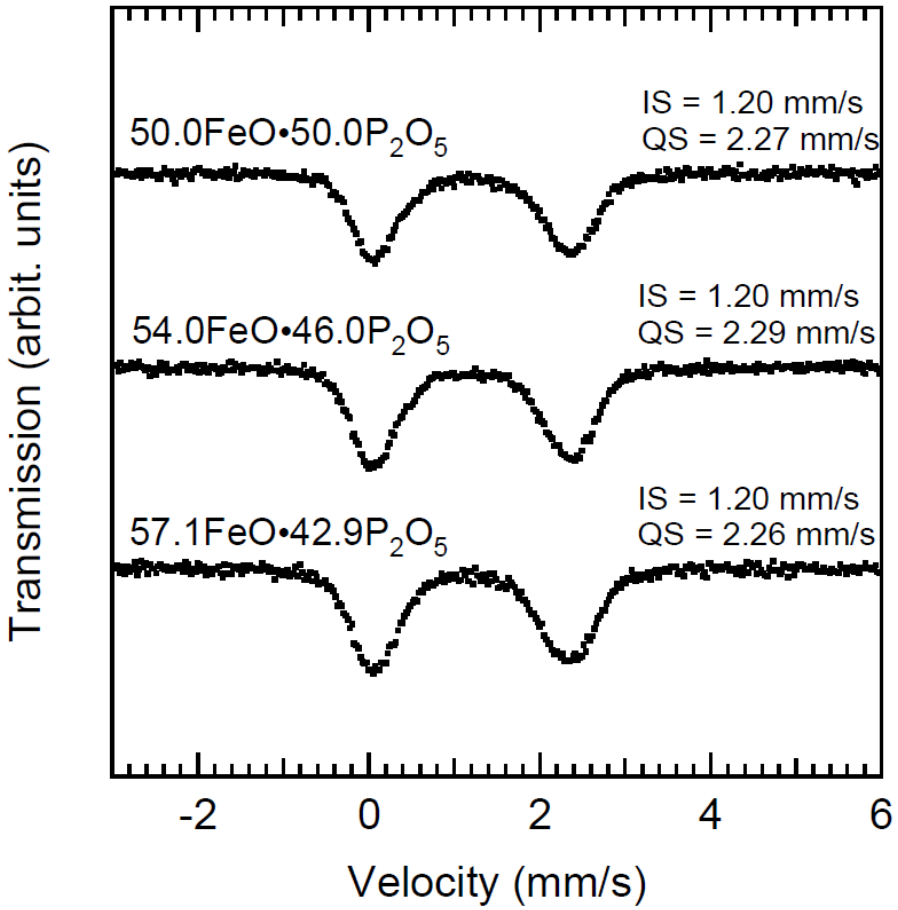

Figure 4.1: ^{57}Fe Mössbauer spectra at room temperature for the FeO-P_2O_5 glasses with 50.0, 54.0 and 57.1 mol% of FeO. IS and QS denote the isomer shift and the quadrupole splitting, respectively, for the doublet assigned to Fe^{2+}.

much easier to obtain the Fe^{2+} ion when compared with the conventional method such as melting under a flow of reducing gas. The isomer shift (IS) and quadrupole splitting (QS) for the glasses after the remelting are summarized in Fig. 4.1. The value of IS=1.20 mm/s corresponds to Fe^{2+} ions octahedrally coordinated by O^{2-} ions as mentioned in section 1.2.

4.3.2 Optical absorption spectra

Figure 4.2(a) shows the optical absorption spectra of the glasses, which exhibit fairly high transmittance in the wavelength range from 400 to 700 nm. The intense optical absorptions in the ultraviolet and infrared regions are ascribable to the charge transfer transition from O^{2-} to Fe^{2+} and intra-atomic *d-d* crystal field transition, respectively [14]. Although the presence of Fe^{3+} ions can not be detected in the Mössbauer spectra, very weak absorption bands attributed to a tiny amount of Fe^{3+} ions are observed at 400 to 550 nm [13]. As the value of x is increased, the amount of Fe^{3+} ion is apt to increase and hence the glass turns its color from blue greenish into orangish [see Fig. 4.2(b)].

4*.3.3 Temperature dependence of dc susceptibility*

Figure 4.3(a) illustrates the temperature dependence of magnetic susceptibility, $\chi(T)$, and its reciprocal, $\chi^{-1}(T)$, for the $57.1FeO{\cdot}42.9P_2O_5$ glass. The linear dependence of $\chi^{-1}(T)$ on T at high temperatures (30 K $\leq T \leq$ 300 K) reveals that these glasses are paramagnetic in the temperature region; the linear part is describable in terms of the following Curie-Weiss law:

$$\frac{1}{\chi} = \frac{3k_{\mathrm{B}}\left(T-\theta_W\right)}{NM_{\mathrm{B}}{}^2\mu_{\mathrm{B}}{}^2}, \qquad (4.1)$$

where θ_{W} is the Weiss temperature, N the number of magnetic ions per unit mass, μ_{B} the Bohr magneton, M_{B} the effective number of Bohr magnetons, and k_{B} the Boltzmann constant. The value of M_{B} = 5.21 obtained by fitting Eq. (4.1) to the experimental data of $\chi^{-1}(T)$ at high temperatures is slightly higher than the theoretical

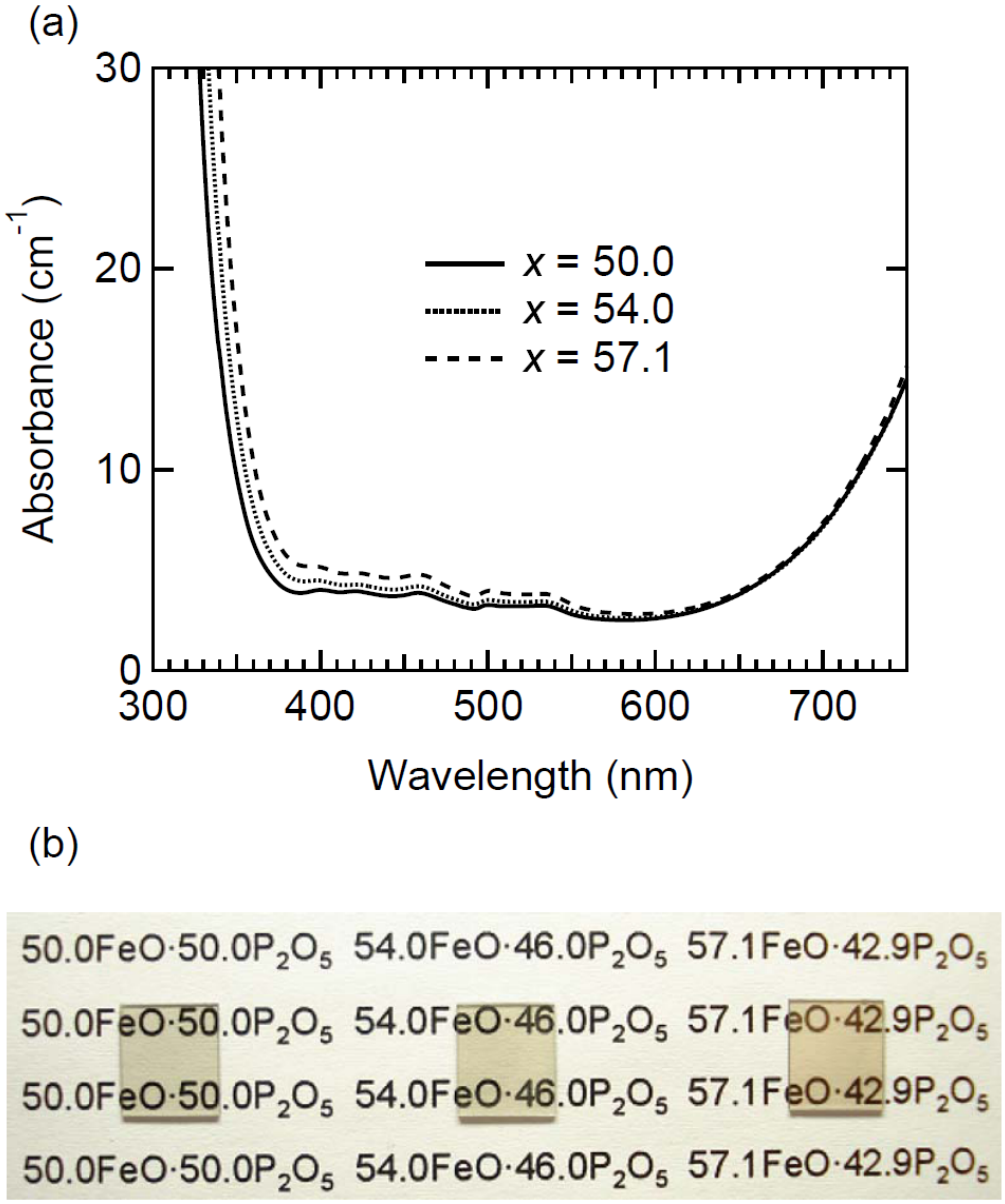

Figure 4.2: (a) Optical absorption spectra for the xFeO·(100-x)P_2O_5 glasses with x=50.0, 54.0 and 57.1. (b) Pictures of the glasses with the thickness of about 450 μm.

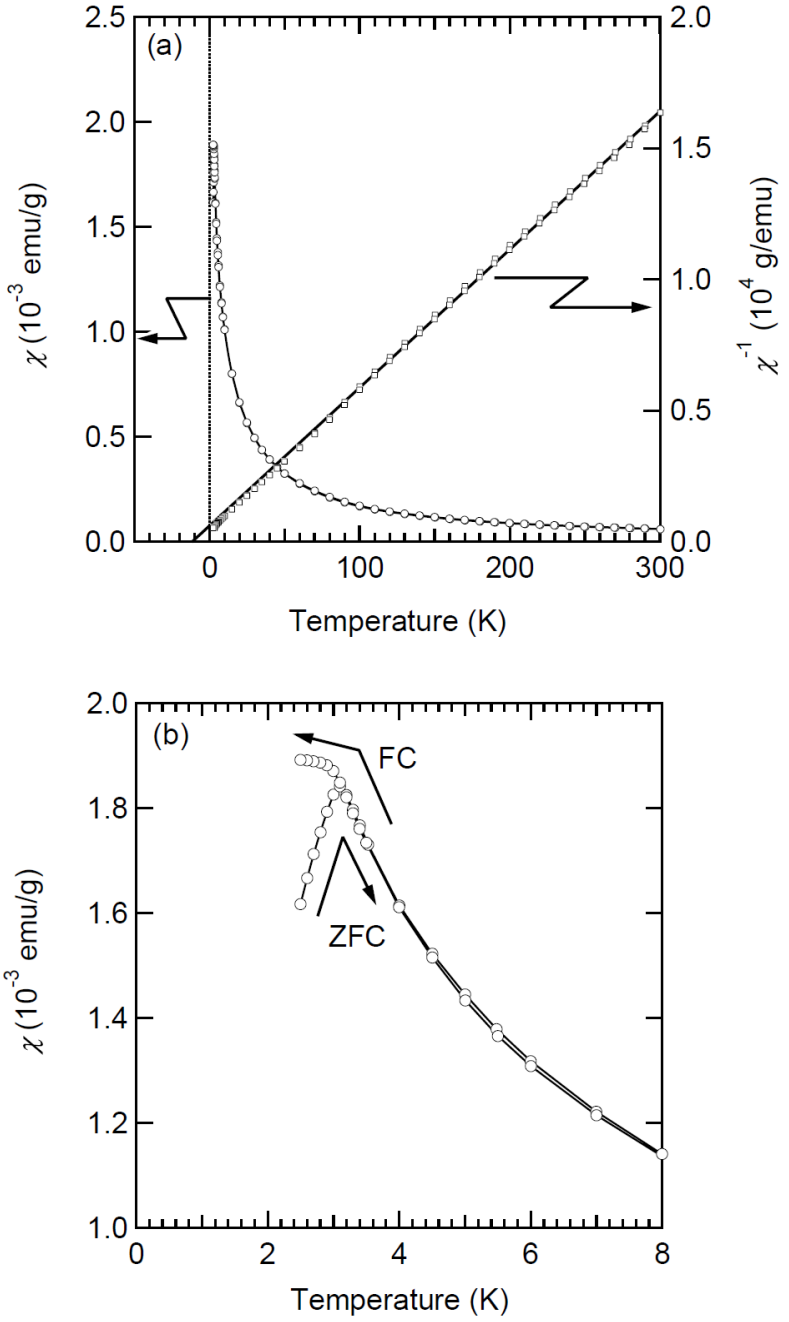

Figure 4.3: (a) Temperature dependence of dc magnetic susceptibility and its reciprocal for the $57.1FeO{\cdot}42.9P_2O_5$ glass. (b) The enlarged view of low temperature region.

spin-only value of Fe^{2+}, i.e., 4.82 presumably due to the contribution of unquenched orbital magnetic moment. The Fig. 4.3(b) shows $\chi(T)$ in the low temperature region. $\chi(T)$'s in ZFC and FC deviate from each other at the temperature where $\chi(T)$ in the ZFC run exhibits a maximum. This behavior of $\chi(T)$ is characteristic of the spin glass. As summarized in Table 1.4, the spin freezing temperature is 2.2, 2.6 and 3.1 K and θ_W is -8.6, -9.0 and -11.6 K for xFeO·(100-x)P_2O_5 glasses with x = 50.0, 54.0 and 57.1, respectively. The negative value of θ_W means that the antiferromagnetic interaction is dominant among the magnetic moments of Fe^{2+} ions in the glasses.

4.3.4 Faraday effect

The wavelength dependence of Verdet constant, V, for the glasses is illustrated in Fig. 4.4. For paramagnets, $V=\theta/(Hl)$, where θ is the Faraday rotation angle, H is the applied magnetic field, and l is the length of light path in the material. The absolute value of V monotonically increases as the wavelength of incident light, λ, becomes shorter. A similar tendency was observed for the rare-earth-containing glasses. The relation between V and λ for the glasses containing rare-earth ions has been analyzed in terms of the Van Vleck-Hebb theory using the following equation:

$$V = \frac{4\pi^2 \chi}{g\mu_B ch} \sum_i C_i \left(1 - \frac{\lambda^2}{\lambda_i^2}\right)^{-1}, \qquad (4.2)$$

where g is the Landé factor, μ_B is the Bohr magneton, c is the velocity of light, h is the Plank constant, C_i is related to the transition probability, and λ_i is the transition wavelength. The subscript i denotes the electronic transition which contributes to the Faraday effect. The approximation taking only single electronic transition into account has been used to explains the wavelength dependence of V of rare-earth-containing glasses [4-7]. However, the dependence of V of the iron phosphate glasses on λ can not be interpreted by this single oscillator model, but described well by considering two optical transitions, i.e., the charge transfer transition

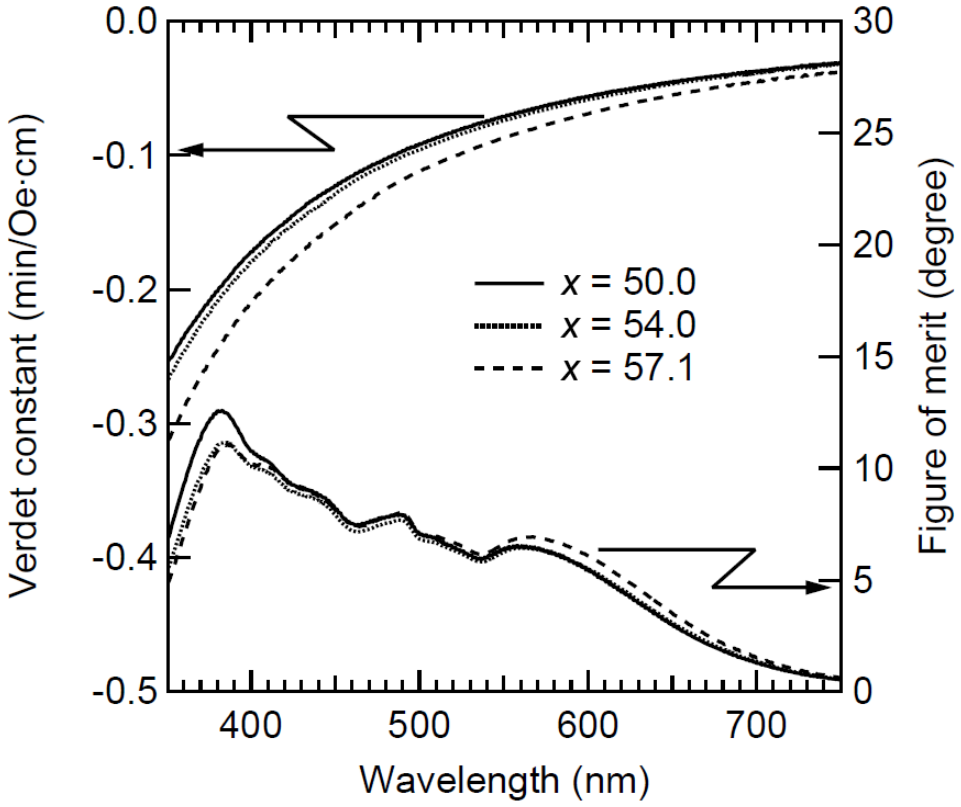

Figure 4.4: Wavelength dependence of Verdet constant and magneto-optical figure of merit for the xFeO·(100-x)P_2O_5 glasses with x=50.0, 54.0 and 57.1.

and the crystal field transition in the ultraviolet and infrared regions, respectively. For instance, the analysis using Eq. (4.2) yields C_1=8.6×10^{-45} J·cm^3, λ_1=214 nm, C_2=1.1×10^{-46} J·cm^3 and λ_2=1100 nm for 57.1FeO·42.9P_2O_5 glass. The value of C_1 corresponding to the charge transfer transition is much larger than that of C_2 corresponding to the *d*-*d* transition. This fact indicates that the charge transfer transition mainly contributes to the Faraday effect due to the large oscillator strength.

Also shown in Fig. 4.4 is the magneto-optical figure of merit defined as $|\theta|/\alpha$, where θ is the Faraday rotation angle and α is the absorbance. $|\theta|/\alpha$ is an important factor from a point of view of practical applications. For all the glasses, $|\theta|/\alpha$ exhibits a maximum at around 380 nm. For instance, $|\theta|/\alpha$ of 50.0FeO·50.0P_2O_5 glass is 13 ° at 380 nm under *H*=15 kOe. Since the wavelength like 380 nm corresponds to the emission of blue laser diodes, the present glasses are expected as a candidate for optical devices such as an optical isolator in such a short wavelength region. The amplitude of *V* for the present glasses is several times smaller than or comparable to those for the rare-earth-containing glasses; for instance, at 405 nm, *V* is -0.204 and -0.560 min/cm·Oe for 57.1FeO·42.9P_2O_5 and 25.4Tb_2O_3·74.6P_2O_5 glasses, respectively, both of which are phosphate glasses and have almost the same effective transition wavelength [14]. Another advantage of the present glasses lies in the fact that both iron oxide and phosphoric acid, i.e., the starting materials for the glasses, are much more inexpensive and available when compared with the rare-earth oxides which have been practically utilized as a component of glass materials for Faraday rotators.

4.4 Conclusion

In conclusion, the glasses with *x*FeO·(100-*x*)P_2O_5 (mol%) [*x* = 50.0, 54.0, 57.1] composition exhibit farely high transmittance in the visible region, although the glasses contain a large amount of 3*d* transition metal ions. The glasses have large Faraday

rotation angle in the near-ultraviolet to blue region. The large effective transition probability comparable to those reported for the rare-earth-containing glasses stems from the large oscillator strength of charge transfer transition from O^{2-} to Fe^{2+}. Considering that Fe is an abundant element in the crust of the earth, the achievement of FeO-based glass materials which shows high transmittance as well as large Faraday effect in the near-ultraviolet to blue region is of great importance.

References in Chapter 4

[1] R. A. Verhelst, R. W. Kline, A. M. de Graaf and H. O. Hooper, *Phys. Rev. B* **11**, 4427 (1975).

[2] A. Ito, E. Torikai, H. Yamauchi, and Y. Syono, *J. Phys. C: Solid State phys.* **15**, 2759 (1982).

[3] J. P. Sanchez, J. M. Friedt, R. Horne, and A. J. Van Duyneveldt, *J. Phys. C* **17**, 127 (1984).

[4] N. F. Borrelli, *J. Chem. Phys.* **41**, 3289 (1964).

[5] K. Tanaka, K. Hirao and N. Soga, *Jpn. J. Appl. Phys.* **34**, 4825 (1995).

[6] K. Tanaka, K. Fujita, N. Soga, J. Qiu and K. Hirao, *J. Appl. Phys.*, 83 (1997) 840.

[7] K. Tanaka, K. Fujita, N. Matsuoka, K. Hirao and N. Soga, *J. Mater. Res.* **13**, 1989 (1998).

[8] T. Hayakawa, M. Nogami, N. Nishi and N. Sawanobori, *Chem. Mater.* **14**, 3223 (2002).

[9] G. K. Marasinghe, M. Karabulut, C. S. Ray, D. E. Day, M. G. Shumsky, W. B. Yelon, C. H. Booth, P. G. Allen and D. K. Shuh, *J. Non-Cryst. Solids* **222**, 144 (1997).

[10] C. S. Ray, X. Fang, M. Karabulut, G. K. Marasinghe and D. E. Day, *J. Non-Cryst. Solids* **249**, 1 (1999).

[11] M. Karabulut, G. K. Marasinghe, C. S. Ray, D. E. Day, G. D. Waddill, C. H. Booth, P. G. Allen, J. J. Bucher, D. L. Caulder and D. K. Shuh, *J. Non-Cryst. Solids* **306**, 182 (2002).

[12] D. A. Nolet, *J. Non-Cryst. Solids* **37**, 99 (1980).

[13] R. Carl, S. Gerlach and C. Rüssel, *J. Non-Cryst. Solids* **352**, 244 (2007).

[14] S. B. Berger, C. B. Rubinstein, C. R. Kurkjian and A. W. Treptow, *Phys. Rev.* **133**, A723 (1964).

CHAPTER 5: Structural and magnetic properties of disordered $CdFe_2O_4$ thin films fabricated via sputtering method

5.1 Introduction

Cadmium ferrite ($CdFe_2O_4$) possesses a normal spinel structure as its stable phase, where the Cd^{2+} and Fe^{3+} ions occupy the tetrahedral sites (A sites) and the octahedral sites (B sites), respectively, in the face-centered-cubic close packing of the oxide ions. The Fe^{3+} ions in the B sites form a pyrochlore lattice. Hence, strong magnetic frustration based on the geometry is generated in the three-dimensional network of corner-sharing tetrahedra like the pyrochlore lattice when its vertices are occupied by spins with antiferromagnetic interaction among nearest neighbors. Although it is well known that the normal spinel type of $CdFe_2O_4$ behaves like an antiferromagnet with a Néel temperature of 13 K, strictly speaking, spin freezing occurs with only short-range correlation at 13 K and no long-range order is observed down to 0.1 K due to the geometrical frustration, as revealed by Kamazawa *et al*. using neutron scattering experiments [1].

The stable phase of zinc ferrite ($ZnFe_2O_4$) also has a normal spinel structure. Like $CdFe_2O_4$, $ZnFe_2O_4$ shows the geometrical frustration which prevents the magnetic moments of the Fe^{3+} ions in the B sites from long-range order down to 1.5 K [2]. However, nonzero magnetization and high magnetic transition temperature can be observed for the $ZnFe_2O_4$ nanoparticles fabricated by co-precipitation method [3] and high energy ball-milling [4] and for the $ZnFe_2O_4$ thin films derived by gas-phase deposition methods such as sputtering [5,6] and pulsed laser ablation [7]. These non-equilibrium processes yield a metastable phase of $ZnFe_2O_4$. The large magnetization and the high magnetic transition temperature are attributed to such a metastable structure that a site exchange between Zn^{2+} in the A site and Fe^{3+} in the B

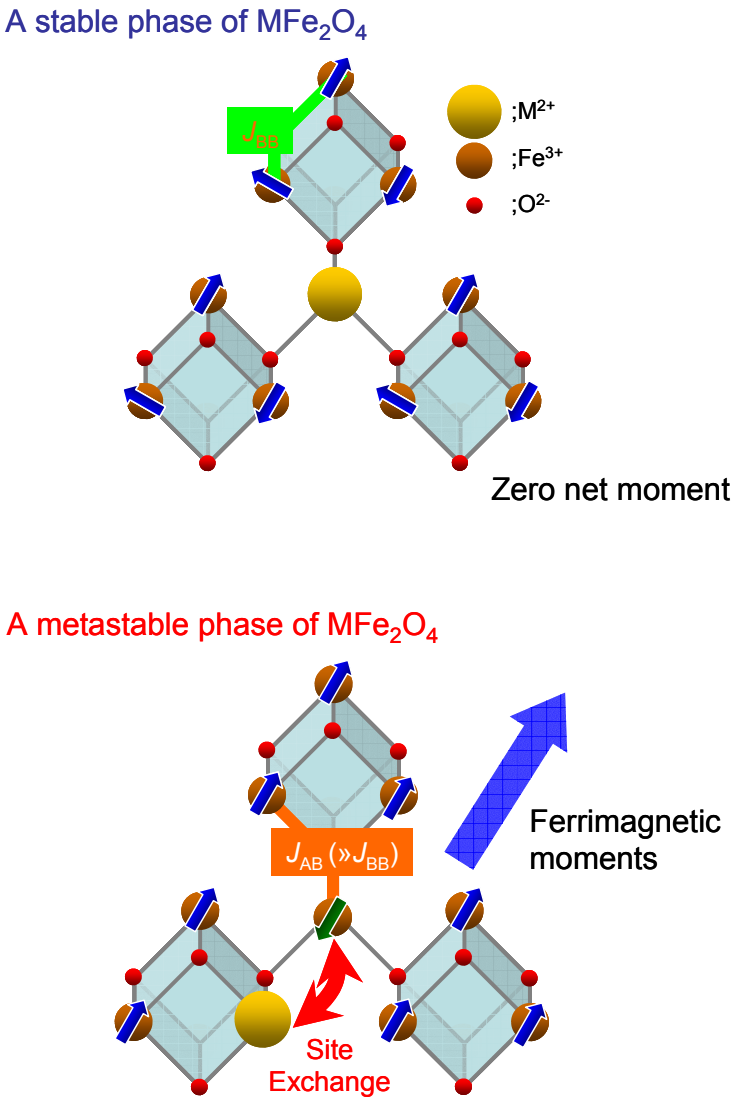

Figure 5.1: Schematic image of a mechanism for the enhancement of magnetization due to a site exchange between the tetrahedral (A) and octahedral (B) sites in normal spinel oxide MFe_2O_4.

site takes place. The schematic image of this mechanism is illustrated in Fig. 5.1. The strong superexchange interaction between the Fe^{3+} ions in the A and B sites leads to a ferrimagnetic order even above room temperature, although the magnetic order may be restricted within a localized region due to a random distribution of cations. The net moments generated by the site exchange exhibit cluster-spin glass behavior.

Recently, ferromagnetic properties have been observed for ultrafine particles of $CdFe_2O_4$ prepared via co-precipitation [8] and ball-milling processes [9]. The ferromagnetic behavior are thought to stem from the site inversion between Cd^{2+} ions in the A sites and Fe^{3+} ions in the B sites. Chapter 5 reports the structural and magnetic properties of $CdFe_2O_4$ thin films prepared by the sputtering method; it is demonstrated that the sputtered $CdFe_2O_4$ thin films exhibit large magnetization and high magnetic transition temperature. The effects of heat treatment on the magnetic and structural properties of the sputtered $CdFe_2O_4$ thin films are also reported.

5.2 Experimental procedure

$CdFe_2O_4$ thin films were prepared by utilizing a radio frequency (rf) sputtering method (ULVAC RFS-200). CdO and Fe_2O_3 (hematite) powders were weighed so that the molar ratio of Fe_2O_3 to CdO was 1.25. The powders mixed thoroughly were compacted into a mould made of copper and used as a target. The composition of sputtering target was different from that of stoichiometric $CdFe_2O_4$ because resultant sputtered thin films were richer in CdO than the target as described below. Thin films were deposited on a silica glass substrate under conditions that the rf power was 100 W, the atmosphere was O_2 and the gas pressure was 1.5×10^{-2} Torr. Deposited films were annealed at 200 and 400 °C in air for 3 h. The bulk sample was also fabricated via solid state reaction. CdO and Fe_2O_3 powders weighed so that the molar fractions of CdO and Fe_2O_3 were equivalent to each other were thoroughly mixed and pressed into

a pellet. Covered with CdO powder, the pellet was calcined at 800 °C for 3 h in air.

It was confirmed by energy dispersive x-ray spectroscopy and Rutherford backscattering spectroscopy (RBS) that both the as-deposited film and the bulk sample had stoichiometric compositions of $CdFe_2O_4$. X-ray diffraction (XRD) analysis was performed using Cu K_α radiation (Rigaku RINT2500) to identify the crystal structure of films. Fe-*K* edge x-ray absorption near edge structure (XANES) was obtained to explore the local structure of Fe ions by using x-ray-fluorescence-yield mode at BL01B1 beamline in SPring-8, Harima, Japan. The microstructure of thin films was observed by transmission electron microscopy (TEM) at an accelerating voltage of 200 kV. Magnetic properties of the samples were examined by using a superconducting quantum interference device magnetometer (Quantum Design MPMS-XL).

5.3 Results and discussion

5.3.1 Structural properties of $CdFe_2O_4$ sputtered thin films

Figure 5.2 illustrates XRD patterns of the as-deposited and annealed thin films. The diffraction lines in the patterns of all the films indicate that a single phase of $CdFe_2O_4$ precipitates in the films. It is found that the diffraction lines become sharper and shift to a higher angle side as the annealing temperature is increased. The narrowing of the diffraction lines suggests that the size of crystallite becomes larger. The crystallite size of the as-deposited film is estimated to be about 6 nm from the broadening of the diffraction lines using the following Scherrer's equation:

$$d = \frac{0.9\lambda}{\beta \cos\theta}, \qquad (5.1)$$

where d is the diameter of crystallite, β the full width at half maximum of diffraction line, θ the diffraction angle, and λ the x-ray wavelength (1.5405 Å for the present case). The shift of the diffraction lines to a high angle side corresponds to a decrease in the

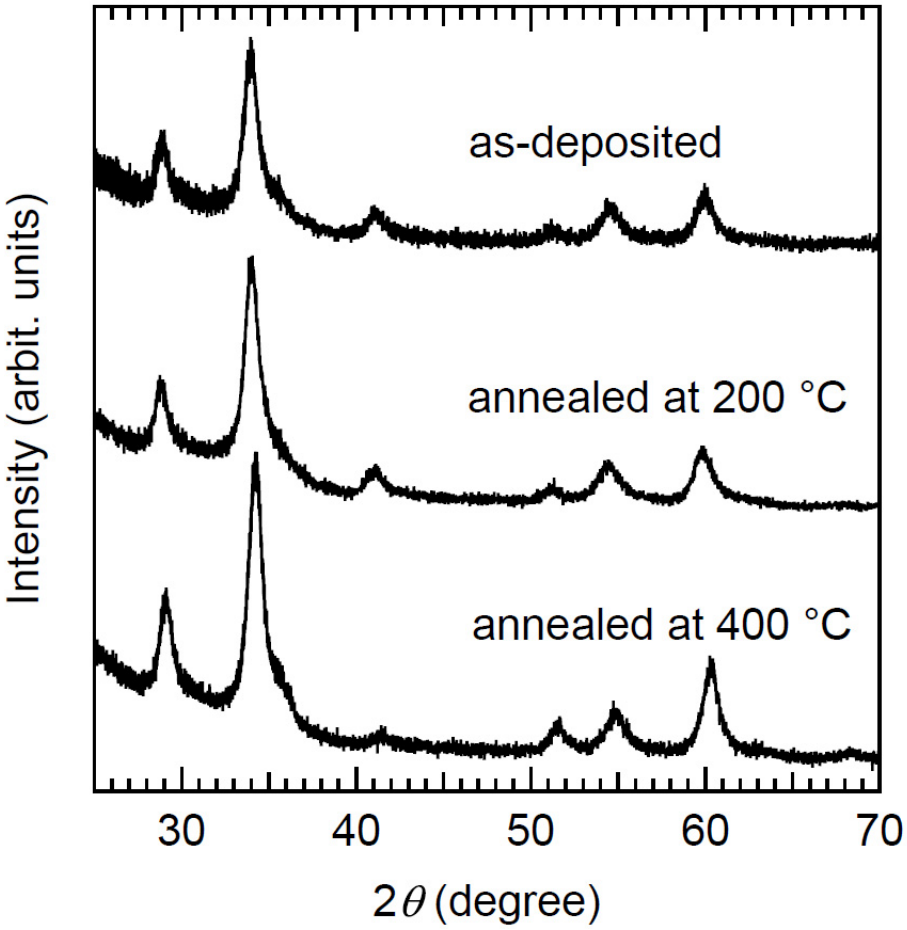

Figure 5.2: X-ray Diffraction patterns for $CdFe_2O_4$ thin films prepared by a sputtering method. The XRD patterns for the as-deposited film and the films annealed at 200 and 400 °C are shown.

lattice parameter. This fact suggests that annealing the as-depodited film at relatively low temperatures like 200 to 400 °C provides the crystals in the film with higher density.

TEM images of the $CdFe_2O_4$ thin films with or without annealing are shown in Figure 5.3. As shown in Fig. 5.3(a), it is revealed that the as-deposited film is composed of single crystalline particles possessing a size of about 5 nm dispersed in an amorphous phase. This is consistent with the crystallite size estimated from the broadened line in the XRD pattern. In the film annealed at 200 °C, crystals slightly larger than those in the as-deposited film are observed, while the amorphous phase still remains [Fig. 5.3(b)]. On the other hand, the TEM image of the film annealed at 400 °C indicates that grain coarsening occurs [Fig. 5.3(c)]. In the film, there are no amorphous regions, but grain boundaries are observed.

Figure 5.4 shows Fe-*K* edge XANES spectra for the films and the bulk sample prepared by solid-state reaction. The intensity of the XANES spectra is normalized by using the intensity at E = 7.100 and 7.140 keV, both of which are off-sides of Fe-*K* edge. As the annealing temperature is increased for the thin films, the main absorption bands centered at E = 7.129 keV become sharper and the profile of the spectra approaches that for the bulk sample. A similar variation was observed for $ZnFe_2O_4$ thin films prepared by a sputtering method [10]. Another important point is that the intensity of the pre-edge peak observed at around E = 7.111 keV is reduced by an increase in the annealing temperature. It is well known that the pre-edge peak stems from the Fe^{3+} ions in the A sites for spinel-type crystalline materials [11]. The results suggest that the number of Fe^{3+} ions coordinated by six oxide ions increases as the annealing temperature increases.

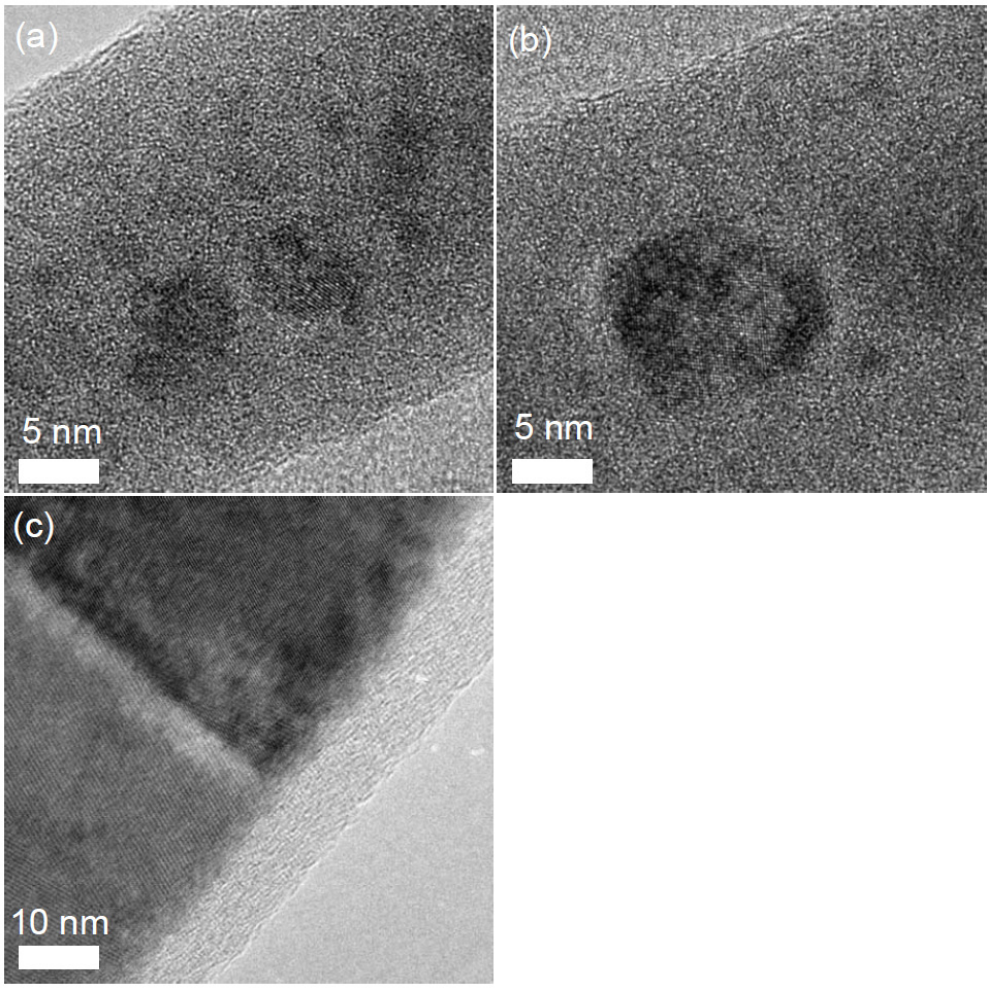

Figure 5.3: TEM images of (a) as-deposited film and films annealed at (b) 200 and (c) 400 °C.

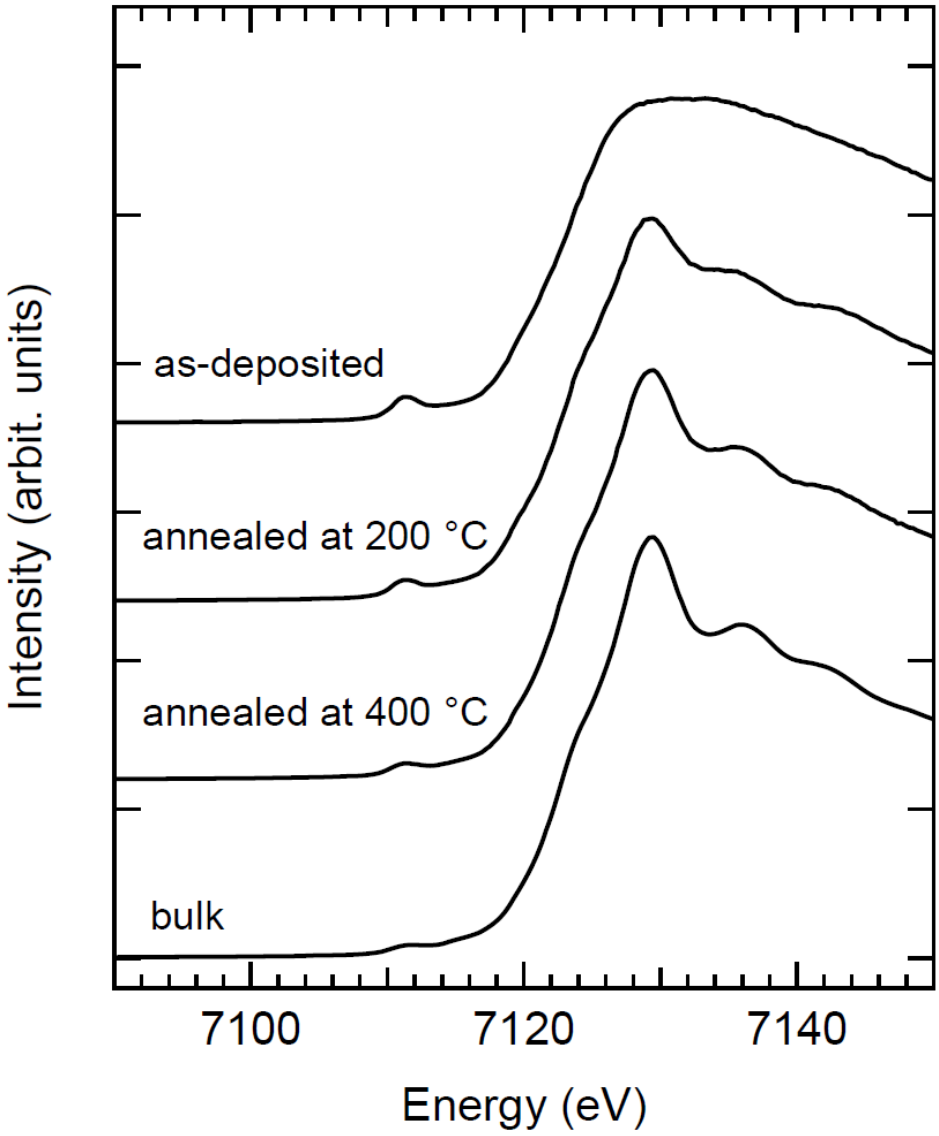

Figure 5.4: X-ray absorption near edge structure spectra of $CdFe_2O_4$ thin films and bulk sample in the vicinity of the Fe-*K* edge.

5.3.2 Magnetic properties of as-deposited $CdFe_2O_4$ sputtered thin films

Figure 5.5 shows the temperature dependence of magnetization measured at varied magnetic fields for the as-deposited $CdFe_2O_4$ thin film. Both field cooling (FC) and zero-field cooling (ZFC) were performed. The magnetization curves exhibit a peak under the condition of ZFC process. The peak temperature shifts to a low temperature side with increase in magnetic field. The deviation between the magnetizations for ZFC and FC conditions is observed when the magnetic field is 3, 50, and 200 Oe. The deviation temperature becomes lower as the magnetic field is increased and, eventually, no deviation is found in the magnetization curve measured at 5000 Oe. The magnetic behavior of as-deposited $CdFe_2O_4$ thin film is quite different from those of bulk $CdFe_2O_4$ as discussed in detail below [see Fig. 5.9]. This may be due to a site exchange between Cd^{2+} in the A site and Fe^{3+} in the B site in the spinel structure. This behavior resembles that observed in cluster-spin glasses and superspin glasses [6,12], suggesting that a ferrimagnetic order occurs only for localized magnetic moments.

In Fig. 5.6, the real part of ac magnetization is shown as a function of temperature for the as-deposited $CdFe_2O_4$ thin film. The amplitude of ac magnetic field H_{ac} was kept to be 3 Oe and the ac frequency f was varied in the range from 0.1 to 1000 Hz. The frequency-dependent spin-freezing temperature $T_f(f)$, defined as a temperature at which the real part of ac susceptibility manifests a maximum, shifts to a higher temperature side with increasing f. The relative shift of $T_f(f)$ per decade of f, i.e., $\Psi=(\Delta T_f/\ T_f)/\Delta(\log f)$ [13], was found to be 0.0075. This value is comparable to those obtained for the spin glasses, i.e., $\sim 10^{-3}$-10^{-2}, while the value is not in the range of the superparamagnets, i.e., $\sim 10^{-1}$ [13,14]. This value suggests that the spin freezing in the present film is not attributed to a simple superparamagnetic blocking but to a collective spin freezing.

The relaxation time of the system, τ, is considered to become $1/f$ at $T_f(f)$. On the

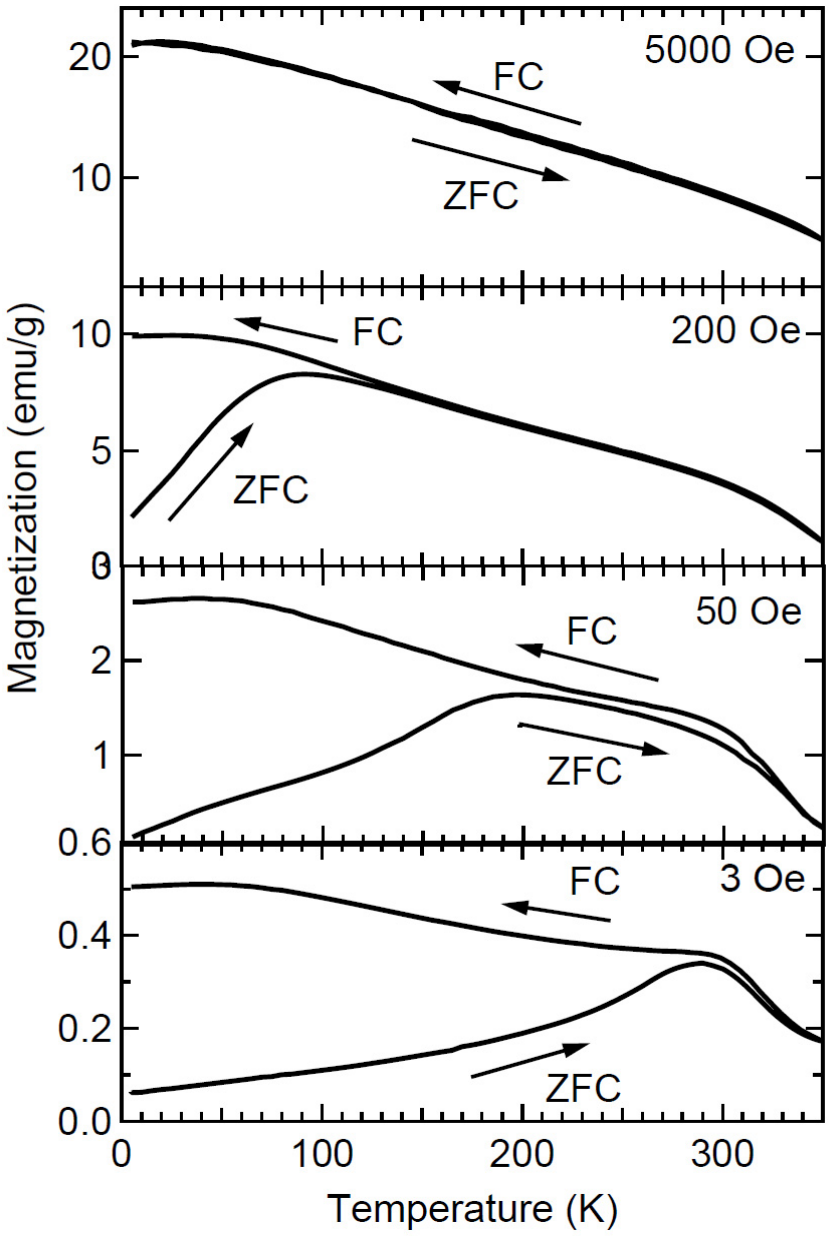

Figure 5.5: Temperature dependence of magnetization measured at a series of magnetic fields for the as-deposited $CdFe_2O_4$ thin film.

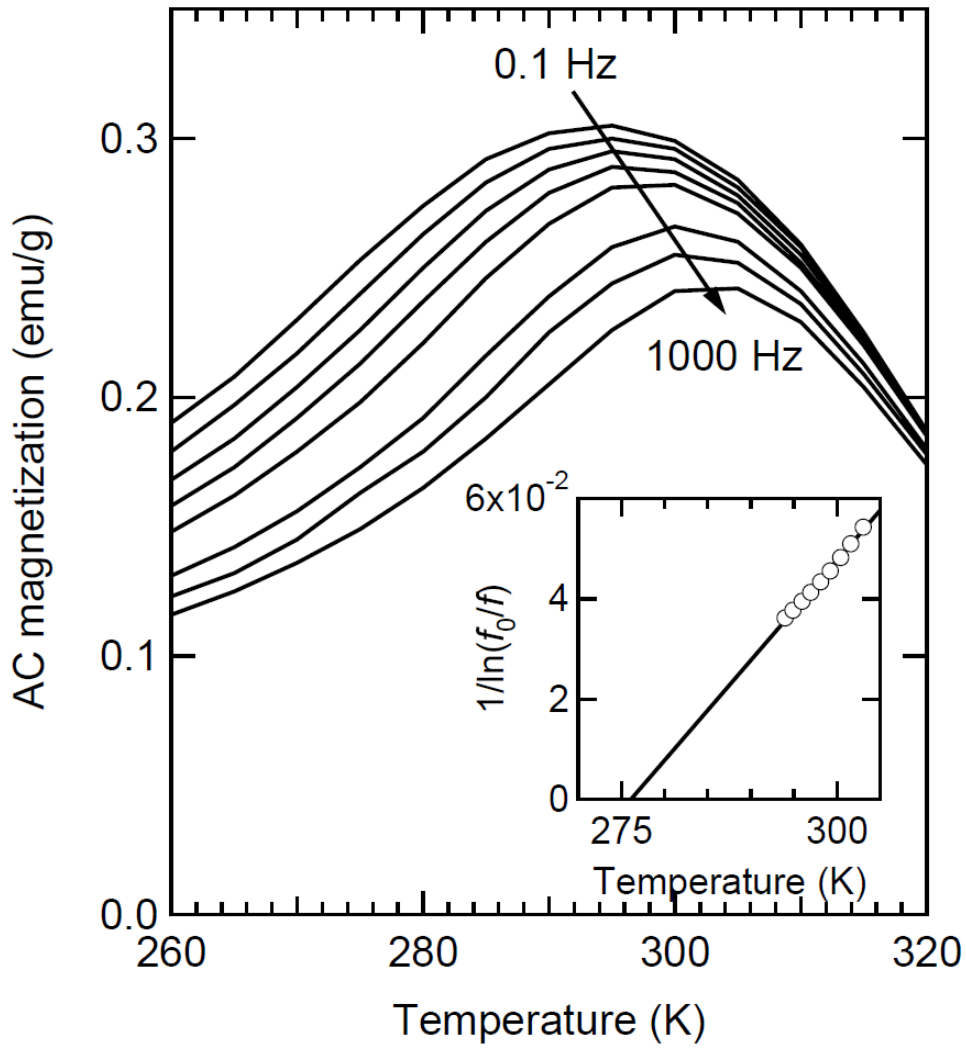

Figure 5.6: Temperature dependence of real part of ac magnetization for the as-deposited $CdFe_2O_4$ thin film measured at H_{ac}=3 Oe. The frequency f is 0.1, 0.3, 1, 3, 10, 100, 300, 500 and 1000 Hz (from top to bottom). The inset of Fig. 5.6 illustrates the relationship between the frequency of magnetic field and the spin freezing temperature. The solid line in the inset indicates the fitting of Eq. (5.4) to the experimental data.

basis of the assumption that the system exhibits critical slowing down at a critical temperature, T_c, the analysis of the data in terms of the power law,

$$\tau = \tau_0 \left(\frac{T_f(f) - T_c}{T_c} \right)^{-zv}, \qquad (5.2)$$

where τ_0 is the characteristic relaxation time of magnetic moments and zv the critical exponent, has been performed. The fitting parameters of zv=13, T_c=285 K, and τ_0=1.5×10^{-19}s are yield by this analysis. The value of zv is in the range of those reported for conventional spin glasses [16,17]. However, the value of τ_0 is too small compared even to the spin flip time of individual magnetic moments belonging to atoms or ions, i.e., 10^{-13}~10^{-12} s. The much larger values of τ_0, i.e., 10^{-6}s, are reported for strongly interacting nanoparticles systems and superspin glasses [16,18]. This is partly because the wide distribution of the size of magnetic clusters makes the magnetic behavior much complicated. On the other hand, for a simple superparamagnet with no inter-particle interactions, the frequency dependence of spin freezing temperature is described in terms of the Arrhenius law,

$$\tau = \tau_0 \exp\left(\frac{E_a}{k_B T} \right), \qquad (5.3)$$

where E_a is the activation energy for the reversal of magnetic particles and k_B is the Boltzmann constant. The analysis using the Eq. (5.3) yields physically unacceptable values of E_a and τ_0. The failure of the Arrhenius law in giving physically acceptable fitting parameters is often compensated by fitting of Vogel-Fulcher empirical law,

$$\tau = \tau_0 \exp\left(\frac{E_a}{k_B (T - T_0)} \right), \qquad (5.4)$$

where E_a and T_0 are the fitting parameters associated with energy and temperature,

respectively. The physical meanings of these parameters are not completely clear although it is suggested that the parameters E_a and T_0 present activation energy of magnetic clusters and inter-cluster interaction or a true transition temperature, respectively [19,20]. Fitting the experimental data to Eq. (5.4) yields the parameter values of $\tau_0=10^{-11}$s, E_a/k_B =502 K, and T_0=276 K. These values are physically acceptable although the signification of the analysis by the Voger-Fulcher law remain to be clear. These results of analyses for the frequency dependence of spin freezing temperature indicate that the spin freezing in the as-deposited $CdFe_2O_4$ thin film can not be explained in terms of a simple superparamagnetic blocking.

To shed light on the nature of magnetically frozen states of the as-deposited $CdFe_2O_4$ thin film, the zero-field cooling memory experiment proposed by Mathieu *et al* [21] has been performed. In this experiment, the system is cooled in zero magnetic field from a high temperature with or without a long stop at a specific temperature T_s situated below the spin freezing temperature. The $\chi(T)$ curve is recorded during the subsequent heating in a measuring magnetic field. Sasaki *et al*. [22] have demonstrated that a memory is imprinted during the aging in the absence of magnetic field only for spin glasses and strongly interacting nanoparticles systems or superspin glasses, but not for non-interacting superparamagnets. Hence, the observation of the memory effect warrants cooperative spin dynamics [14,22-28]. In the present case, the film was cooled to a stopping temperature T_s=250 K, and then kept at T_s for 3 h. After a stop for 3 h, the glass was recooled to 150 K. Subsequently, a magnetic field of 3 Oe was applied and the magnetization curve was measured on heating. The reference magnetization curve was determined by measuring the temperature dependence of zero-field cooled magnetization without any intermittent stops. The results are shown in Fig. 5.7. The memory effect is clearly seen as the dip at T_s. This result strongly evidences that the as-deposited $CdFe_2O_4$ thin film undergoes a collective spin freezing like a superspin glass transition.

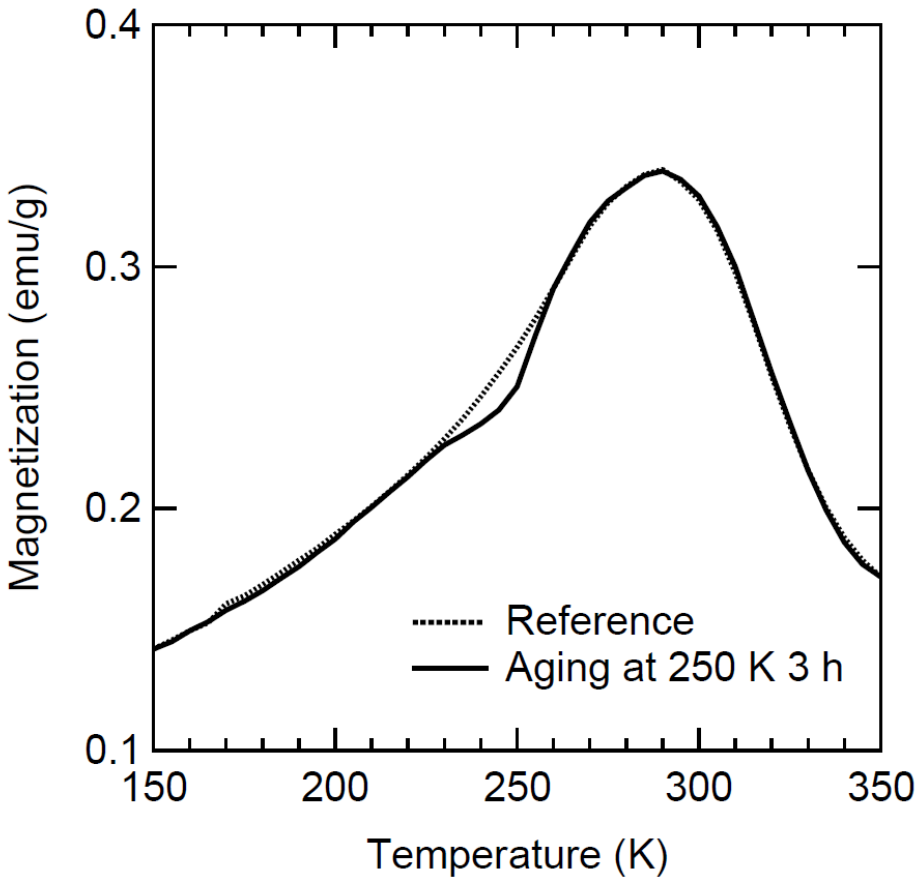

Figure 5.7: The temperature dependence of dc magnetization measured on heating after zero-field cooling with an intermittent stop at T_s=250 K for 3 h. The reference magnetization curve, measured without aging in ZFC process, is also shown.

5.3.2 Effects of heat treatment of magnetic properties of $CdFe_2O_4$ sputtered thin films

Figures 5.8(a) and (b) depict the magnetic field dependence of magnetization for the $CdFe_2O_4$ thin films measured at 5 and 300 K, respectively. All the films show magnetic hysteresis behavior even at room temperature. This may be due to the site exchange between Cd^{2+} in the A site and Fe^{3+} in the B site in the spinel structure. The magnetization of the film annealed at 200 °C is larger than that of the as-deposited film, and the film annealed at 400 °C has smaller magnetization than the as-deposited film.

Temperature dependence of magnetization for the films is shown in Fig. 5.9. Both field cooling (FC) and zero-field cooling (ZFC) were performed for all the films. A magnetic field of 50 Oe was applied for the measurements. For the film annealed at 200 °C, ZFC magnetizations exhibits a broad maximum at around 200 K and ZFC and FC magnetization deviates from each other below 300 K, similarly to the as-deposited film. On the other hand, the magnetic behavior of the thin film annealed at 400 °C resembles that of bulk $CdFe_2O_4$, although the magnitude of magnetization of the film is significantly larger than that of the bulk sample.

Let us consider the effect of annealing on the magnetization of $CdFe_2O_4$ thin film in terms of the structural change of the film induced by the annealing. The annealing at 200 °C causes great enhancement of magnetization up to 36 emu/g at 5 K. This increase is explainable as follows. During the annealing at 200 °C, the crystallization of the amorphous phase and/or the grain growth of the initial crystallites occur, while the random distribution of Fe^{3+} ions in the spinel structure is preserved for the most part. Subsequently, the number of magnetic moments contributing to a ferrimagnetic arrangement is increased. A value of 69.2 emu/g is expected at 0 K for $CdFe_2O_4$ with a cation distribution being perfectly random, the composition of which can be denoted as $[Cd_{0.33}Fe_{0.67}]_A[Cd_{0.67}Fe_{1.33}]_BO_4$. The magnetization of the thin film annealed at 200 °C does not reach such a large value because of the presence of amorphous phase which should possess lower magnetization. On the other hand, the annealing at 400 °C results in a decrease in magnetization. The annealing of the thin films at

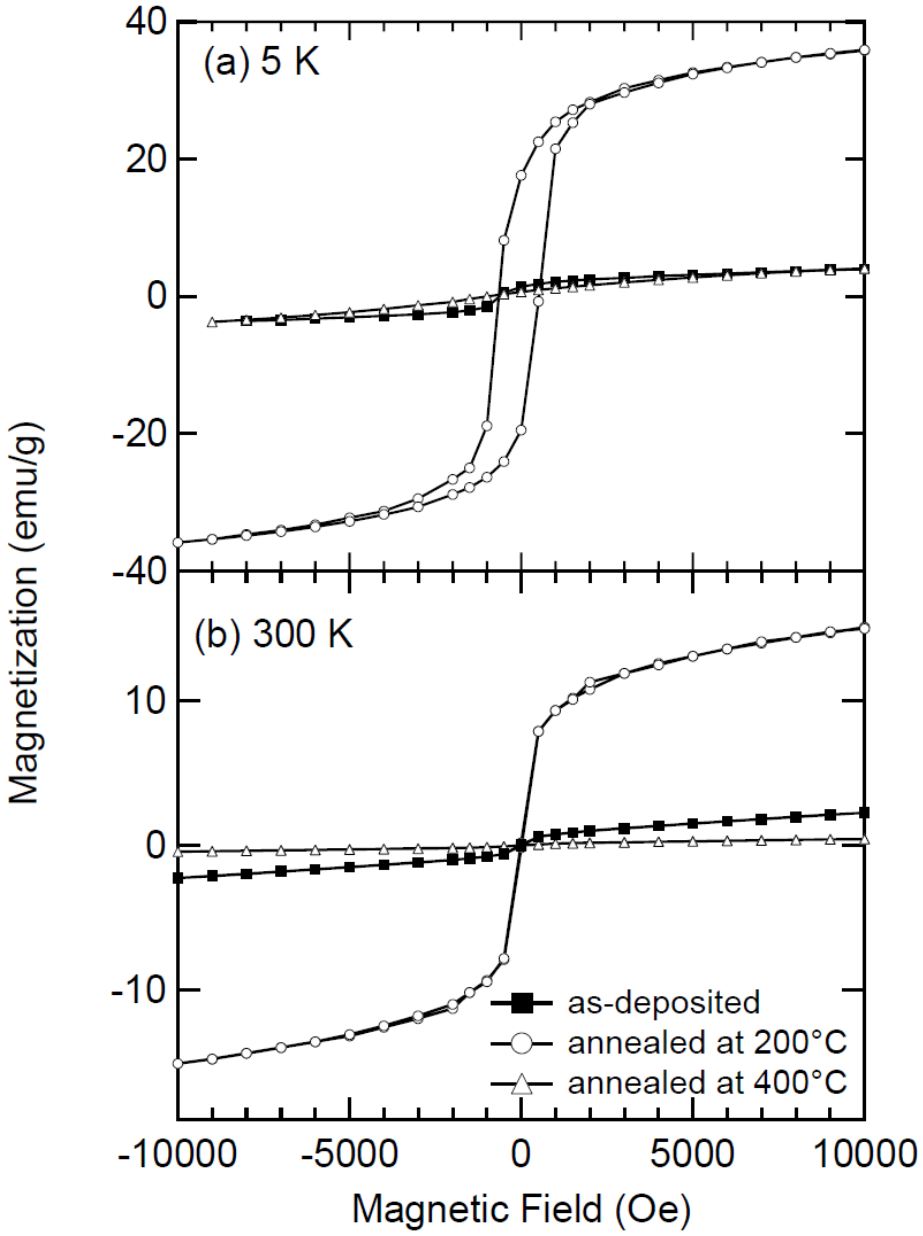

Figure. 5.8: Magnetic field dependence of magnetization for $CdFe_2O_4$ thin films measured at (a) 5 and (b) 300 K.

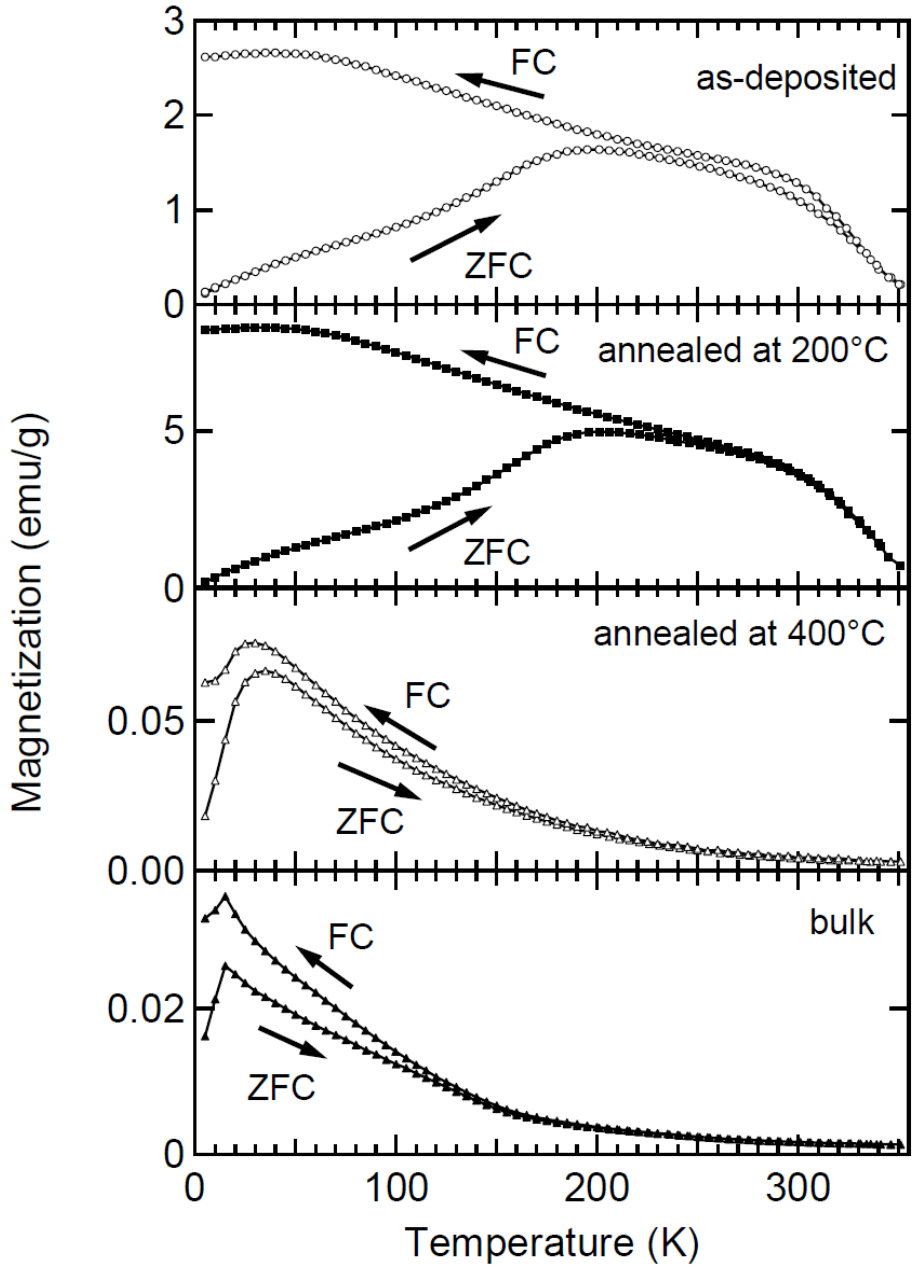

Figure. 5.9: Temperature dependence of magnetization for $CdFe_2O_4$ thin films and bulk $CdFe_2O_4$. Both zero-field and field cooling were performed. A magnetic field of 50 Oe was applied for the measurement.

high temperatures such as 400 °C likely brings about the grain coarsening and the formation of $CdFe_2O_4$ with normal spinel structure, a thermodynamically stable phase, leading to the magnetic behavior similar to that of bulk $CdFe_2O_4$. It is considered that the thin film annealed at 400 °C shows larger magnetization than the bulk sample because the conversion into the normal spinel structure is not completed even after the annealing for 3 h.

Lastly, it is worth referring to another possible mechanism for the high magnetization of the $CdFe_2O_4$ nanocrystals. According to recent research on nanoparticles of spinel ferrites such as $MgFe_2O_4$ and $NiFe_2O_4$, the magnetization of nanocrystals larger than those of the corresponding bulk crystals is explained in terms of the competition between the effects of spin canting and site exchange of cations on the surface regions of nanoparticles, while the interior of the nanocrystals has the same structure and magnetic properties as the bulk crystals [29]-[31]. It should be noted that the magnetization decreases monotonously as the annealing temperature becomes higher in those systems. This behavior is clearly inconsistent with the present $CdFe_2O_4$ thin films, where the film annealed at 200 °C has magnetization higher than the as-deposited film, indicating that the mechanism of the spin canting does not rationalize well the case of this study. Nevertheless, more detailed information is required to confirm that a random distribution of cations prevails not only in the surface region but also in the interior region of the nanocrystals [10].

5.4 Conclusion

A large magnetization and a high magnetic transition temperature were obtained for the as-deposited $CdFe_2O_4$ thin film prepared by a sputtering method. It is thought that the random distribution of the cations in the structure of $CdFe_2O_4$ nanocrystals, where the Fe^{3+} ions occupy not only the B sites but also the A sites, causes a cluster-spin or superspin glass like magnetic ordering. The annealing of the film at 200 °C leads to grain growth as well as crystallization of $CdFe_2O_4$ with a random distribution of cations from the amorphous phase, resulting in the enhancement of magnetization. The grain coarsening of normal spinel $CdFe_2O_4$ crystalline phases takes place when the thin film is annealed at 400 °C. In consequence, the film annealed at 400 °C exhibits magnetic properties similar to those of bulk $CdFe_2O_4$.

References in Chapter 5

[1] K. Kamazawa, S. Park, S. H. Lee, T. J. Sato, and Y. Tsunoda, *Phy*. *Rev*. B **70**, 024418 (2004).

[2] K. Kamazawa, Y. Tsunoda, H. Kadowaki, and K. Kohn, *Phy*. *Rev*. B **68**, 024412 (2003).

[3] S. J. Stewart, S. J. A. Figueroa, J. M. Ramallo López, S. G. Marchetti, J. F. Bengoa. R. J. Prado and F. G. Requejo, *Phy*. *Rev*. B **75**, 073408 (2007).

[4] G. F. Goya, H. R. Rechenberg, M. Chen, and W. B. Yelon, *J*. *Appl*. *Phys*. **87**, 8005 (2000).

[5] K. Tanaka, S. Nakashima, K. Fujita, and K. Hirao, *J*. *Phys*.: *Condens*. *Matter.* **15**, L469 (2003).

[6] S. Nakashima, K. Fujita, K. Tanaka, and K. Hirao, *J*. *Phys*.: *Condens*. *Matter*. **17**, 137 (2005).

[7] Y. Yamamoto, H. Tanaka, and T. Kawai, *Jpn*. *J*. *Appl*. *Phys*. **40**, L545 (2001).

[8] M. Yokoyama, E. Ohta, T. Sato, and T. Sato, "Magnetic properties of ultrafine particles and bulk metarial of cadmium ferrite," *J*. *Magn*. *Magn*. *Mater*. **183**, 173 (1998).

[9] C. N. Chinnasamy, A. Narayanasamy, N. Ponpandian, R. Justin Joseyphus, K. Chattopadhyay, K. Shinoda, B. Jeyadevan, K. Tohji, K. Nakatsuka, and J.-M. Greneche, *J*. *Appl*. *Phys*. **90**, 527 (2001).

[10] S. Nakashima, K. Fujita, K. Tanaka, K. Hirao, T. Yamamoto, and I. Tanaka, *Phy*. *Rev*. B **75**, 174443 (2007).

[11] K. Matsumoto, F. Saito, T. Toyoda, K. Ohkubo, K. Yamawaki, T. Mori, K. Hirano, M. Tanaka, and S. Sasaki, *Jpn*. *J*. *Appl*. *Phys*. **39**, 6089 (2000).

[12] M. D. Mukadam, S. M. Yusuf, P. Sharma, S. K. Kulshreshtha, and G. K. Dey, *Phy*. *Rev*. B **72**, 174408 (2005).

[13] J. A. Mydosh, *Spin glasses: an Experimental Introduction* (Taylor &Francis Ltd., London, 1993).

[14] S. Sahoo, O. Petracic, W. Kleemann, S. Stappert, G. Dumpich, P. Nordblad, S. Cardoso and P. P. Freitas, *Appl. Phys. Lett.* **82**, 4116 (2003).

[15] B. Antic, G. F. Goya, H. R. Rechenberg, V. Kusigerski, N. Jovic and M. Mitric, *J. Phys.: Condens. Mater.* **16**, 651 (2004).

[16] C. Djurberg, P. Svedlindh, P. Nordblad, M. F. Hansen, F. Bodker and S. Morup, *Phys. Rev. Lett.* **79**, 5154 (1997).

[17] K. Gunnarsson, P. Svedlindh, P. Nordblad, L. Lundgren, H. Aruga and A. Ito, *Phys. Rev. Lett.* **61**, 754 (1988).

[18] M. F. Hansen, P. E. Jönsson, P. Nordblad and P. Svedlindh, *J. Phys.: Condens. Mater.* **14**, 4901 (2002).

[19] S. Shtrikman and E. P. Wohlfarth, *Phys. Lett.* **85A**, 467 (1981).

[20] S. Shtrikman and E. P. Wohlfarth, *J. Magn. Magn. Mater.* **31-34**, 1421 (1983).

[21] R. Mathieu, P. Jönsson, D. N. H. Nam, and P. Nordblad, *Phys. Rev. B* **63**, 92401 (2001).

[22] M. Sasaki, P. E. Jönsson, H. Takayama and H. Mamiya, *Phys. Rev. B* **71**, 104405 (2005).

[23] Xi Chen, S. Bedanta, O. Petracic, W. Kleemann, S. Sahoo, S. Cardoso and P. P. Freitas, *Phys. Rev. B* **72**, 214436 (2005).

[24] S. Sahoo, O. Petracic, W. Kleemann, P. Nordblad, S. Cardoso and P. P. Freitas, *Phys. Rev. B* **67**, 214422 (2003).

[25] O. Cador, F. Grasset, H. Haneda and J. Etourneau, *J. Magn. Magn. Mater.* **268**, 232 (2004).

[26] C. R. Sankar and P. A. Joy, *Phys. Rev. B* **72**, 132407 (2005).

[27] J. Du, B. Zhang, R. K. Zheng and X. X. Zhang, *Phys. Rev. B* **75**, 014415 (2007).

[28] Sunil Nair, A. K. Nigam, A. V. Narlikar, D. Prabhakaran and A. Boothroyd, *Phys. Rev. B* **74**, 132407 (2006).

[29] K. Matsumoto, F. Saito, T. Toyoda, K. Ohkubo, K. Yamawaki, T. Mori, K. Hirano, M. Tanaka, and S. Sasaki, *Jpn*. *J*. *Appl*. *Phys*. **39**, 6089 (2000).

[30] V. Šepelák, I. Bergmann, D. Menzel, A. Feldhoff, P. Heitjans, F. J. Litterst, and K. D. Becker, *J*. *Magn*. *Magn*. *Mater*. **316**, e764 (2007).

[31] V. Šepelák, A. Feldhoff, P. Heitjans, F. Krumeich, D. Menzel, F. J. Litterst, I. Bergmann, and K. D. Becker, *Chem*. *Mater*. **18**, 3057 (2006).

[32] V. Šepelák, I. Bergmann, A. Feldhoff, P. Heitjans, F. Krumeich, D. Menzel, F. J. Litterst, S. J. Campbel, and K. D. Becker, *J. Phys. Chem. C* **111**, 5026 (2007).

Summary

In the present thesis, with a view to shed light on chemistry and physics of random magnetic systems, the preparation and characterization of the random magnetic oxides including bulk oxide glasses, amorphous oxide films, and nanocrystalline oxide films were performed; their magnetic and magneto-optical properties were investigated in detail. The origin of magnetic transitions and the nature of magnetically ordered phases were discussed on the basis of the static and dynamic magnetic behavior and thermo-magnetic properties. In particular, the scaling analysis on critical slowing down and the investigation of magnetic aging and memory effects proved to be significant tools to clarify the complicated magnetic properties. The random magnetic oxides manifest a wide variety of magnetic properties in close connection with their structural and chemical properties. The results obtained are summarized as follows.

In Chapter 1, the magnetic properties of bulk iron-containing oxide glasses were investigated in detail. In Section 1.1, the Fe_2O_3-TeO_2 glasses were proved to be categorized as a typical spin glass by examining spin dynamics including magnetic aging and memory effects as well as critical slowing down. The random distribution of magnetic moments and the prevailing AFM interactions between them inevitably causes magnetic frustration of geometrical origin in the alignment of magnetic moments. The combination of randomness and frustration leads to a spin glass phase transition. In Section 1.2, the dependence of magnetic properties on the valence state of iron ions in the mixed valence iron phosphate glasses was discussed. The glasses as well as the Fe_2O_3-TeO_2 glasses are also classified as a conventional spin glass. Magnetic frustration is relieved with an increase in the fraction of the amount of Fe^{2+} ions partly due to the strong single-ion anisotropy of Fe^{2+} ions. In Section 1.3, the coexistence of spin glass and cluster-spin glass phases were clarified in the Fe_2O_3-Bi_2O_3-B_2O_3 glass system. The studies of magnetic aging and memory effects

and exchange bias effects revealed that the two magnetic phases are present accompanied with specific interfaces between them. This magnetic phase separation may be due to the inhomogeneous distribution of iron ions.

In Chapter 2, the amorphous Fe_2O_3-R_2O_3 (R = La, Gd and Tb) thin films were fabricated via a radio frequency sputtering method. The Fe_2O_3-La_2O_3 thin films exhibit magnetic behavior like those of spin glasses. In Fe_2O_3-R_2O_3 (R = Gd and Tb) systems, the magnetic moments due to the iron ions form a spin glass phase while those of gadolinium and terbium ions remain to be included in a paramagnetic phase.

In Chapter 3, the dominance of ferromagnetic interactions was discovered in the Eu^{2+}-based bulk oxide glasses. The reentrant spin glass behavior was observed for the glasses with a high concentration of Eu^{2+} ions. The reentrant spin glass nature of the present system indicates that the ferromagnetic interactions are favored but the antiferromagnetic ones are not negligible, reflecting the amorphous nature of the system.

In Chapter 4, it was found that the divalent iron phosphate glasses exhibit fairly high transmittance in the visible region, although the glasses contain a large amount of 3*d* transition metal ions. The glasses have large Faraday rotation angle in the near-ultraviolet to blue region due to the large oscillator strength of charge transfer transition from O^{2-} to Fe^{2+}. The possibility of applying FeO-based glass materials to magneto-optical devices was discussed.

In Chapter 5, a large magnetization and a high magnetic transition temperature were obtained for as-deposited $CdFe_2O_4$ thin film prepared by a sputtering method. It is thought that a random distribution of cations in the structure of $CdFe_2O_4$ nanocrystals, where the Fe^{3+} ions occupy not only the B sites but also the A sites, causes a cluster-spin or superspin glass like magnetic ordering. The dependence of structural and magnetic properties on annealing temperature was investigated.

List of Publications

Chapter 1

"Spin dynamics in Fe_2O_3-TeO_2 glass: Experimental evidence for an amorphous oxide spin glass"

H. Akamatsu, K. Tanaka, K. Fujita, and S. Murai

Physical Review B **74**, 012411 (2006).

"Magnetic properties of disordered oxides with iron and manganese ions"

K. Tanaka, H. Akamatsu, S. Nakashima, and K. Fujita

Journal of Non-Crystalline Solids **354**, 1346 (2008).

"Magnetic properties of mixed valence iron phosphate glasses"

H. Akamatsu, S. Oku, K. Fujita, S. Murai, and K. Tanaka

to be submitted to *Physical Review B*

"Spin dynamics in oxide glass of Fe_2O_3-Bi_2O_3-B_2O_3 system"

H. Akamatsu, K. Tanaka, K. Fujita, and S. Murai

Journal of Magnetism and Magnetic Materials **310**, 1506 (2007).

"Magnetic phase transitions in Fe_2O_3-Bi_2O_3-B_2O_3 glasses"

H. Akamatsu, K. Tanaka, K. Fujita, and S. Murai

Journal of Physics: Condensed Matter **20**, 235216 (2008).

Chapter 2

"Magnetic Properties of Amorphous Fe_2O_3-R_2O_3 (R = La, Gd and Tb) Thin Films Fabricated by Sputtering Method"

H. Akamatsu, S. Murai, K. Fujita, and K. Tanaka

Advanced Materials Research **39-40**, 207 (2008).

Chapter 3

"Eu^{2+}-based oxide glasses with ferromagnetic interactions"

H. Akamatsu, K. Fujita, S. Murai, and K. Tanaka

to be submitted to *Physical Review Letters*

Chapter 4

"Magneto-optical properties of transparent divalent iron phosphate glasses"

H. Akamatsu, K. Fujita, S. Murai, and K. Tanaka

Applied Physics Letters **92**, 251908 (2008).

Chapter 5

"Structural and Magnetic Properties of $CdFe_2O_4$ Thin Films Fabricated via Sputtering Method"

H. Akamatsu, Y. Zong, Y. Fujiki, K. Kamiya, K. Fujita, S. Murai, and K. Tanaka

IEEE Transactions on Magnetics **44**, 2796 (2008).

Acknowledgments

The present thesis has been carried out under the direction of Professor Katsuhisa Tanaka at Graduate School of Engineering, Kyoto University.

The author wishes to express his sincere gratitude to Professor Katsuhisa Tanaka for his continuous encouragement and valuable advice all through the duration of the present work. The author is also grateful to Professor Toshinobu Yoko and Professor Kazuyuki Hirao for guidance and discussion in preparing the present thesis. The author is greatly indebted to Associate Professor Koji Fujita for his informative discussion, helpful advice, and sincere supports. The author also thanks Mr. Shunsuke Murai for helpful assistance.

Experimental supports for Mössbauer spectroscopy measurements by Dr. Mitsuo Tosaki are greatly acknowledged. The author would like to thank Professor Masaki Azuma, Professor Yuichi Shimakawa, and the students at their laboratory for specific heat measurements and informative discussions. The author also thanks Dr. Seisuke Nakashima, Dr. Hojo Hajime, Mr. Kazuma Kugimiya, Mr. Yosefu Fujiki, Mr. Kazuaki Kamiya, Mr. Satoshi Oku, and Mr. Jun Kawabata for their experimental supports and fruitful discussions.

Hearty thanks are made to all the students of Tanaka's laboratory and Hirao's laboratory for their collaboration and everyday activities. Especially his colleagues, Dr. Xiangeng Meng, Mrs. Sakiko U. Goto, Mr. Hideaki Murase, Mr. Kazuya Fukui, Mr. Akihiro Shiota, Ms. Akiko Kawase, and Mrs. Yanfua Zong contributed to my happiest time.

An acknowledgement is extended to the financial support by a Grant-in-Aid for Scientific Research (No.20·6726) from the Ministry of Education, Culture, Sports, Science and Technology, Japan.

Finally, the author would like to express his sincere gratitude to his parents, Mikiyoshi Akamatsu and Etsuko Akamatsu, for their understanding, supports, and hearty encouragements.

Kyoto, 2009 Hirofumi Akamatsu